REPAIR EVALUATIONS OF DEPRESSED TRANSVERSE CRACKS IN ASPHALT PAVEMENTS IN DISTRICT 6

FINAL REPORT

ODOT TASK ORDER NUMBER 2160-20-02

Submitted to:
Office of Research and Implementation
Oklahoma Department of Transportation

Submitted by:
Sagar Ghos, M.Sc.*
Syed Ashik Ali, Ph.D.*
Matias M. Mendez Larrain, M.Sc., P.E.*
Kenneth Ray Hobson, P.E.*
Dar Hao Chen, Ph.D., P.E.[#]
Musharraf Zaman, Ph.D., P.E.*
Michael Behm, Ph.D.[+]
*School of Civil Engineering and Environmental Science (CEES)
[+]School of Geology and Geophysics
The University of Oklahoma
[#]Texas A&M Transportation Institute

August 2021

SI* (MODERN METRIC) CONVERSION FACTORS

APPROXIMATE CONVERSIONS TO SI UNITS

SYMBOL	WHEN YOU KNOW	MULTIPLY BY	TO FIND	SYMBOL
		LENGTH		
in	inches	25.4	millimeters	mm
ft	feet	0.305	meters	m
yd	yards	0.914	meters	m
mi	miles	1.61	kilometers	km
		AREA		
in^2	square inches	645.2	square millimeters	mm^2
ft^2	square feet	0.093	square meters	m^2
yd^2	square yard	0.836	square meters	m^2
ac	acres	0.405	hectares	Ha
mi^2	square miles	2.59	square kilometers	km^2
		VOLUME		
fl oz	fluid ounces	29.57	milliliters	mL
gal	gallons	3.785	liters	L
ft^3	cubic feet	0.028	cubic meters	m^3
yd^3	cubic yards	0.765	cubic meters	m^3
		NOTE: volumes greater than 1000 L shall be shown in m^3		
		MASS		
oz	ounces	28.35	grams	g
lb	pounds	0.454	kilograms	kg
T	short tons (2000 lb)	0.907	megagrams (or "metric ton")	Mg (or "t")
		TEMPERATURE (exact degrees)		
^oF	Fahrenheit	5 (F-32)/9 or (F-32)/1.8	Celsius	^oC
		ILLUMINATION		
fc	foot-candles	10.76	lux	Lx
fl	foot-Lamberts	3.426	candela/m^2	cd/m^2
		FORCE and PRESSURE or STRESS		
lbf	poundforce	4.45	newtons	N
lbf/in^2	poundforce per square inch	6.89	kilopascals	kPa

APPROXIMATE CONVERSIONS FROM SI UNITS

SYMBOL	WHEN YOU KNOW	MULTIPLY BY	TO FIND	SYMBOL
		LENGTH		
mm	millimeters	0.039	inches	in
m	meters	3.28	feet	ft
m	meters	1.09	yards	yd
km	kilometers	0.621	miles	mi
		AREA		
mm^2	square millimeters	0.0016	square inches	in^2
m^2	square meters	10.764	square feet	ft^2
m^2	square meters	1.195	square yards	yd^2
ha	hectares	2.47	acres	Ac
km^2	square kilometers	0.386	square miles	mi^2
		VOLUME		
mL	milliliters	0.034	fluid ounces	fl oz
L	liters	0.264	gallons	Gal
m^3	cubic meters	35.314	cubic feet	ft^3
m^3	cubic meters	1.307	cubic yards	yd^3
		MASS		
g	grams	0.035	ounces	Oz
kg	kilograms	2.202	pounds	Lb
Mg (or "t")	megagrams (or "metric ton")	1.103	short tons (2000 lb)	T
		TEMPERATURE (exact degrees)		
^oC	Celsius	1.8C+32	Fahrenheit	^oF
		ILLUMINATION		
lx	lux	0.0929	foot-candles	Fc
cd/m^2	candela/m^2	0.2919	foot-Lamberts	Fl
		FORCE and PRESSURE or STRESS		
N	newtons	0.225	poundforce	lbf
kPa	kilopascals	0.145	poundforce per square inc h	lbf/in^2

*SI is the symbol for the International System of Units. Appropriate rounding should be made to comply with Section 4 of ASTM E380.
(Revised March 2003)

TABLE OF CONTENTS

LIST OF TABLES

LIST OF FIGURES

ACKNOWLEDGMENTS

The authors would like to acknowledge the financial support provided by the Oklahoma Department of Transportation (ODOT) for this Task Order. In addition, ODOT District 6 staff played a key role in achieving important milestones of this Task Order including selection of test section, planning for repairing cracks, milling and trenching of cracks, providing traffic control and conducting field tests. Specifically, the research team is thankful to Ron McDaniel and Jon Logan from ODOT District 6 for their assistance in this Task Order. The field component of this Task Order would not be possible without the active involvement of FPTInfrastructures. The authors are grateful to the company for providing material and technical support for constructing Fibrecrete repair sections. Also, authors would like to thank Dr. Michael Behm and his team for Ground Penetrating Radar (GPR) tests, Dr. Naji Khouri and Michael Schmitz for Falling Weight Deflectometer (FWD) tests, and Dr. Kelvin Wang and his team at Oklahoma State University (OSU) for conducting PaveVision3D and Pave 3D 8K surveys. Special thanks are extended to staff members at the School of Civil Engineering and Environmental Science (CEES) and Shared Business Service Center (SBSC), for their invaluable assistance throughout this Task Order.

EXECUTIVE SUMMARY

Transverse cracking is one of the major problems in asphalt pavements in north-western (Panhandle) regions of Oklahoma. The eastbound lane and shoulder of US-270 in Harper County northwest of Woodward, Oklahoma has experienced significant transverse cracking. The extent and probable causes of the transverse cracking at US-270 were documented during the Phase 1 of this forensic investigation (ODOT Task Order 2160-18-07). The purpose of this Task Order (2160-20-02) was to evaluate the effectiveness of two transverse crack repair methods, namely (1) trenching and patching using Fibrecrete and (2) trenching and patching using HMA. Performance of these repair methods were investigated periodically using physical inspection, Falling Weight Deflectometer (FWD), Ground Penetrating Radar (GPR), Face Dipstick, Straightedge, PaveVision3D and Pave 3D 8K. An evaluation of the "do no repair or do nothing" scenario was considered to document the improvement of the proposed repair methods. The key findings from this investigation are summarized below:

i. The Fibrecrete repair was observed to fully suppress transverse cracking.
ii. Repair with coarse HMA with no tack coat may not produce satisfactory results. The reflective cracks on the test section were found to propagate 2-in. in one year through the HMA layer. The use of coarse (S3) HMA may be responsible for this faster propagation of cracks. Additional cracking may have occurred due to no tack coat.
iii. The initial compaction of the HMA and Fibrecrete layer resulted in an increase in the rut depths after repair. The IRI of the Fibrecrete- and HMA-repaired sections were found to be comparable.
iv. No significant changes in the crack geometry were observed for the controlled cracks over the observation period (1 year). However, cracks may widen, and more rutting may occur over time, if no-repair activity is pursued.

The following rehabilitation options (lowest cost to highest cost) were evaluated as repair options for the transverse cracks on US-270:

1. Crack seal, overlay 2-in. with S4 (PG 70-28 OK) mix;
2. Crack seal, overlay 2-in. with S4 (PG 70-28 OK) mix and 3-in. with S3 (PG 70-28 OK) mix;
3. Crack seal, mill most cracks, Fibrecrete, overlay with 2-in. S4 (70-28 OK) mix; and
4. Crack seal, mill all cracks, Fibrecrete, overlay with 2-in. S4 (PG 70-28 OK) mix.

Please note that, the Option 2 is similar to the rehabilitation project implemented in US-270 by District 6 on June 2021. However, based on the LCCA results and the results from the three evaluations, Fibrecrete repair methods were recommended for US-270. Other options, such as high polymer mixes may be considered, but were not investigated and evaluated in this Task Order.

1. INTRODUCTION

Cracking is one of the most common distresses in flexible pavements [1-3]. According to West et al. [3], more than 85% of asphalt pavements in the United States experience some form of cracks, which includes transverse cracking, reflective cracking, fatigue cracking and longitudinal cracking. About 45% of asphalt pavements experience transverse cracking and reflective cracking in their service lives [3]. The eastbound lane and shoulder of US-270 in Harper County northwest of Woodward, Oklahoma has experienced significant transverse cracking. Figure 1.1 shows a photographic view of the transverse cracks observed in US-270. According to ODOT District 6 staff, the pavement section was built in the 1980s and depressed transverse cracks have been observed since at least 2008. The extent and probable causes of the transverse cracking at this site were documented during the Phase 1 of this forensic investigation (ODOT Task Order 2160-18-07). With significant time lag, it was difficult to identify the real causes of these depressed transverse cracks. However, it was evident from the field and laboratory tests that the base supports were still structurally sound, and the main issue resided with the cracks in the asphalt layer. The two most probable causes of the surface cracks, identified during Phase 1, were: (1) inability of the asphalt binder to resist low temperature cracking under extreme weather conditions including large thermal cycles with a rapid drop or rise in temperature; and/or (2) brittleness of the asphalt mixes due to aging. In addition, a number of recommendations were provided to minimize the transverse cracking problem in Oklahoma. The current Task Order (ODOT Task Order 2160-20-02) was a follow-up of the previous Task Order and aimed at evaluating the effectiveness of different repair options for depressed transverse cracks in US-270.

A number of repair and remedial options, such as trenching and patching with special materials, milling and overlay with HMA, and adding polymers to the HMA overlay, are currently in practice to eliminate transverse cracks in asphalt pavements [4]. However, the effectiveness of these options depends on the nature and extents of the problem specific to the repair site [3]. Among the available repair options, patching with polymer modified patching materials and HMA are popular methods among the Departments of Transportation (DOTs) and contractors due to ease of operations [4-5]. Fibrecrete is a polymer modified asphalt material containing mineral fillers, chopped fibers, sand and graded granite aggregates [5]. Although flexible in nature, Fibrecrete is strong enough to handle heavy traffic and the stresses of changing temperatures and seasons [6]. Also, use of Fibrecrete can limit the joint and crack movement due to thermal expansion and contraction, and vibration [6]. In this Task Order, a comparative evaluation of two

transverse cracking repair options was conducted on a selected test section of US-270. Also, an attempt was made to identify suitable transverse crack repair options for Oklahoma pavement. The specific objectives of this Task Order are:

i. To evaluate the effectiveness of two repair methods, namely (1) trenching and patching using Fibrecrete and (2) trenching and patching using HMA for transverse cracks observed in US-270.
ii. To compare performance of the repaired sections with non-repaired (control) sections.
iii. To conduct a Life Cycle Cost Analysis (LCCA) to identify a suitable repair option for transverse cracks inUS-270.

(a) (b) (c)

Figure 1.1 Transverse cracks observed in US-270: (a) view from the top; (b) width of crack; and (c) depth of crack

1.1 Scope of Work

The Task Order was divided into the following steps: selection of site; repair of selected cracks; and assessment of performance using non-destructive testing. A kickoff meeting was held on June 30, 2020, among the OU team and ODOT staff to discuss the location of the crack sections and devise the testing plan. The selection of the cracks was made based on findings from ODOT Task Order 2160-18-07. Three transverse cracks were selected for each repair method. Also, three non-repaired (i.e., “do nothing”) cracks were selected as control. The locations of these cracks were relatively close to each other to minimize the extent of traffic control. The performance of two repair methods and control was evaluated using physical observation, Falling Weight Deflectometer (FWD), Ground Penetrating Radar (GPR), Straightedge, Face Dipstick and PaveVision3D and Pave 3D 8K. These tests were scheduled to be conducted at approximately: (1) before the repairs; (2) five months after the repairs, and (3)

ten months after the repair. The first repair evaluation (Evaluation #1, before the repair) was performed on July 22, 2020. Both Fibrecrete and HMA repairs were completed on July 24, 2020. Then, Evaluation #2 was performed on November 18, 2020 using FWD, GPR, straightedge and face Dipstick. Also, the physical condition of the repair was inspected during Evaluation #2. The final evaluation (Evaluation #3) was planned on May 19, 2021 but cancelled due to severe weather condition. Evaluation #3 was then performed on June 2, 2021 (approximately 11 months after repair). The performance of the Fibrecrete and HMA repairs was compared with each other and with the control cracks. Also, the changes in the performance of the repaired sections over time were evaluated by comparing Evaluations #1, #2 and #3.

2. METHODOLOGY

2.1 Project Location and Testing Plan

A 3,650-ft long segment of US-270 starting from 3.0 miles east of the US-283/US-270 junction and extending to 2 miles east in District 6 was selected for this study, as shown in Figure 2.1. The starting and ending coordinates of this test section were (36°37'20.93"N, 99°49'54.94"W) and (36°37'20.84"N, 99°50'8.42"W), respectively. At this test section, a total of 9 transverse cracks were selected for the evaluation. The cracks were selected based on the findings of the Phase 1 investigation (ODOT Task Order 2160-18-07). The GPS coordinates of these cracks are presented in Table 2.1. As shown in Table 2.1, Cracks #5, #7, and #9 were repaired using Fibrecrete and Cracks #12, #18, and #27 were repaired using HMA. The other three cracks, namely Cracks #29, #30, and #32, were used as control (“do nothing”) for comparison purpose. As noted previously, three evaluations were performed on these sections using physical observation, GPR, FWD, Face Dipstick, Straightedge, PaveVision3D and Pave 3D 8K.

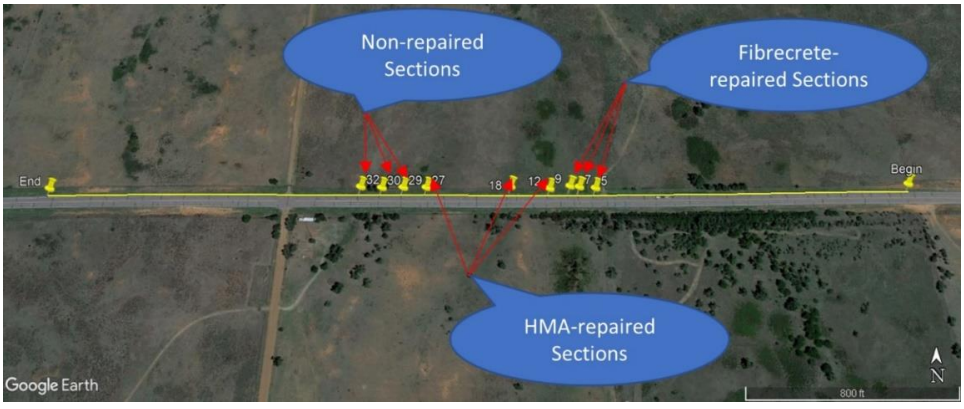

Figure 2.1 Google satellite image of the test section

Table 2.1 Locations of the repaired cracks

ID	Latitude	Longitude	Repair Methods
Begin	36°37'20.86"N	99°49'39.97"W	--
End	36°37'20.77"N	99°50'24.58"W	--
#5	36°37'20.83"N	99°49'56.14"W	Fibrecrete
#7	36°37'20.87"N	99°49'56.98"W	
#9	36°37'20.91"N	99°49'57.46"W	
#12	36°37'20.79"N	99°49'58.54"W	HMA
#18	36°37'20.89"N	99°50'0.57"W	
#27	36°37'20.82"N	99°50'4.96"W	
#29	36°37'20.82"N	99°50'6.17"W	No repair
#30	36°37'20.80"N	99°50'7.28"W	
#32	36°37'20.84"N	99°50'8.38"W	

2.2 Repair of Transverse Cracks

Figures 2.2 and 2.3 show the Fibrecrete and HMA repair activities for Cracks #5 and #12, respectively. Both the Fibrecrete and HMA repairs were performed on July 24, 2020. The east bound lanes of the test section were closed, and traffic control was setup by ODOT to ensure safety during repair activities. For the purpose of the Fibrecrete repairs, the shoulder and the outside lane, along the transverse cracks, were milled to 2-inch deep and 24-inch wide using a milling machine, as shown in Figures 2.2 (a). The milled trench was then swept and cleaned to remove dust (Figure 2.2 (b)). After cleaning, the Fibrecrete material was laid on the milled trench. The material was prepared on the site by a technician from the company (FPTInfrastructures). First, a layer of the heated Fibrecrete mastic was laid on the trench using a shovel (Figure 2.2 (c)). Then, uniformly graded crushed stone chips were spread on the heated Fibrecrete mastic and mixed using the shovel as shown in Figure 2.2 (d). Finally, another layer of heated Fibrecrete mastic was laid on the top. Then the repaired cracks were leveled with respect to the existing pavement using the shovel. No additional compaction was required for the Fibrecrete repair. Figure 2.2 (e) shows the photographic view of the repaired Crack #5. The HMA repairs were conducted with the help of District 6 staff. For HMA repair, similar milling and trenching as Fibrecrete were performed on Cracks #12, #18, and #27. Asphalt mix (S3 HMA with PG 64-22 binder) was collected from a local asphalt plant. The heated HMA was laid in the milled trench using a front-end loader and leveled with shovels (Figure 2.3 (a)). Then the HMA layer was compacted using a hand-operated vibratory compactor as shown in Figure 2.3 (b). Figure 2.3 (c) shows the photographic view of the

repaired Crack #12. The photographs of the crack repair activities for Cracks #7, #9, #18 and #27 are presented in Appendix A.

(a) (b) (c) (d) (e)

Figure 2.2 Fibrecrete repair at Crack #5: (a) milling; (b) sweeping of dust; (c) laying of Fibrecrete mastic; (d) mixing with aggregate; and (e) final repaired crack

(a)

(b)

(c)

Figure 2.3 HMA repair at Crack #12: (a) laying of HMA; (b) compaction using hand-held compactor; and (c) final repaired crack

2.3 Field Testing

Three evaluations with Straightedge, GPR, FWD and Face Dipstick were conducted at the test site to evaluate the effectiveness of the repair works. Evaluations #1, #2 and #3 were conducted on July 22, 2020, November 18, 2020, and June 2, 2021, respectively. Evaluations using the PaveVision3D was performed on April 26, 2019 (before repair) and using Pave 3D 8kon November 28, 2020 (five months after repair). In addition to field testing, all 9 cracks were inspected carefully during each evaluation by taking photographs and documenting physical changes.

Straight Edge Measurement: A 12-ft. Straightedge was placed transversely across the outside lane following the crack, as shown in Figure 2.4. The measurements were taken at the

middle of the repair width. The rut gauge blocks were placed at the two largest deflections to measure rut depths in 1/8-in. depth intervals. These deflections usually occurred at the wheel paths. A 10-ft. Straight Edge was placed longitudinally along the two-wheel paths. Maximum rut depths were recorded using a rut gauge with 1/8-in. increment. The results of Straightedge measurements are discussed subsequently.

Ground Penetrating Radar (GPR): The GPR tests were conducted at all 9 cracks to determine the extent of cracks, moisture, and other anomalies. The GPR data were collected by forming longitudinal and transverse grids. The grid was centered on the transverse crack and included both shoulder and the outside eastbound lane. A Sensors & Software Pulse Ekko GPR equipment with 1,000 MHz antenna was used for collecting the GPR data. Figure 2.5 shows a photographic view of the GPR data collection at the test site. The ReflexW software was used for processing the GPR data. The longitudinal and transverse profiles of each crack locations were determined from the collected data. The results from the three evaluations were compared and discussed in the subsequent section.

Falling Weight Deflectometer (FWD) Test: The structural condition assessment of pavement layers plays a critical role to select maintenance and rehabilitation strategies by the state transportation agencies. Falling Weight Deflectometer (FWD) is a deflection-testing device commonly used to determine structural capacity of pavement layers. Typically, crack repairs are not expected to improve structural capacity substantially as the main purpose is to improve functionality and extend pavement life. However, it is expected that the maintenance repairs may slow the pavement deterioration, thus may deter the increase in deflection in FWD test. A total of nine FWD tests was conducted during each evaluation. A JILS-20 FWD equipment with a 12-in. diameter loading plate and seven geophone sensors (W1 to W7) was used for the FWD tests. The FWD load plate was positioned at approximately 3-ft away from the transverse cracks. Figure 2.6 shows the photographic view of the FWD tests conducted at the test site. The MODULUS 7.0 program was used to analyze the FWD data and calculate the normalized maximum deflection of W1 and W7 sensors (with respect to 9-kip load) and modulus of the pavement layers.

Face Dipstick Measurement: Face Dipstick was used to measure the pavement profile, rutting, and International Roughness Index (IRI). Figure 2.7 shows a photo of the Face Dipstick measurement on Both pavement profiles and rutting were measured in the transverse direction twice, once in the forward direction and once in the backward direction.

PaveVision3D and Pave 3D 8K: The collection of data for Evaluation #1 (before repair) at the site was conducted on April 26, 2019 by the OSU team using PaveVision3D. The begin and end positions of the 3D image data collection were located at (36.622456, -99.828987) and (36.622410, -99.840904), respectively. Therefore, the image data was collected and analyzed on a 0.6-mile-long pavement section. The PaveVision3D was used for automated pavement condition survey at 1 mm resolution. The collected data was saved by image frame with the dimension of 2,048 mm in length and 4,096 mm in width. Please note that this evaluation was performed as a part of the Phase 1 investigation (ODOT Task Order 2160-18-07).

The Evaluation #2 (after repair) for surface data collection was conducted on November 28, 2020 by the WayLink/OSU team. The image data was collected and analyzed for a 0.73-mile-long pavement section beginning at (36.622448, -99.827812) and ending at (36.622414, -99.840866). A newer version of the PaveVision3D, namely Pave 3D 8K, was used for pavement condition survey at 0.5 mm resolution. The latest iteration of the Pave3D 8K vehicle is shown in Figure 2.8. The collected data was saved by image frames with a dimension of 2,048 mm in length and 4,096 mm in width. The collected data was used for calculating transverse rutting and longitudinal roughness.

A third evaluation, after 11 months of repair, was planned around the middle June 2021. However, the team had to cancel the evaluation as an overlay was already constructed on top of the test section.

Figure 2.4 Photographic view of straightedge measurement in US-270

Figure 2.5 Photographic view of GPR testing in US-270

Figure 2.6 Photographic view of the FWD testing in US-270

Figure 2.7 Face Dipstick measurement in US-270 test site

Figure 2.8 Pave3D 8k Vehicle parked on the shoulder of US-270 test site

3. RESULTS AND DISCUSSIONS

3.1 Physical Inspection of the Cracks

Figures 3.1, 3.2 and 3.3 show the photographs of Fibrecrete-repaired, HMA-repaired and control section, respectively. From physical inspection, the Fibrecrete-repaired sections were found to perform better as compared to HMA-repaired sections. No reflective cracking was observed in the Fibrecrete-repaired sections during after repair evaluations, i.e., Evaluation #2 and #3. However, during Evaluation #3 (11-months after repair), reflective cracks were found in all three HMA-repaired sections, as shown in Figures 3.2 (a), 3.2 (b) and 3.2 (c). Also, cracking along the edges of HMA-repaired sections were observed during Evaluation #3. However, no

significant changes in the crack geometry over time were observed for the control cracks (Figure 3.3).

(a) (b) (c)

Figure 3.1 Photographs of Fibrecrete-repaired cracks during Evaluation #3: (a) Crack #5; (b) Crack #7; and (c) Crack #9

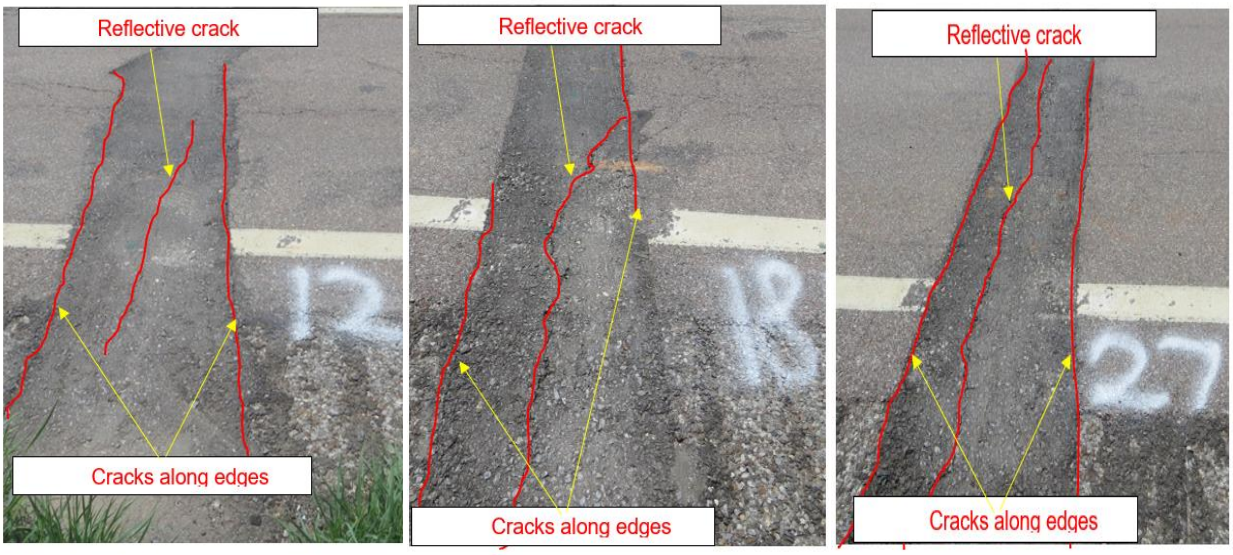

(a) (b) (c)

Figure 3.2 Photographs of HMA-repaired cracks during Evaluation #3: (a) Crack #12; (b) Crack #18; and (c) Crack #27

(a) (b) (c)

Figure 3.3 Photographs of control cracks during Evaluation #3: (a) Crack #29; (b) Crack #30; and (c) Crack #32

3.2 Ground Penetrating Radar (GPR) Testing

Figures 3.4, 3.5 and 3.6 show the GPR test results of Cracks #5, #12 and #30, respectively. As shown in Figure 3.4, the Fibrecrete repaired sections did not exhibit any new surface crack. Also, the propagation of the underlying transverse cracks was observed to stop due to the use of the Fibrecrete layer. However, from the GPR analyses, the HMA repaired sections were found to exhibit the propagation of the reflective cracks. For example, for Crack #12 (Figure 3.5), the presence of the reflective cracking in the HMA layer was prominent in Evaluation #3. As observed during physical inspection, these cracks already propagated through the HMA sections and edges between the new and existing HMA. Figure 3.6 presents the profiles of non-repaired (control) cracked section (Crack #30). Similar to physical inspection, the GPR analyses revealed no significant changes in the crack geometry over time for the control cracks. Additional results of the GPR tests can be found in Appendix B.

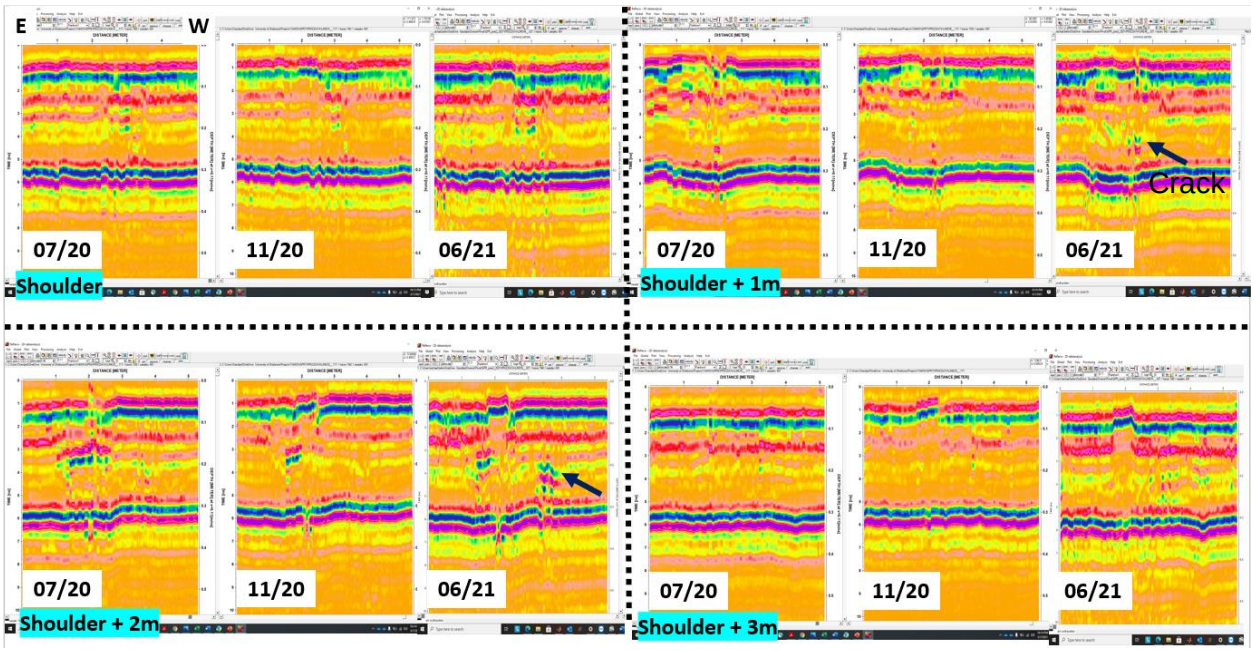

Figure 3.4 Longitudinal profile near the Crack #5 (Fibrecrete repair)

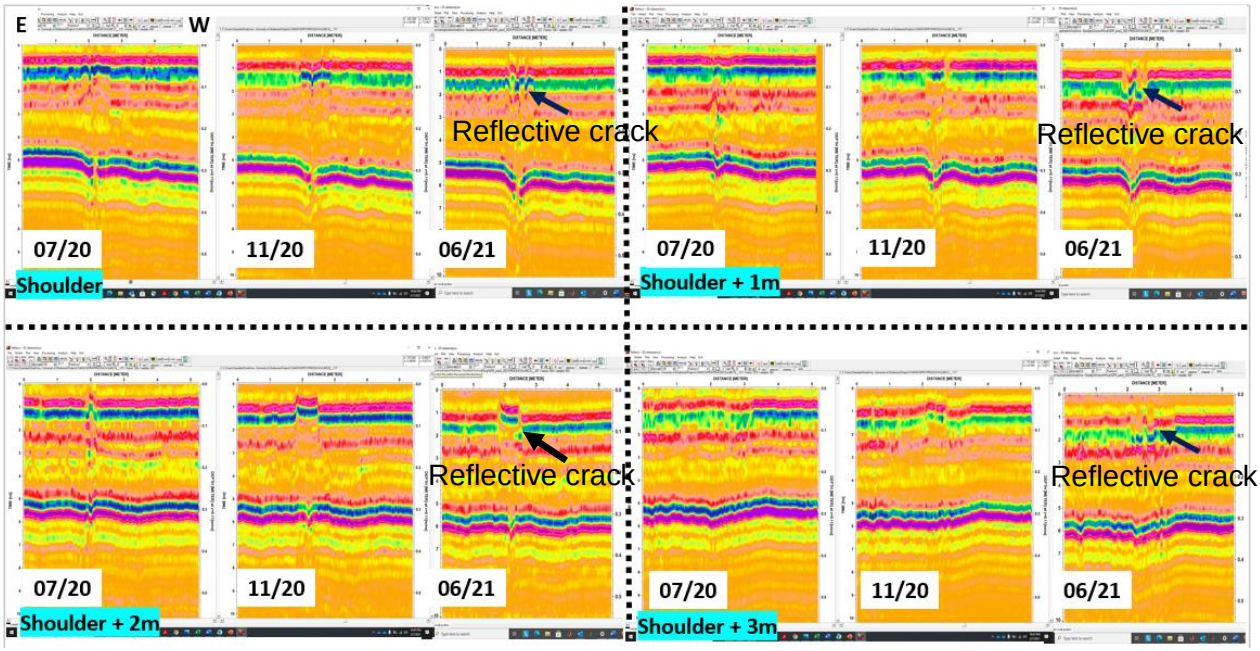

Figure 3.5 Longitudinal profile near the Crack #12 (HMA repair)

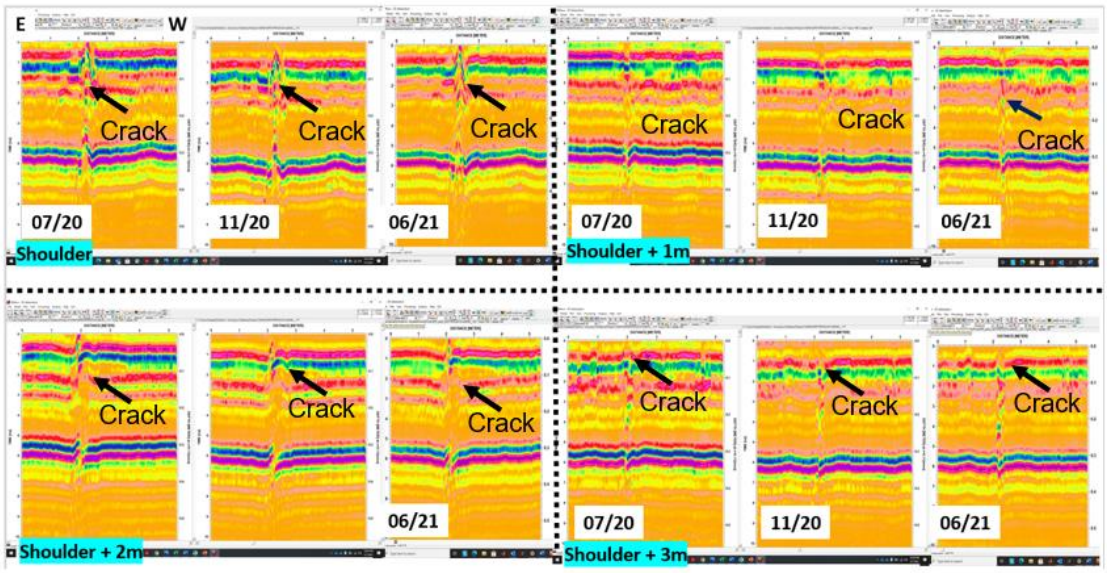

Figure 3.6 Longitudinal profile near the Crack #30 (control)

3.3 Falling Weight Deflectometer (FWD) Testing

Figures 3.7 (a) and (b) show the variations of normalized (9-kip) deflections for the W1 and W7 sensors, respectively, at the test site for all three evaluations. The W1 sensor shows deflection at the center of the FWD loading plate which represents the overall pavement structural condition at the time of testing. The W7 sensor indicates the deflection at 60 inches from the load center which is an indicator of subgrade strength. The air temperatures during Evaluation #1, #2 and #3 ranged from 96°F to 101°F, 80°F to 81°F, and 80°F to 86°F, respectively. Figure 3.7 (a) shows that the FWD tests near control cracks for all three evaluations exhibited lower W1 deflections than the Fibrecrete- and HMA- repaired sections. The results indicated that the stiffnesses of the control sections were the highest among the three sections. Also, from Figure 3.7 (a), all the FWD tests were found to exhibit lower W1 deflections for Evaluation #2 (4-month after repair) than Evaluation #1 (before repair). Even the control cracked section exhibited lower W1 deflections for Evaluation #2 than Evaluation #1. It was hypothesized that the lower W1 deflections resulted from the lower pavement temperatures during Evaluation #2.

As shown in Figures 3.7 (a) and (b), deflections for both sensors (W1 and W7) collected during Evaluation #3 were higher than those collected during Evaluation #1 and Evaluation #2. It was believed that the presence of higher moisture content in the base and subgrade layers was responsible for these higher deflections. There were almost three-week of continuous rains before the Evaluation #3 on June 2, 2021. During the evaluation, pools of standing water were

observed in areas with ruts. Although, the temperature during data collection was slightly higher for Evaluation #3 than Evaluation #2, the higher moisture contents of the base and subgrade layers were believed to be the primary contributor for the higher W1 deflections during Evaluation #3.

Back-calculation analyses using MODULUS 7 were performed for the FWD data collected during all three evaluations. Figures 3.8 (a), (b) and (c) show the back-calculated layer moduli for Evaluations #1, #2 and #3, respectively. The layer moduli for all the sections were found to be the highest during Evaluation #2. As mentioned earlier, this may have resulted from the lower pavement temperature. Also, the pavement layer moduli were found to be lower for Evaluation #3 than Evaluation #2. For example, the average subgrade modulus reduced from 10.4 ksi to 7.6 ksi (Figures 3.8 (a) and (c)) possibly because of the three-week rains before the evaluation on June 2, 2021.

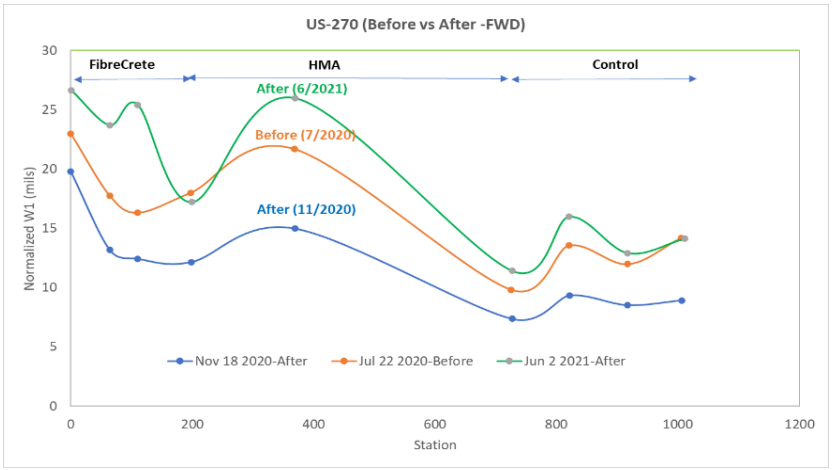

(a)

(b)

Figure 3.7 Variation of normalized (a) W1; and (b) W7 deflections with FWD stations

TTI MODULUS ANALYSIS SYSTEM (SUMMARY REPORT) (Version 7.0)

District:
County :
Highway/Road:

	Thickness(in)	MODULI RANGE(psi) Minimum	Maximum	Poisson Ratio Values
Pavement:	12.06	100,000	1,040,000	H1: v = 0.35
Base:	12.00	10,000	200,000	H2: v = 0.35
Subbase:	0.00			H3: v = 0.00
Subgrade:	109.82(by DB)	10,000		H4: v = 0.40

Station	Load (lbs)	Measured Deflection (mils): W1	W2	W3	W4	W5	W6	W7	Calculated Moduli values (ksi): SURF(E1)	BASE(E2)	SUBB(E3)	SUBG(E4)	Absolute ERR/Sens	Dpth to Bedrock
0.000	8,740	22.33	17.41	10.05	7.52	4.58	3.01	2.25	100.0	10.0	0.0	9.4	6.94	112.0 *
64.000	8,910	17.58	14.08	9.81	8.00	5.15	3.41	2.49	154.5	10.0	0.0	9.3	1.47	124.9 *
110.000	9,010	16.34	13.40	9.07	7.39	4.76	3.26	2.45	169.6	10.2	0.0	10.2	2.84	150.2 *
197.000	8,940	17.88	14.37	9.29	7.27	4.59	3.21	2.47	133.9	10.4	0.0	10.4	4.08	172.0 *
368.000	8,810	21.24	17.20	11.01	8.70	5.31	3.48	2.56	102.2	10.0	0.0	8.6	2.95	118.1 *
725.000	9,160	10.00	8.13	6.05	5.11	3.57	2.48	1.18	331.9	22.5	0.0	12.7	0.84	49.7
820.000	9,060	13.63	11.42	8.10	6.77	4.53	3.11	2.33	238.4	10.9	0.0	10.7	2.06	149.5
917.000	9,130	12.15	10.29	7.49	6.31	4.38	3.06	2.31	292.7	13.0	0.0	10.8	1.86	163.8
1005.000	8,740	13.77	10.76	7.65	6.25	4.06	2.64	2.10	198.8	11.9	0.0	11.9	0.72	110.0 *
Mean:		16.10	13.01	8.72	7.04	4.55	3.07	2.24	191.3	12.1	0.0	10.4	2.64	133.9
Std. Dev:		4.11	3.14	1.53	1.06	0.53	0.33	0.42	81.9	4.0	0.0	1.3	1.94	62.4
Var Coeff(%):		25.51	24.14	17.58	15.11	11.57	10.78	18.81	42.8	33.2	0.0	12.4	73.33	46.6

FibreCrete

HMA

Control

Subgrade Modulus

(a)

TTI MODULUS ANALYSIS SYSTEM (SUMMARY REPORT) (Version 7.0)

District:
County :
Highway/Road:

	Thickness(in)	MODULI RANGE(psi) Minimum	Maximum	Poisson Ratio Values
Pavement:	12.06	100,000	1,040,000	H1: v = 0.35
Base:	12.00	10,000	200,000	H2: v = 0.35
Subbase:	0.00			H3: v = 0.00
Subgrade:	189.82(by DB)	10,000		H4: v = 0.40

Station	Load (lbs)	Measured Deflection (mils): W1	W2	W3	W4	W5	W6	W7	Calculated Moduli values (ksi): SURF(E1)	BASE(E2)	SUBB(E3)	SUBG(E4)	Absolute Dpth to ERR/Sens	Bedrock	
0.000	8,840	19.42	15.52	9.69	7.74	5.14	3.51	2.56	110.4	11.0	0.0	11.0	2.91	140.9	*
64.000	9,010	13.19	10.23	8.86	7.60	5.42	3.83	2.84	325.6	10.5	0.0	10.5	2.61	179.9	*
110.000	8,740	12.07	10.83	8.08	6.95	5.10	3.67	2.88	323.2	10.8	0.0	10.8	1.68	214.5	*
198.000	9,030	12.19	10.46	7.88	6.66	4.67	3.35	2.58	294.9	12.3	0.0	12.3	1.40	213.2	*
369.000	8,910	14.83	12.36	8.88	7.44	5.24	3.67	2.76	211.7	11.1	0.0	11.1	1.40	172.3	*
727.000	8,980	7.34	6.14	4.90	4.35	3.32	2.50	2.23	553.7	39.7	0.0	15.2	0.28	300.0	
821.000	9,110	9.44	8.24	6.58	5.72	4.34	3.27	2.60	502.8	16.4	0.0	12.6	0.81	290.2	
917.000	8,960	8.48	7.60	6.13	5.44	4.13	3.14	2.54	629.5	13.3	0.0	13.1	0.81	300.0	
1006.000	8,740	8.66	7.54	6.07	5.32	3.86	2.82	2.41	510.7	14.0	0.0	14.0	1.32	240.6	*
Mean:		11.74	9.88	7.45	6.36	4.58	3.31	2.60	384.7	15.5	0.0	12.3	1.47	213.9	
Std. Dev:		3.80	2.89	1.60	1.19	0.72	0.43	0.21	172.8	9.3	0.0	1.6	0.85	55.6	
Var Coeff(%):		32.41	29.22	21.50	18.80	15.63	13.09	7.93	44.9	60.2	0.0	13.1	57.75	26.0	

FibreCrete

HMA

Control

Subgrade Modulus

(b)

TTI MODULUS ANALYSIS SYSTEM (SUMMARY REPORT) (Version 7.0)

District:
County :
Highway/Road:

	Thickness(in)	MODULI RANGE(psi) Minimum	Maximum	Poisson Ratio Values
Pavement:	12.06	100,000	1,040,000	H1: v = 0.35
Base:	12.00	10,000	200,000	H2: v = 0.35
Subbase:	0.00			H3: v = 0.00
Subgrade:	128.52(by DB)	10,000		H4: v = 0.40

	Station	Load (lbs)	Measured Deflection (mils): W1	W2	W3	W4	W5	W6	W7	Calculated Moduli values (ksi): SURF(E1)	BASE(E2)	SUBB(E3)	SUBG(E4)	Absolute ERR/Sens	Dpth to Bedrock	
FibreCrete	1.000	8,840	26.14	21.09	12.23	9.36	5.83	3.93	2.88	100.0	10.0	0.0	7.5	10.41	129.9	*
	64.000	8,910	23.45	19.69	15.01	12.52	8.35	5.44	3.81	126.6	10.0	0.0	5.6	3.97	124.0	*
	110.000	8,810	24.88	20.12	13.06	10.43	6.76	4.54	3.31	100.0	10.0	0.0	6.9	4.20	134.7	*
HMA	199.000	9,060	17.31	14.73	11.11	9.26	6.23	4.30	3.26	194.2	10.0	0.0	7.9	2.31	169.2	*
	369.000	8,840	25.51	21.12	14.64	11.90	7.63	5.01	3.56	100.0	10.0	0.0	6.0	4.35	124.8	*
	727.000	9,060	11.48	9.66	7.66	6.65	4.83	3.49	2.75	376.7	14.0	0.0	9.9	0.31	227.6	
Control	820.000	9,010	15.98	13.47	10.56	8.92	6.37	4.40	3.62	240.7	10.0	0.0	7.7	0.90	163.7	*
	917.000	8,910	12.78	11.12	9.01	7.97	5.80	4.13	3.72	372.8	10.0	0.0	8.1	1.16	212.9	*
	1011.000	9,040	14.17	12.15	9.70	8.29	5.77	3.93	2.90	282.1	10.0	0.0	8.5	2.16	149.9	*
	Mean:		19.08	15.91	11.44	9.48	6.40	4.35	3.31	210.3	10.4	0.0	7.6	3.31	152.6	
	Std. Dev:		5.90	4.60	2.51	1.87	1.06	0.59	0.39	114.0	1.3	0.0	1.3	3.05	30.3	
	Var Coeff(%):		30.91	28.94	21.92	19.77	16.60	13.61	11.91	54.2	12.9	0.0	17.2	92.28	19.8	

Subgrade Modulus

(c)

Figure 3.8 Back-calculated moduli: (a) Evaluation #1; (b) Evaluation #2; and (c) Evaluation #3

3.4 Face Dipstick Measurement

Table 3.1 presents the Face Dipstick results for Evaluations #2 and #3. After two evaluations, Fibrecrete-repaired sections were found to perform better in rutting as compared to the HMA-and control sections. As presented in Table 3.1, the average rut depths for the Fibrecrete-repaired sections were found as 5.78-mm (0.23-in.) and 9.90-mm (0.39-in.) after Evaluations #2 and #3, respectively. For the HMA-repaired sections, the rut depths were found as 7.86-mm (0.31-in.) and 10.23-mm (0.4-in.) after Evaluations #2 and #3, respectively. The control sections exhibited the highest rut depths during Evaluations #2 and #3 with 19.97-mm (0.79-in.) and 20.35-mm (0.80-in.) rutting, respectively. However, the changes in the rut depths at the Fibrecrete-repaired sections from Evaluation #2 and Evaluation #3 were higher compared to the HMA- and control sections. This is primarily caused by the lower stiffness of the Fibrecrete materials. Also, the rut depths at all three Fibrecrete-repaired sections were more consistent as compared to the HMA- and non-repaired sections, as evident from Table 3.1. In terms of IRI, the HMA-repaired sections performed better as compared to the Fibrecrete-repaired and control sections. For example, during Evaluation #3, the average IRI for the HMA-repaired sections was observed to be 233 in./mile, whereas for the Fibrecrete-repaired and control sections the IRI values were 327 in./mile and 499 in./mile, respectively. Additional Face Dipstick measurements results can be found in Appendix C.

3.5 Straightedge Measurement

Figures 3.9, 3.10 and 3.11 show the transverse and longitudinal (right and left wheel paths) profiles of Crack #7 (Fibrecrete-repaired), #18 (HMA-repaired) and #32 (control), respectively. The profiles of all the cracks can be found in Appendix D. By comparing the straightedge measurements of different sections, it was found that the Fibrecrete-repaired sections performed well as compared to the HMA-repaired and control sections. Deflections or depressions in both transverse and longitudinal directions were found to decrease after repairing with Fibrecrete, as evident in Figures 3.9 (a), (b) and (c). However, as shown in Figure 3.10 (a), with time, the surface deflections in the transvers direction increased for the HMA-repaired section. Also, deflections for the control sections were not found to change significantly after 11-months of repair, as shown in Figure 3.11.

Table 3.1 Summary of Face Dipstick measurements

ID	Latitude	Longitude	P1 Offset (0.10 mi.)	P2 Offset (Ft.)	E2 Avg. Rut (mm)	E3 Avg. Rut (mm)	E2 Avg. IRI (in./mi.)	E3 Avg. IRI (in./mi.)	E2 Avg. Rut (mm)	E3 Avg. Rut (mm)	E2 Avg. IRI (in./mi.)	E3 Avg. IRI (in./mi.)
Begin P1	36.622456	-99.828987	0		**Avg. Each Location**				**Avg. Each Set**			
Begin P2	36.622448	-99.827812		0								
5	36.622453	-99.832261	0.182	1303	5.97	9.27	451	483	5.78	9.90	266	327
7	36.622464	-99.832294	0.183	1312	6.05	10.14	151	221				
9	36.622475	-99.832628	0.202	1410	5.31	10.29	197	278				
12	36.622442	-99.832928	0.219	1498	7.18	9.7	173	194	7.86	10.23	228	233
18	36.622469	-99.833492	0.25	1663	11	13.67	291	337				
27	36.62245	-99.834711	0.317	2020	5.39	7.31	220	167				
29	36.62245	-99.835047	0.336	2118	20.73	22.17	399	461	19.97	20.35	456	499
30	36.622444	-99.835356	0.353	2209	19.25	20.78	454	528				
32	36.622456	-99.835661	0.37	2298	19.94	18.1	516	507				
End P2	36.62241	-99.840904		3833								
End P1	36.62241	-99.840904	0.661									

Note: P1 and P2 represent Phase 1 (2160-18-06) Phase 2 (2160-20-02), respectively.

E2 and E3 represents Evaluation #2 and Evaluation #3, respectively.

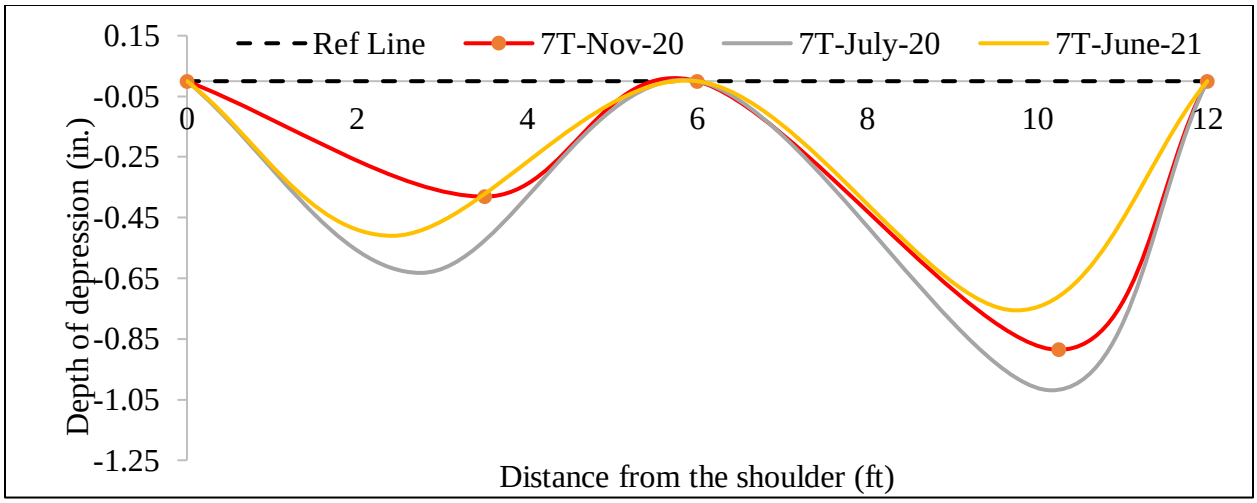

(a)

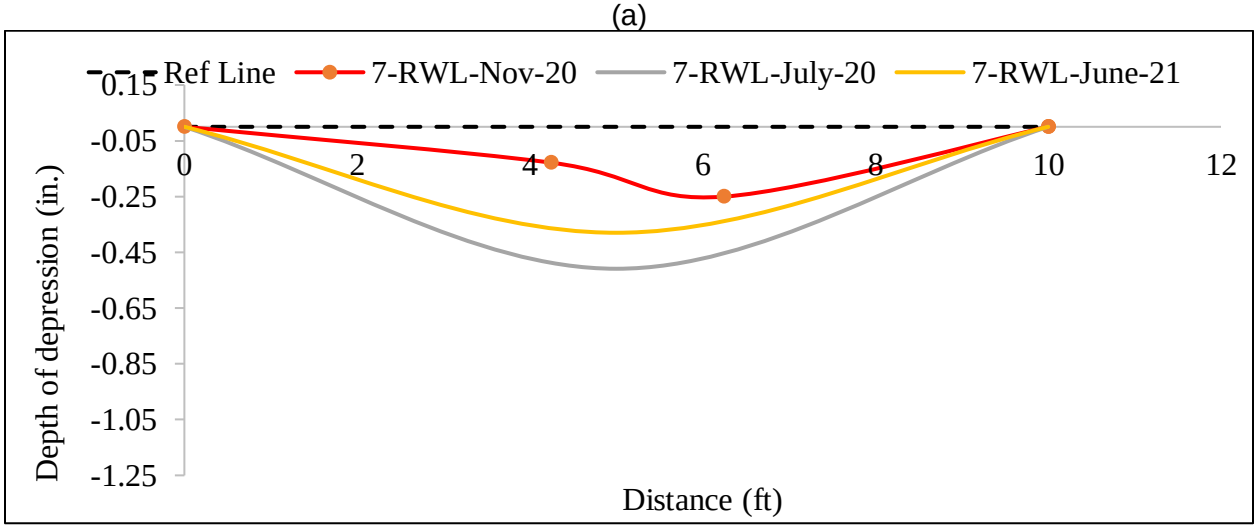

(b)

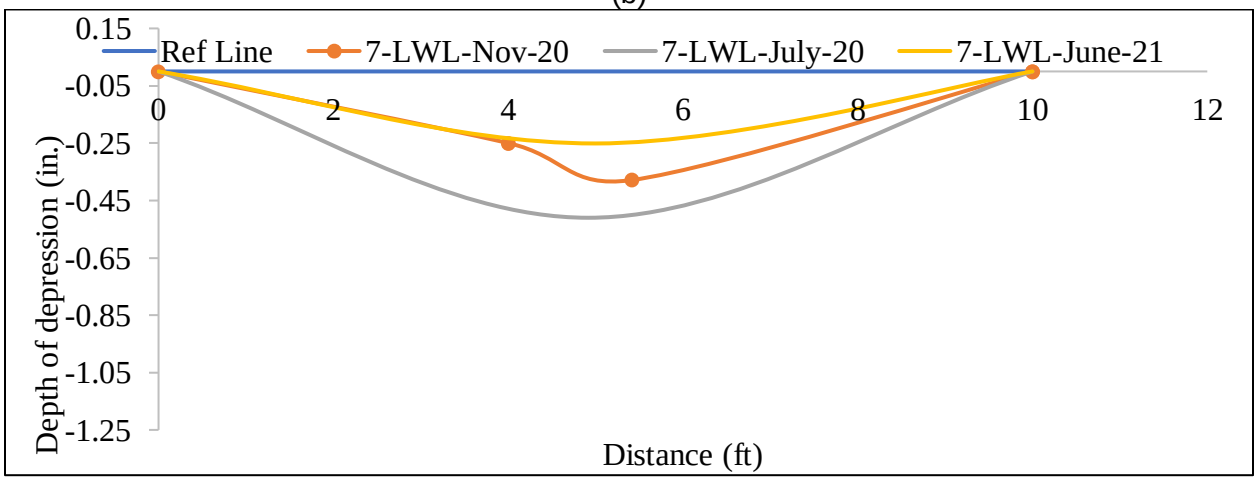

(c)

Figure 3.9 Straightedge measurements at Crack #7: (a) transverse profile; (b) longitudinal profile along right wheel-path; and (c) longitudinal profile along left wheel-path

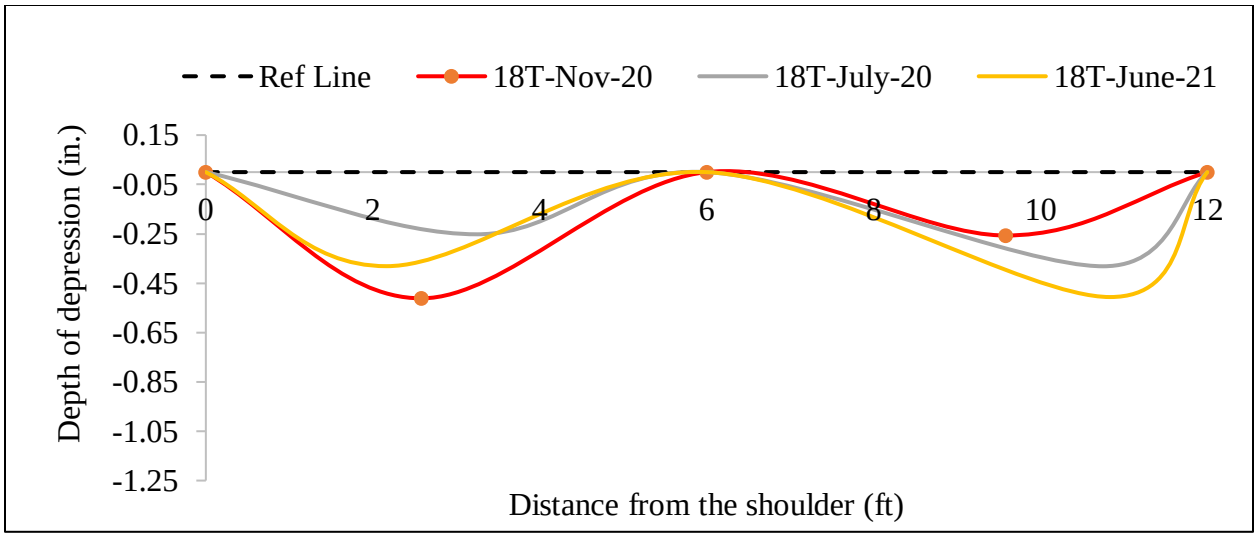

(a)

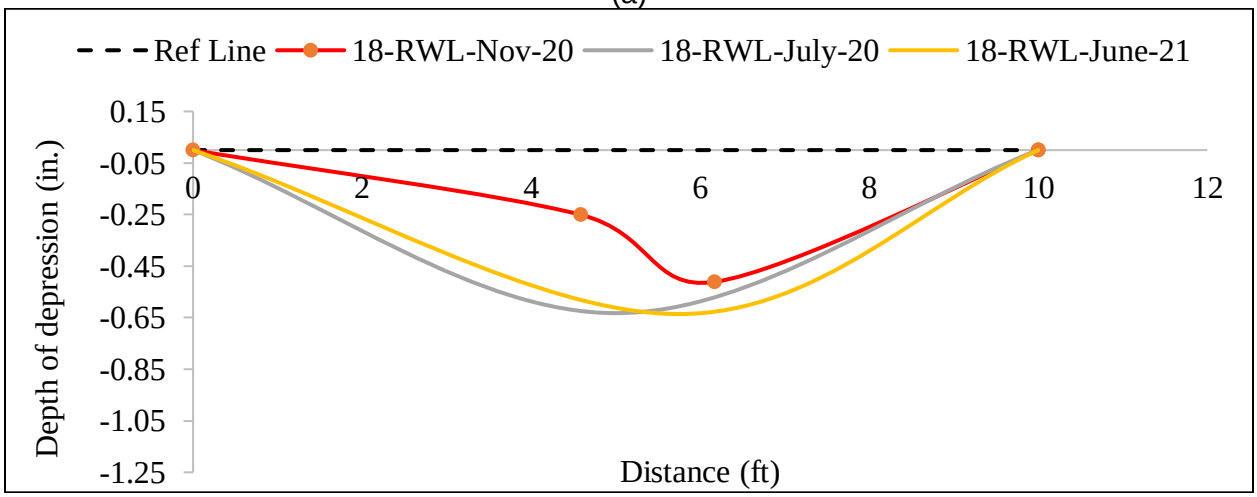

(b)

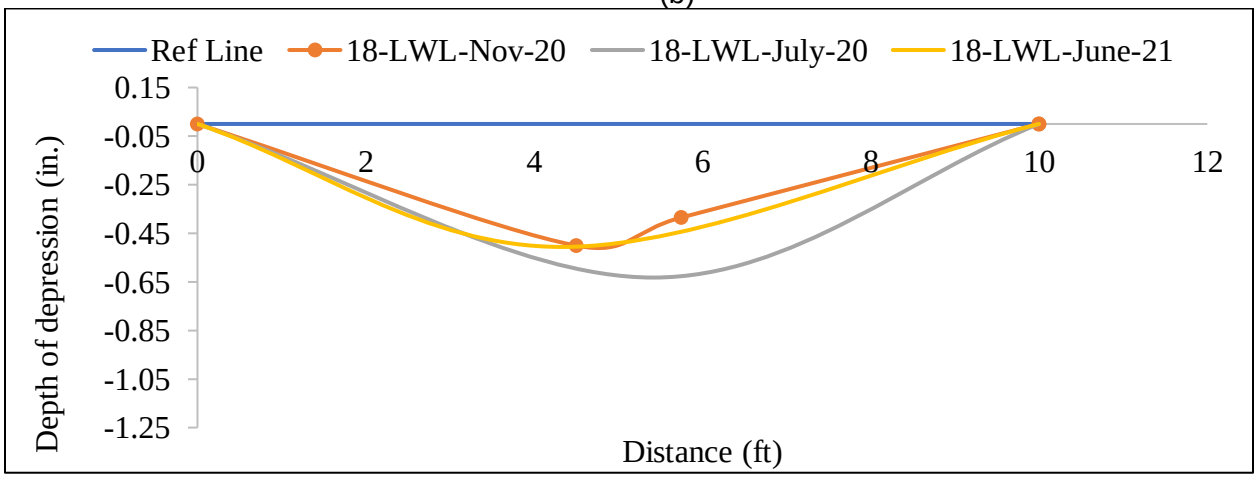

(c)

Figure 3.10 Straightedge results at Crack #18: (a) transverse profile; (b) longitudinal profile along right wheel-path; and (c) longitudinal profile along left wheel-path

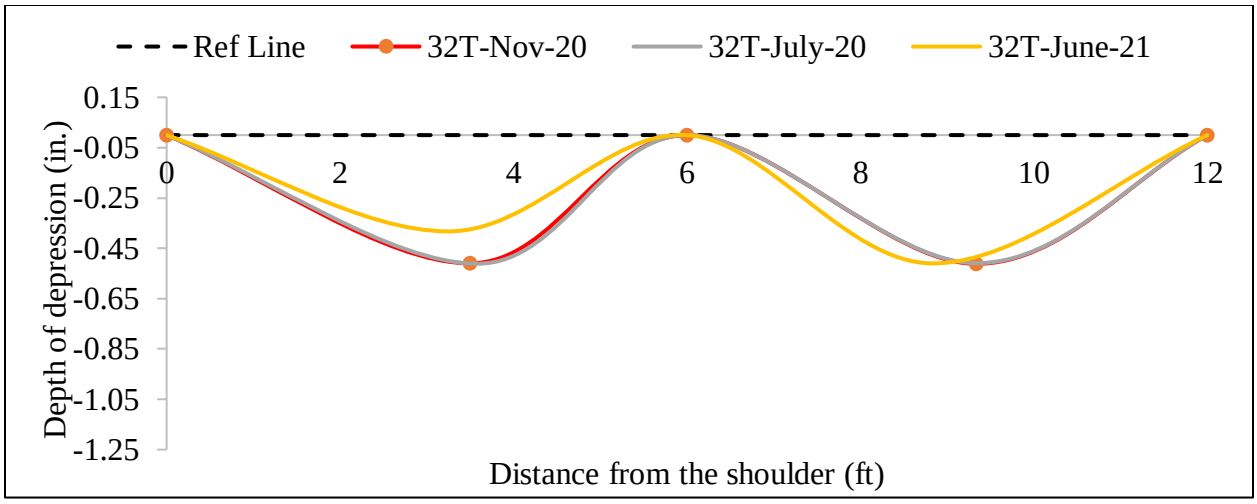

(a)

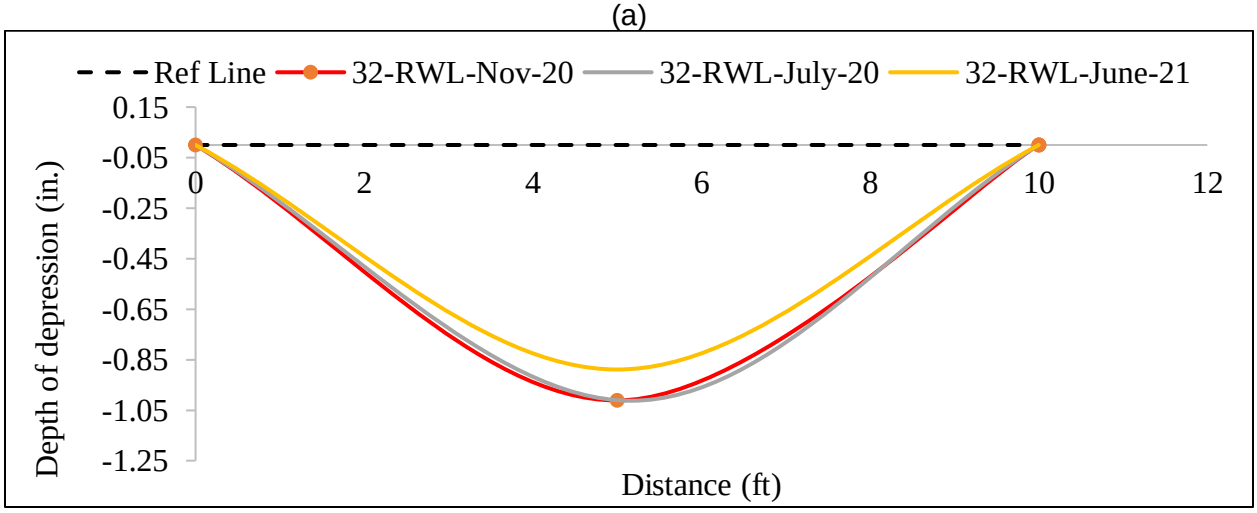

(b)

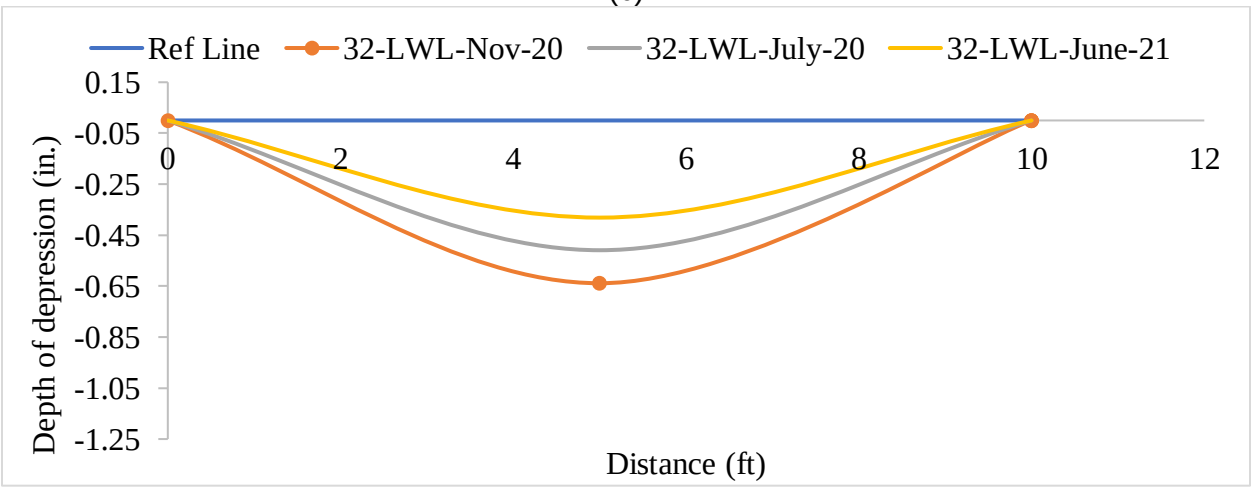

(c)

Figure 3.11 Straightedge results at Section #32: (a) transverse profile; (b) longitudinal profile along right wheel path; and (c) longitudinal profile along left wheel path

3.6 PaveVision3D and Pave3D 8K Survey

Table 3.2 shows a summary of the Evaluations #1 and #2 performed using the PaveVision3D and Pave 3D 8K, respectively. From Table 3.2, Evaluation #2 was found to exhibit higher rut depths and IRI for all the sections than Evaluation #1. The increase in the rut depths and IRI of the repaired sections may have resulted from the initial consolidation of the Fibrecrete and HMA due to traffic. Also, the Fibercrete-repaired sections were found to exhibit higher rut depths (6.96-mm or 0.27 in.) as compared to the HMA-repaired (3.7-mm or 0.15-in.) and control sections (3.34-mm or 0.13 in.). These results indicated that the Fibercrete is relatively flexible and less stiff than the HMA and expected to perform better in resisting cracking. Based on the IRI values from Evaluation #2, the Fibercrete-repaired sections were found to perform similar to the HMA-repaired and control sections, as evident from Table 3.2. The average IRI of the Fibercrete-repaired, HMA-repaired and control sections during Evaluation #2 were found as 185-in/mile, 186-in/mile and 187-in/mile, respectively. Additional results from the PaveVision3D and Pave 3D 8K can be found in Appendix E.

Table 3.2 Summary of PaveVision3D and Pave 3D 8K analysis

ID	Latitude	Longitude	P1 Offset (0.1 mile)	P2 Offset (ft)	P1 Avg. Rut (mm)	P2 Avg. Rut (mm)	P1 Avg. IRI (in/mile)	P2 Avg. IRI (in/mile)	P1 Avg. Rut (mm)	P2 Avg. Rut (mm)	P1 Avg. IRI (in/mile)	P2 Avg. IRI (in/mile)
Begin P1	36.622456	-99.828987	0	0	Avg. Each Location				Avg. Each Set			
Begin P2	36.622448	-99.827812										
5	36.622448	-99.832261	0.182	1303	2.13	6.57	169	185	2.2	6.96	170	185
7	36.622464	-99.832294	0.183	1312	1.19	6.07	170	185				
9	36.622475	-99.832628	0.202	1410	2.56	8.23	172	185				
12	36.622442	-99.832928	0.219	1498	2.46	3.52	178	186	1.92	3.7	179	186
18	36.622469	-99.833492	0.25	1663	1.95	4.51	189	185				
27	36.62245	-99.834711	0.317	202	1.36	3.08	170	188				
29	36.62245	-99.835047	0.336	2118	1.22	2.86	190	204	1.68	3.34	178	187
30	36.622444	-99.835356	0.353	2209	1.7	3.34	173	187				
32	36.622456	-99.835661	0.37	2298	2.11	3.83	171	170				
End P2	36.62241	-99.840904		3833								
End P1	36.62241	-99.840904	0.661									

Note: P1 represents Phase 1 (2160-18-07) Evaluation #1

P2 represents Phase 2 (2160-20-02) Evaluation #2

4. REHABILITATION OPTIONS AND COST ANALYSIS

Based on the results obtained from the field tests from the three evaluations presented in the preceding sections and findings from ODOT Task Order 2160-18-07, the following repair options were evaluated for the rehabilitation of the test section in US-270 (see Table 4.1). Of these options, Option 2 was used on US-270 for repairing transverse cracks.

Table 4.1 Cost analysis of rehabilitation options

Option	Pay Item	Units	Cost/Unit	No. Units	Cost	Total Cost	Expected Life (Years)
1	Crack Sealing Asphalt Pavement	LF	$0.75	6547	$4,910.25	$100,220.40	6
	2-in. S4 (PG 70-28 OK)	Ton	$103.61	920	$95,310.15		
2	Crack Sealing Asphalt Pavement	LF	$0.75	6547	$4,910.25	$211,877.05	10
	2-in. S4 (PG 70-28 OK)	Ton	$103.61	920	$95,310.15		
	3-in. S3 (PG 70-28 OK)	Ton	$80.92	1380	$111,656.65		
3	Crack Sealing Asphalt Pavement	LF	$0.75	5632	$4,224.00	$117,142.23	11
	Fibrecrete	CF	$66.54	252	$16,768.08		
	Cold Milling Pavement	SY	$20.00	42	$840.00		
	2-in. S4 (PG 70-28 OK)	Ton	$103.61	920	$95,310.15		
4	Crack Sealing Asphalt Pavement	LF	$0.75	5280	$3,960.00	$129,175.93	12
	Fibrecrete	CF	$66.54	428	$28,479.12		
	Cold Milling Pavement	SY	$20.00	71	$1,426.67		
	2-in. S4 (PG 70-28 OK)	Ton	$103.61	920	$95,310.15		

To quantify the cost-benefit of each rehabilitation option, a life cycle analysis (LCCA) was performed using the procedures suggested by the Federal Highway Administration. The LCCA analysis involved the following steps [7-8]:

i. Establish design alternatives [and AP]
ii. Determine [performance period and] activity timing
iii. Estimate costs [agency and user]
iv. Compute [net present value] life cycle costs
v. Analyze results
vi. Reevaluate design strategies

Equivalent Uniform Annual Cost (EUAC) is widely used in LCCA analysis for transportation decision making when service lives differ in length for given alternatives [7]. In this method, all incurred costs expected throughout the service life of an alternative are brought to a base year, summed, and then annualized according to the treatment's service life, as determined by field data and pavement manager's professional judgment. The following equation is used to estimate EUAC:

$$EUAC\ (i\%) = [\Sigma P] * [i(1+i)^n \div (1+i)^n - 1)] \qquad (1)$$

where:

i = discount rate (in this case, 4% as suggested in the literature for highway projects);

P = present value; and

n = pavement treatment anticipated service life.

Based on this analysis, the *per-lane-mile* costs for the four rehabilitation options for US-270 are given in Table 4.2. This is a simplistic evaluation intended to highlight the relative differences between options. Present value after 1st rehabilitation (PV2) is calculated at a discount rate of 4% from the total cost of 2nd rehabilitation (FV) at n years. EUAC is calculated from the sum of present value at year zero (PV1) and the present value after 1st rehabilitation (PV2). User costs were not considered in this analysis. Based upon the input data (treatment type, expected service life and total initial cost), options 3 and 4 yield similar (lower) EUACs than the 1st and 2nd options. The FHWA suggests that a sensitivity analysis be included in LCCA (Step 5 – Analyze Results) to provide a greater insight about the uncertainty that exists within the analyses – specifically: how different assumptions may result in different output (rankings). If the Option 1 scenario shown in the preceding table could be expected to yield one more additional year of service life (7-year life), it would then yield a comparable EUAC of $13,023. At the given cost, the service life of Option 2 would need to be at least 25 years to yield an EUAC of $13,563. The sensitivity analysis provides the evaluator with an indication about how sensitive the output is to the selected service life to inform decision making. The LCCA results should also be placed into context, then reevaluated in accordance with FHWA "good practices" (Step 6). LCCA results should be coupled with other decision-support factors such as "risk, available budgets, and political and environmental concerns" [7]. The output from an LCCA should not be considered as the answer, but merely an indication of the cost effectiveness of alternatives [7].

Table 4.2 Summary of rehabilitation options

ID	Repair	Cost	Life	LCCA (EUAC)
1	Crack Seal, Overlay 2" S4(PG 70-28 OK)	$100,220.40	6	$19,118
2	Crack Seal, Overlays: 2" S4(PG 70-28 OK) and 3" S3(PG 70-28 OK)	$211,877.05	10	$26,123
3	Crack Seal, Mill Most Cracks, Fibrecrete, Overlay 2" S4(PG 70-28 OK)	$117,142.23	11	$13,372
4	Crack Seal, Mill All Cracks, Fibrecrete, Overlay 2" S4(PG 70-28 OK)	$129,175.93	12	$13,764

5. CONCLUSIONS AND RECOMMENDATIONS

The aim of this Task Order was to evaluate the effectiveness of two repair methods, namely (1) trenching and patching using Fibrecrete and (2) trenching and patching using HMA for transverse cracks observed in US-270. Performance of these repair methods was investigated periodically using physical inspection, FWD, GPR, Face Dipstick, Straightedge and PaveVision3D/Pave 3D 8K testing. An evaluation of the “do no repair or do nothing” scenario was considered to help document the improvement of the proposed repair methods. The specific findings of this Task Order are:

i. The physical inspection and GPR results indicated that the propagation of the underlying cracks was fully suppressed by the use of the Fibrecrete layer.

ii. Repair with coarse HMA with no tack coat may not produce satisfactory results. Typically, the rate of the propagation of reflective cracking in HMA layer is 1-in. per year. However, for the studied sections, reflective cracks were found to propagate 2-in. in one year through the HMA layer. The use of coarse (S3) HMA may be responsible for this faster propagation of cracks. Additional cracking may have occurred due to no tack coat.

iii. From Face Dipstick and PaveVision3D/Pave 3D 8K evaluations, both HMA and Fibrecrete were found to exhibit increase in rut depths after repair. This was due to the initial compaction of the HMA and Fibrecrete which happens in the early stage of opening to traffic. However, the IRI of the Fibrecrete- and HMA-repaired sections were found to be comparable.

iv. No significant changes in the crack geometry were observed for the controlled cracks over the observation period (1 year). However, cracks may widen and more rutting may occur over time if no-repair activity is pursued.

v. The LCCA/EUAC shows that the Fibrecrete repair options 3 & 4 were most economical. Option 1 and Option 2 compares if:
   - Option 1 lasts an extra year (from 6 to 7) – note short life of HMA repair
   - Option 2 lasts 25 years (not 10) – not feasible for comparative performance

Based on the LCCA results and the results from the three evaluations, Fibrecrete repair methods are recommended when pavement performance degrades due to similar transverse cracking and rutting. Also, sealing cracks is recommended, as with any standard maintenance practice. Please note that, Option 2 was adopted by District 6 for repairing transverse cracks in the investigated area on June 2021 (Contract ID 210108, NHPP-017N(266)PM 31065(04)).

In addition to the repair options mentioned in the Task Order, other options may be pursued to repair transverse cracks in US-270. Balanced Mix Design (BMD) combined with a chemical Warm Mix Asphalt (WMA) technology may be able to prevent cracking and extend pavement life. An additional benefit of WMA is that by keeping asphalt production temperatures lower, overlaying newly filled cracks will likely not cause a bump at those locations. Also, ODOT has had success mitigating reflective cracking using high polymer mixes like those used for the 2012 NCAT Test Track section N8. In addition, other available commercial materials can be pursued to resolve the problem of transverse cracks in US-270. However, it is recommended to conduct a performance verification and economic feasibility study before pursuing a new material.

REFERENCES

[1] Adlinge, S. S., and Gupta, A. K. (2013). “Pavement Deterioration and Its Causes”. International Journal of Innovative Research and Development, 2(4), pp. 437-450.

[2] Rada, G. R. (2013). “Guide for Conducting Forensic Investigations of Highway Pavements (with supplemental material on CD-ROM) (Vol. 747).” Transportation Research Board.

[3] West, R., Rodezno, C., Leiva, F., and Yin, F. (2018). Development of a Framework for Balanced Mix Design. NCHRP Project 20-07/Task 406, National Center for Asphalt Technology, Auburn University.

[4] Hafez, M., Ksaibati, K., & Atadero, R. (2019). Developing a methodology to evaluate the effectiveness of pavement treatments applied to low-volume paved roads. *International Journal of Pavement Engineering*, *20*(8), 894-904.

[5] Donmyer, T. Polymer Concrete Patching Materials. Louisiana Department of Transportation and Development.

[6] FPTInfrastructure. Website: Fibrecrete hot-appied flexible concrete repairs (fptinfrastructure.com), last access:8/20/2021.

[7] FHWA (2002)." Life-Cycle Cost Analysis Primer". Federal Highway Administration.

[8] Sinha, K. C., & Labi, S. (2011). "*Transportation decision making: Principles of project evaluation and programming"*. John Wiley & Sons.

APPENDIX A: REPAIR ACTIVITIES

Figure A.1 Repair Activities of Crack #5

Figure A.2 Repair Activities of Crack #7

Figure A.3 Repair Activities of Crack #9

Figure A.4 Repair Activities of Crack #12

Figure A.5 Repair Activities of Section #18

Figure A.6 Repair Activities of Crack #27

APPENDIX B: GROUND PENETRATING RADAR

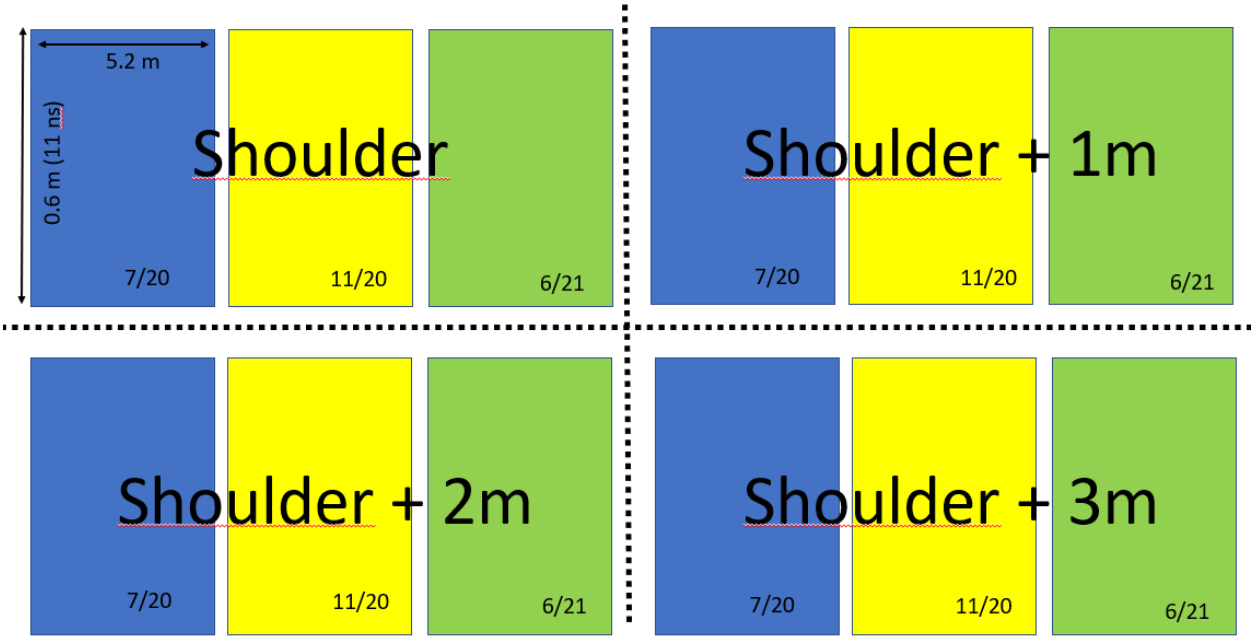

Figure B.1 Layout of Longitudinal Profiles

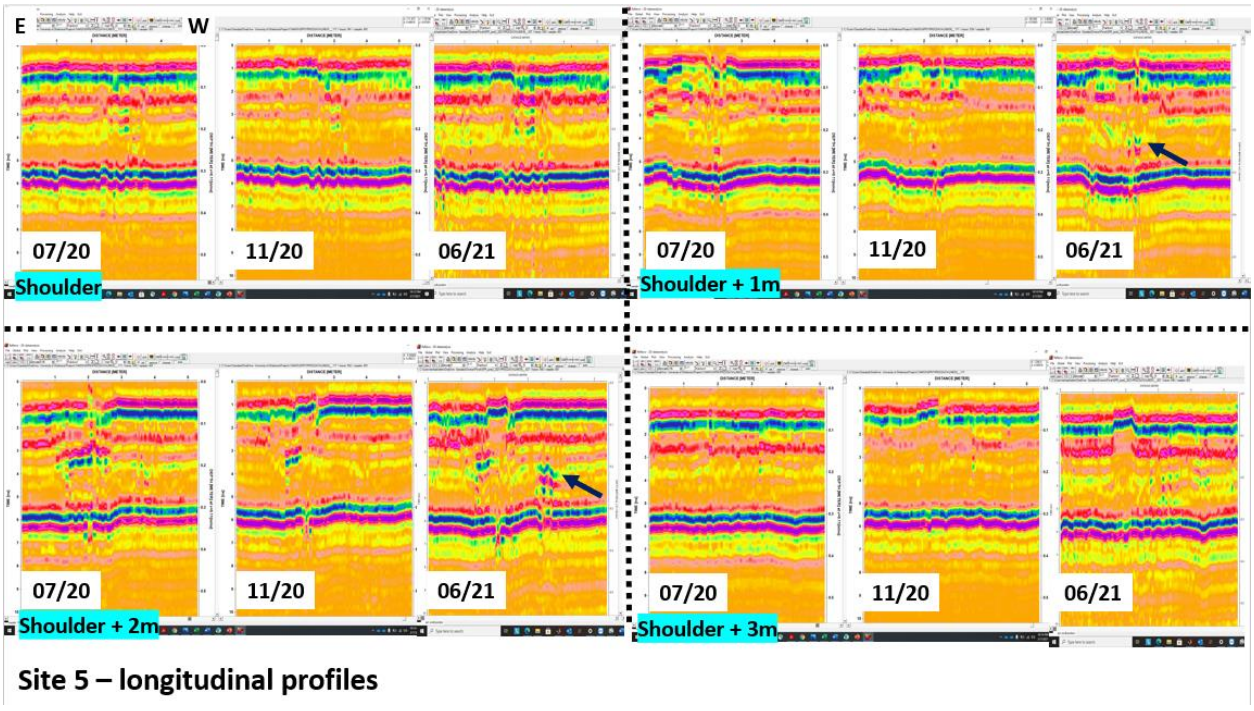

Figure B.2 Longitudinal Profiles of Crack #5

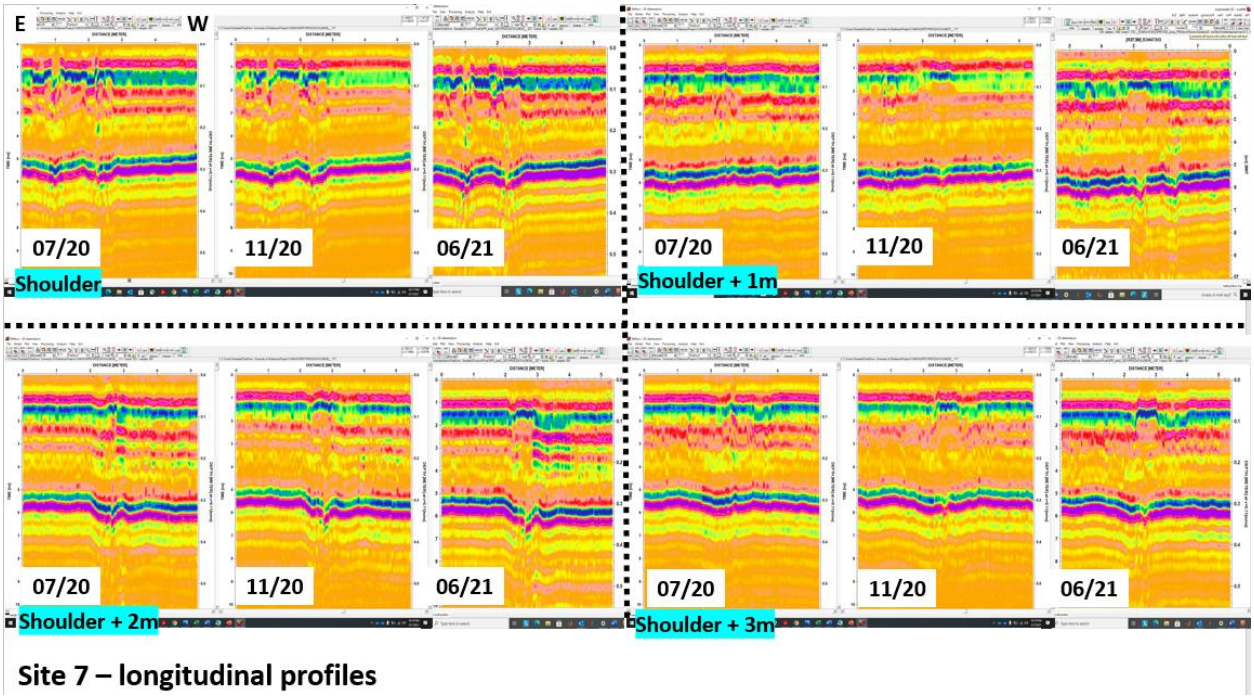

Figure B.3 Longitudinal Profiles of Crack #7

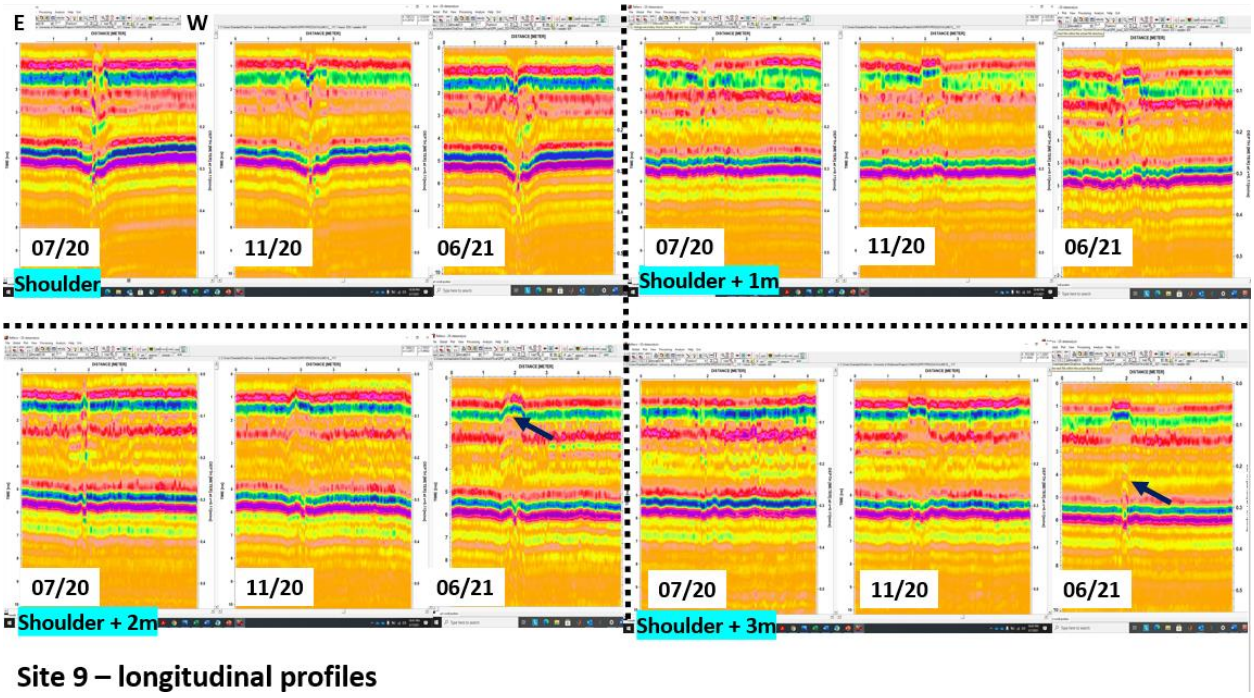

Figure B.4 Longitudinal Profiles of Crack #9

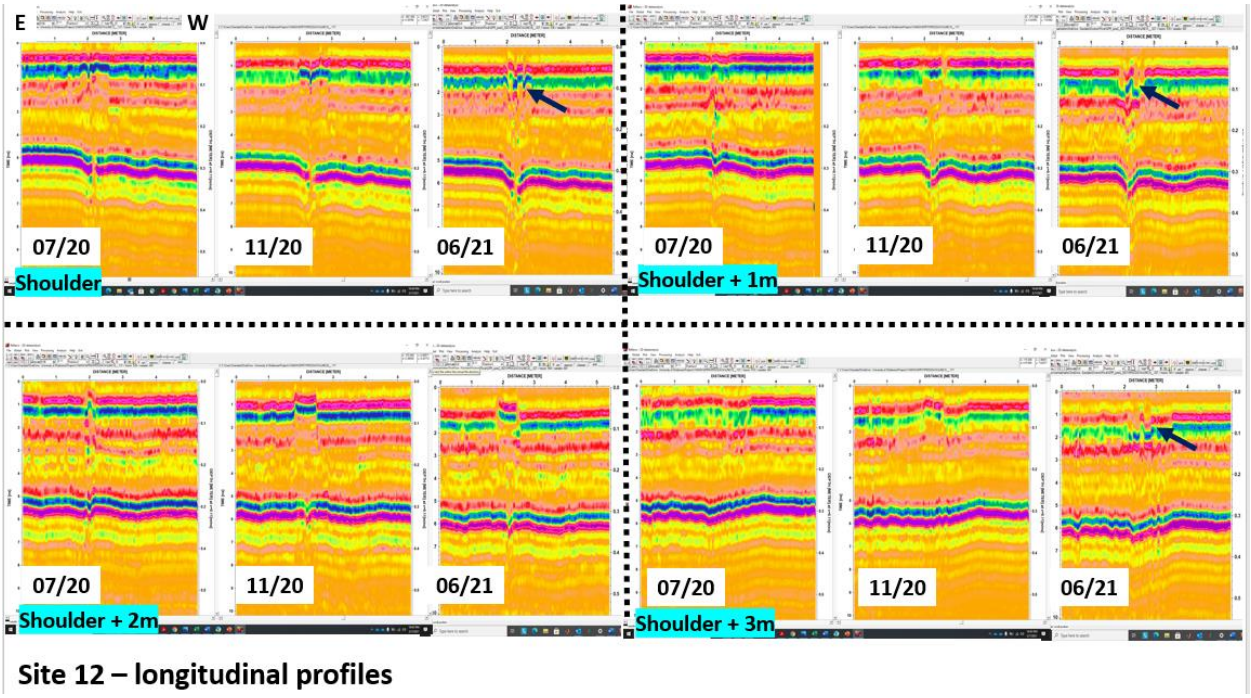

Figure B.5 Longitudinal Profiles of Crack #12

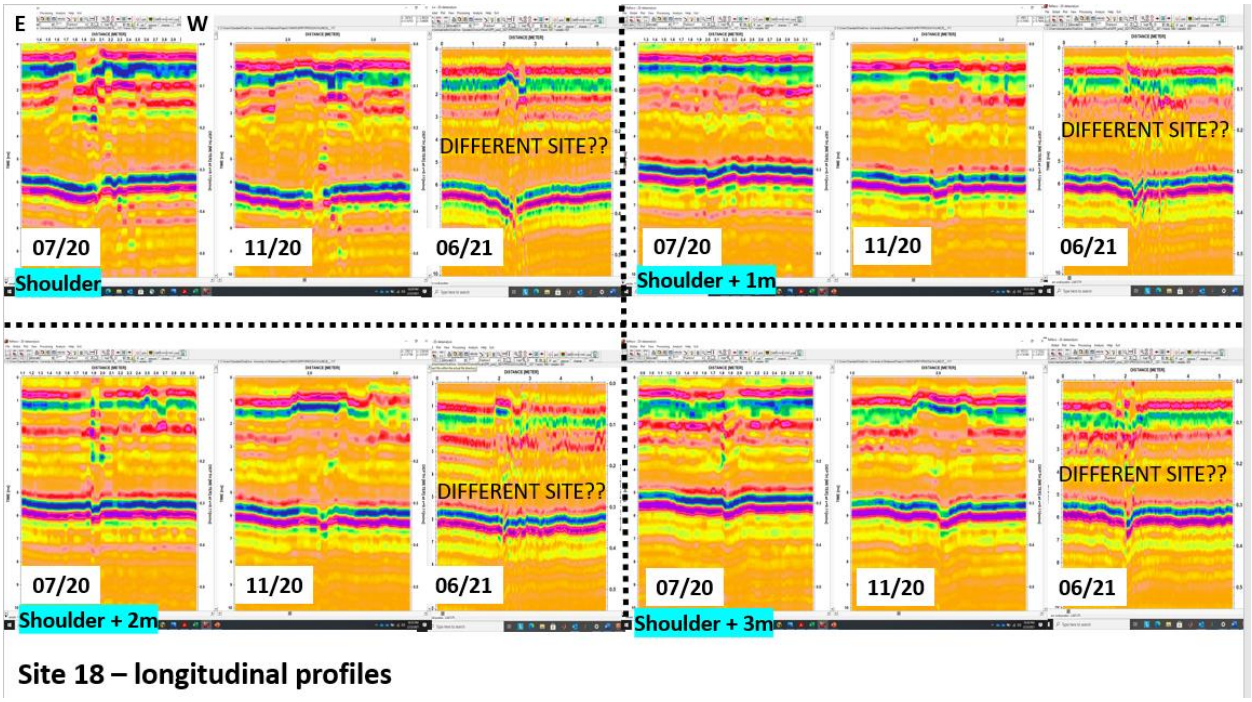

Figure B.6 Longitudinal Profiles of Crack #18

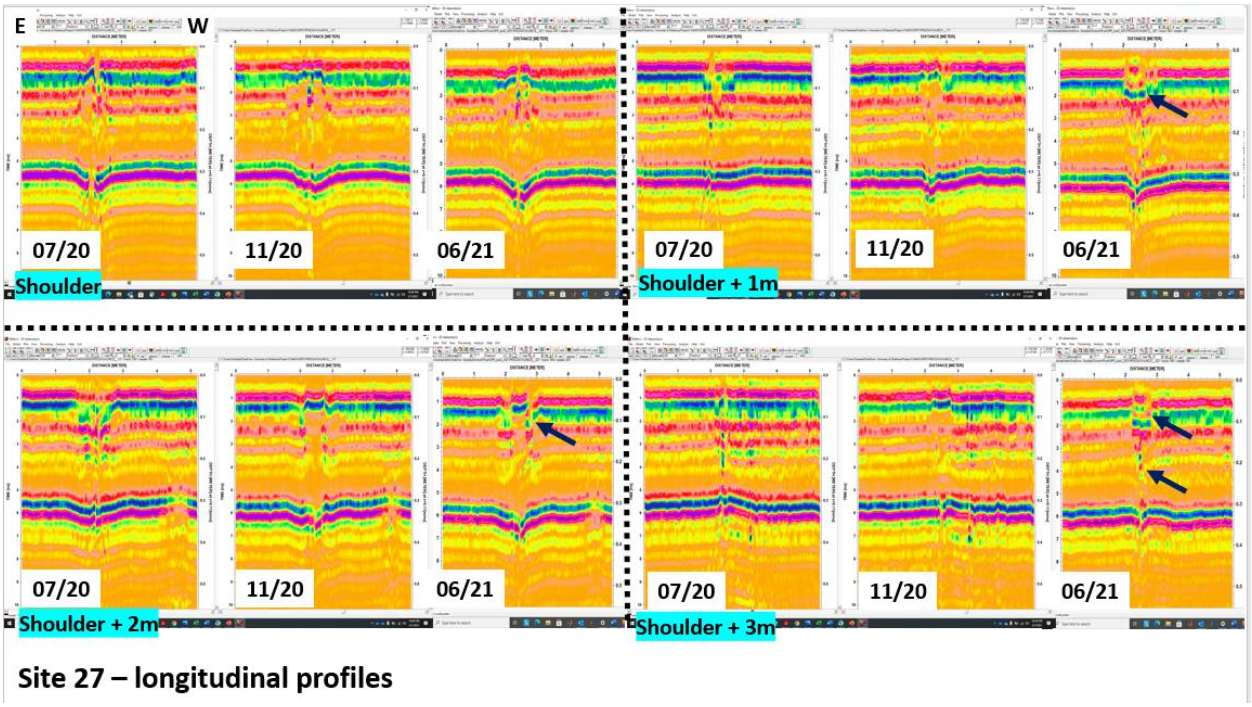

Figure B.7 Longitudinal Profiles of Crack #27

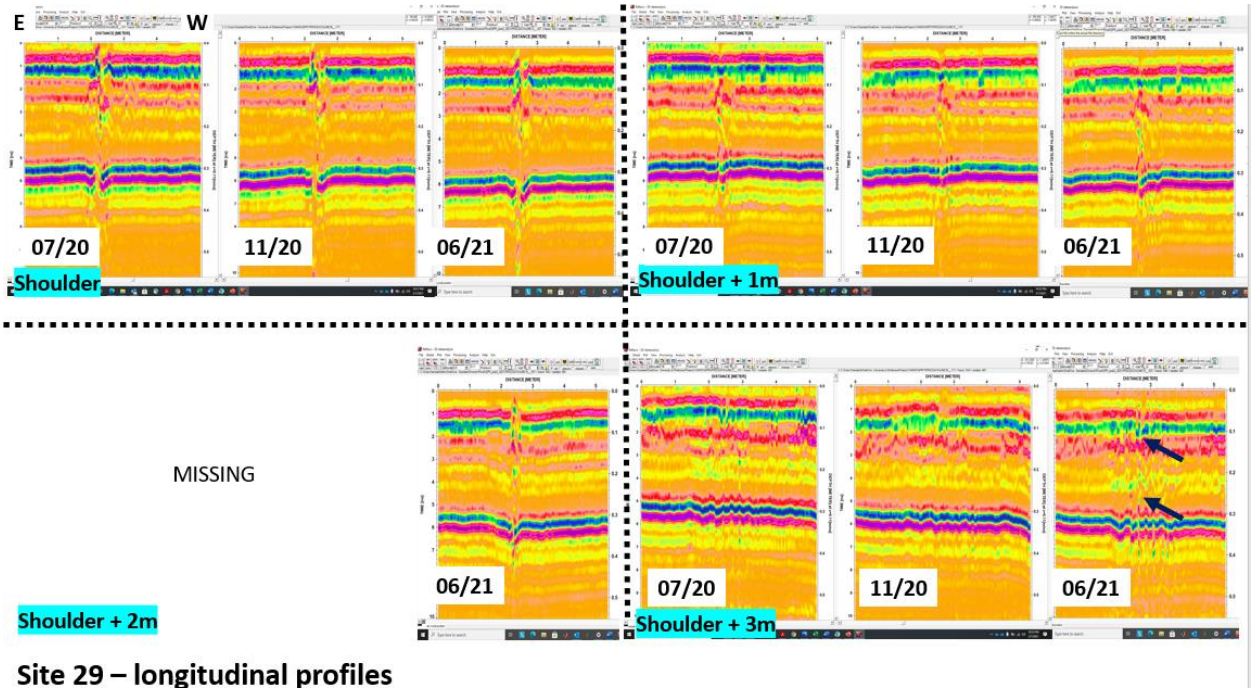

Figure B.8 Longitudinal Profiles of Crack #29

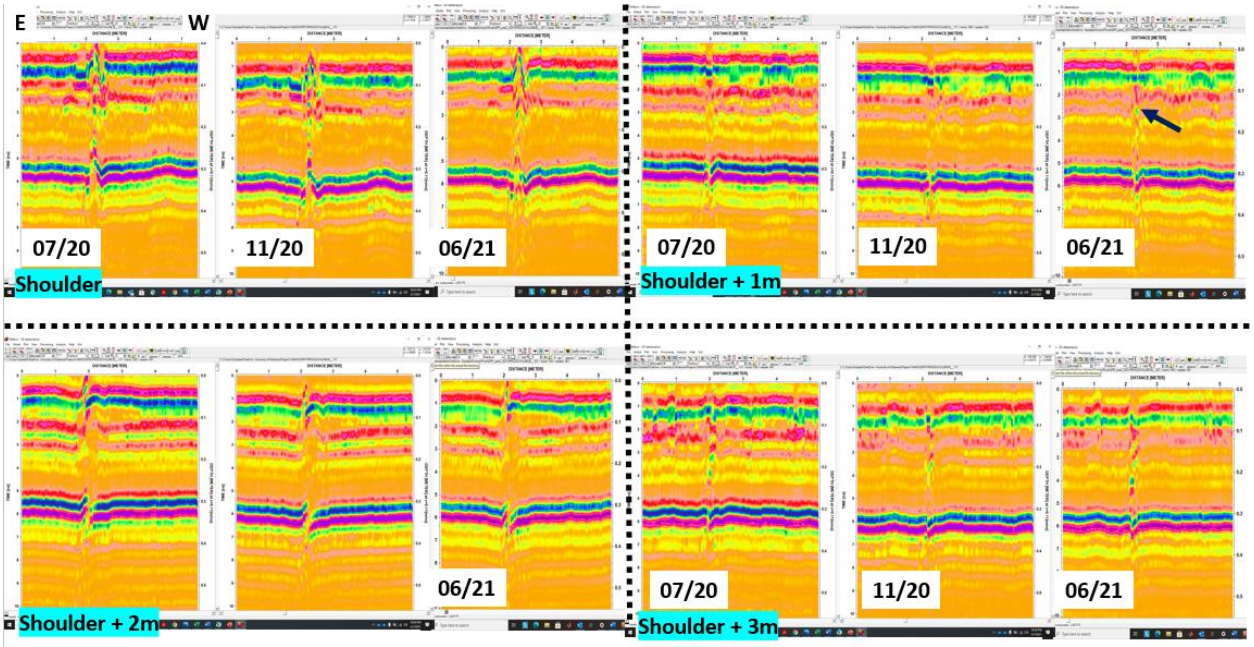

Figure B.9 Longitudinal Profiles of Crack #30

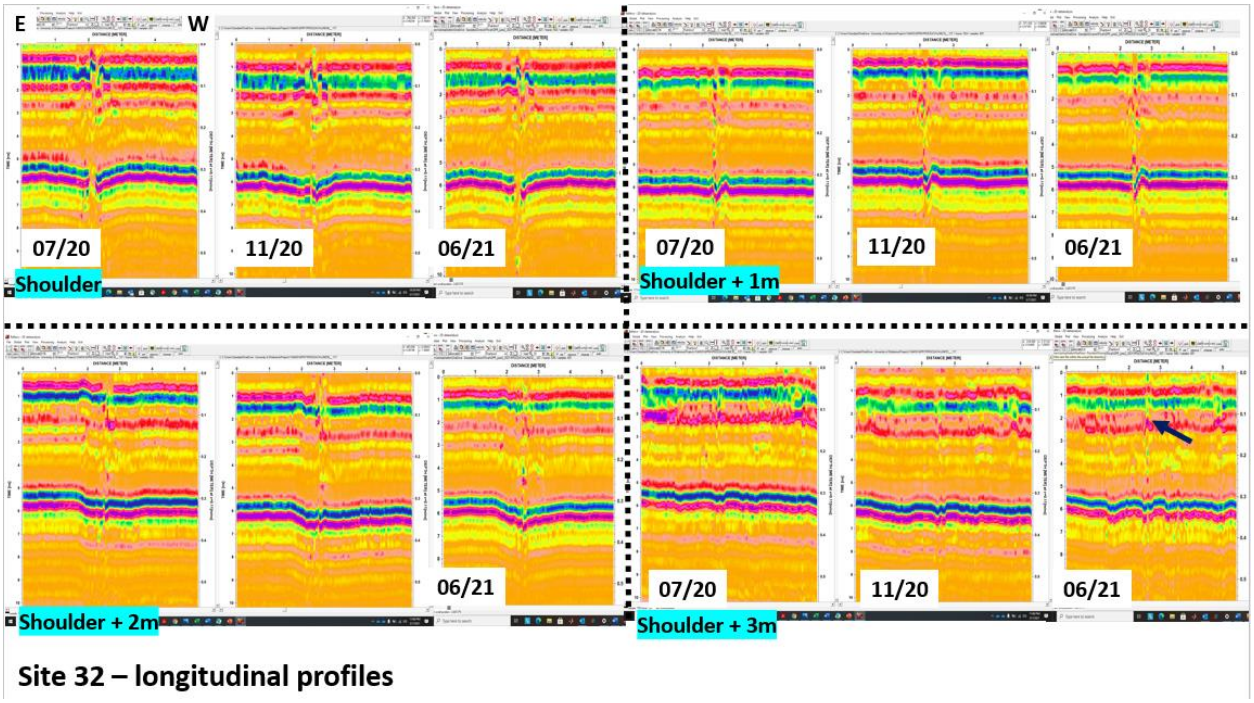

Figure B.10 Longitudinal Profiles of Section #32

APPENDIX C: FACE DIPSTICK

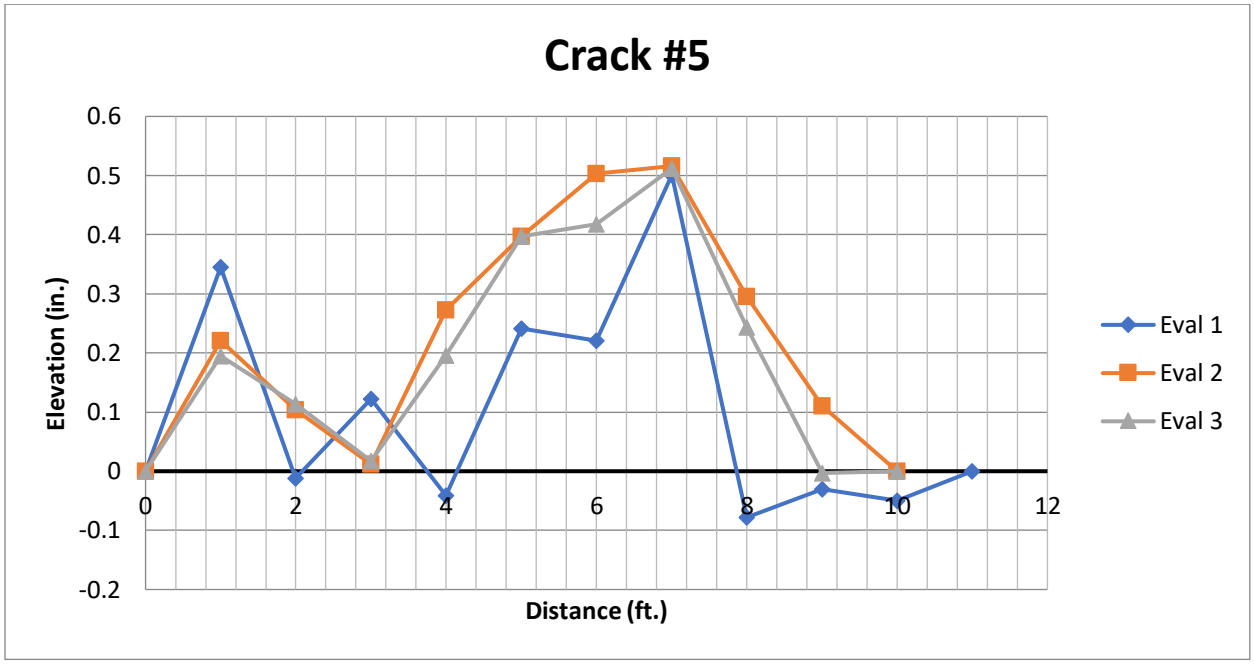

Figure C.1 Transverse Profile of Crack #5

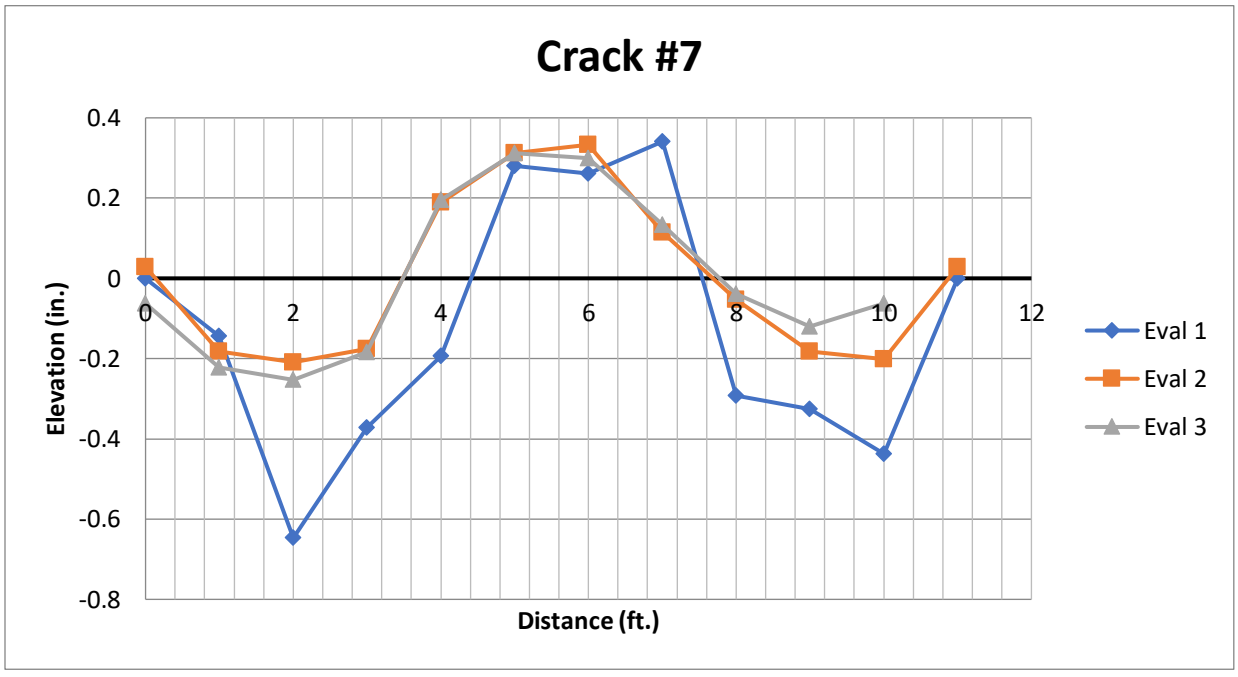

Figure C.2 Transverse Profile of Crack #7

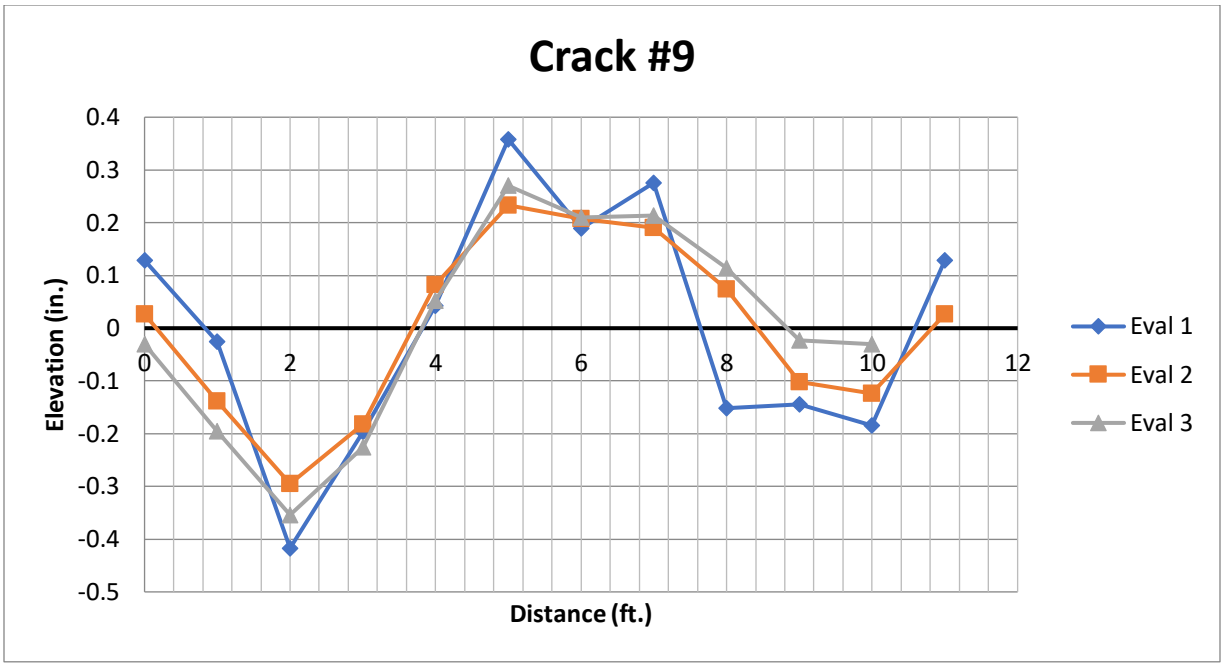

Figure C.3 Transverse Profile of Crack #9

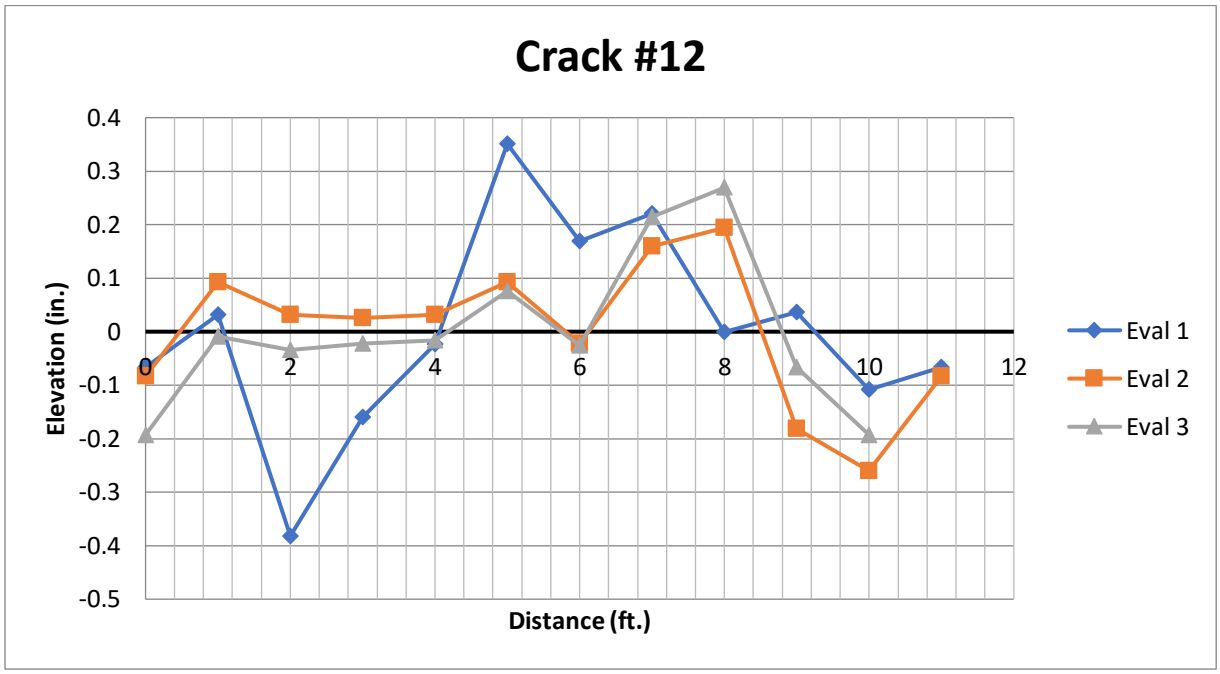

Figure C.4 Transverse Profile of Crack #12

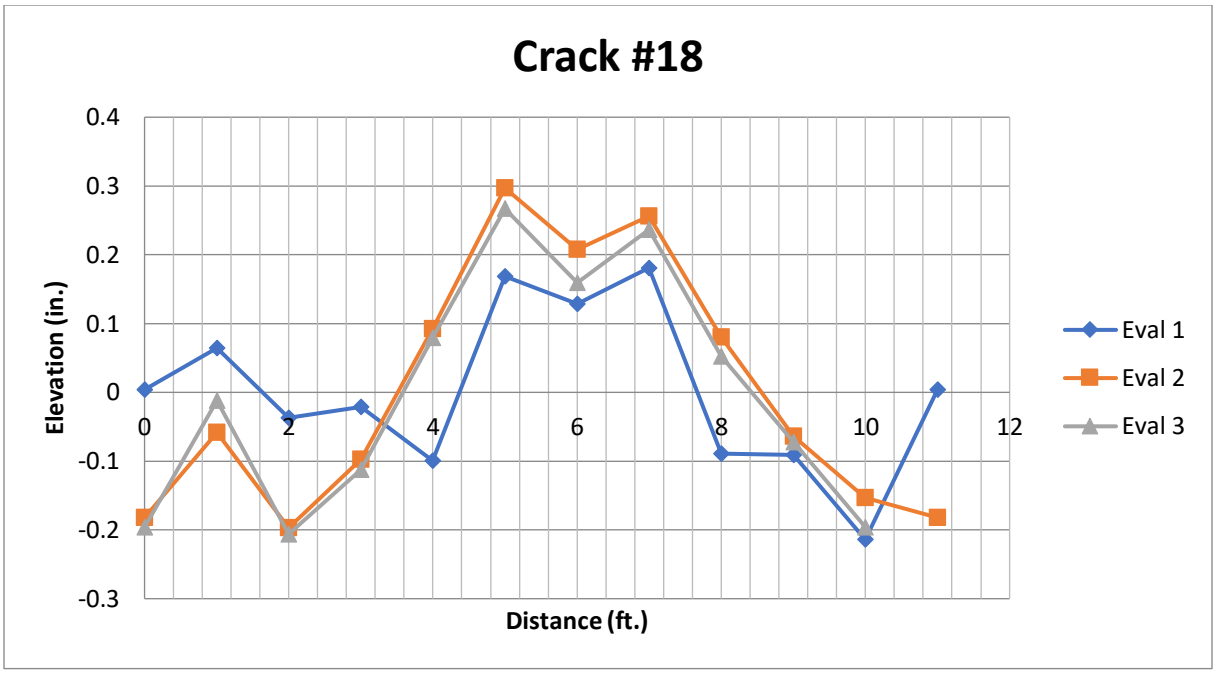

Figure C.5 Transverse Profile of Crack #18

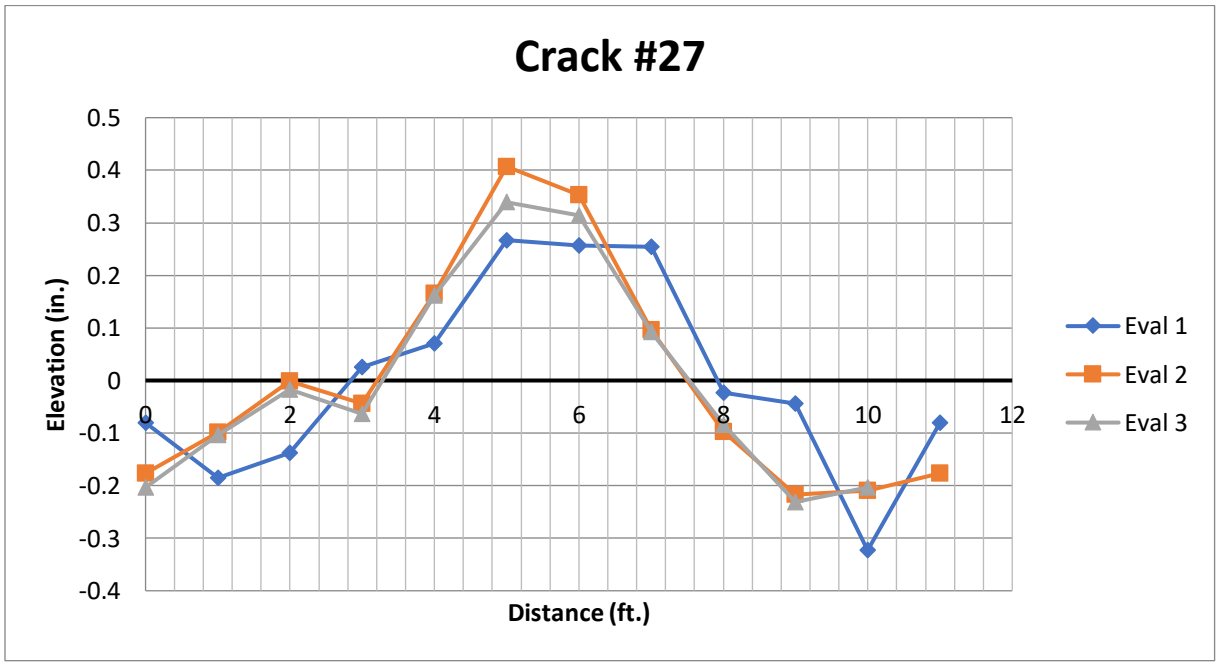

Figure C.6 Transverse Profile of Crack #27

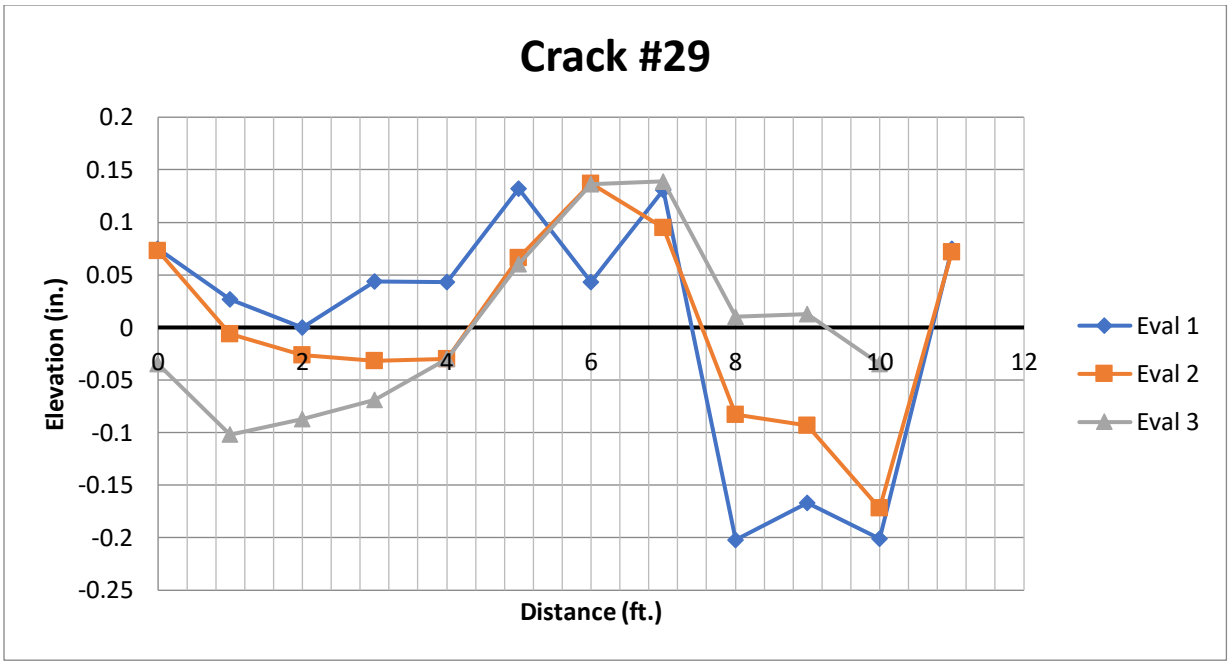

Figure C.7 Transverse Profile of Crack #29

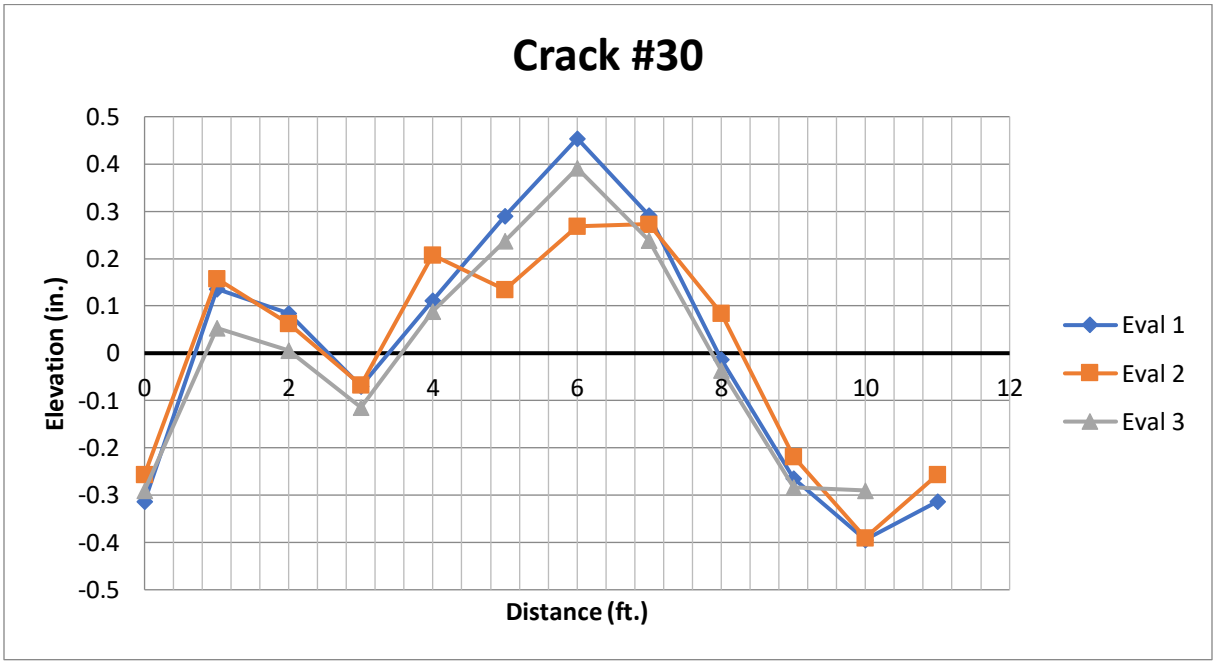

Figure C.8 Transverse Profile of Crack #30

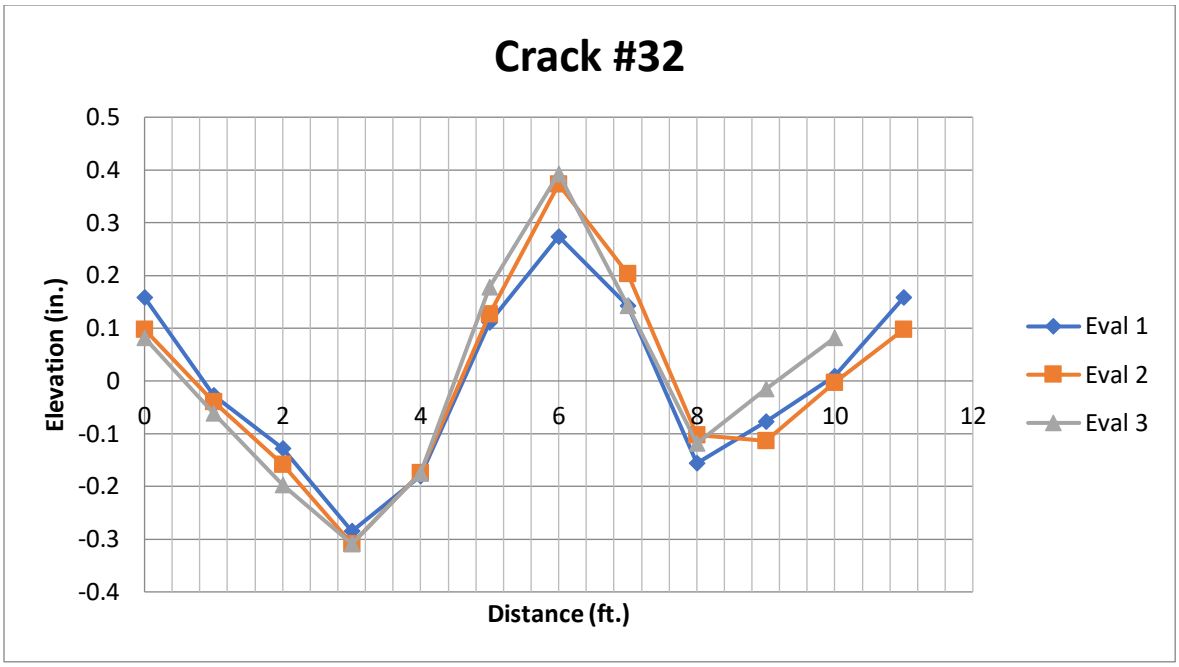

Figure C.9 Transverse Profile of Crack #32

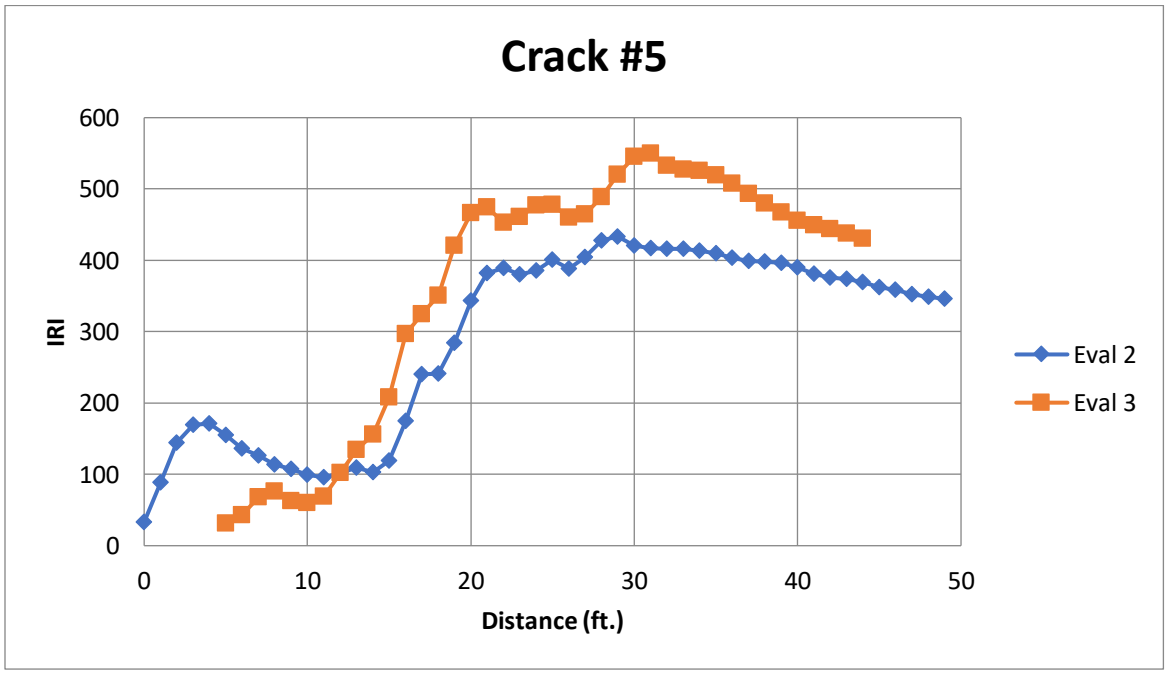

Figure C.10 IRI results of Crack #5

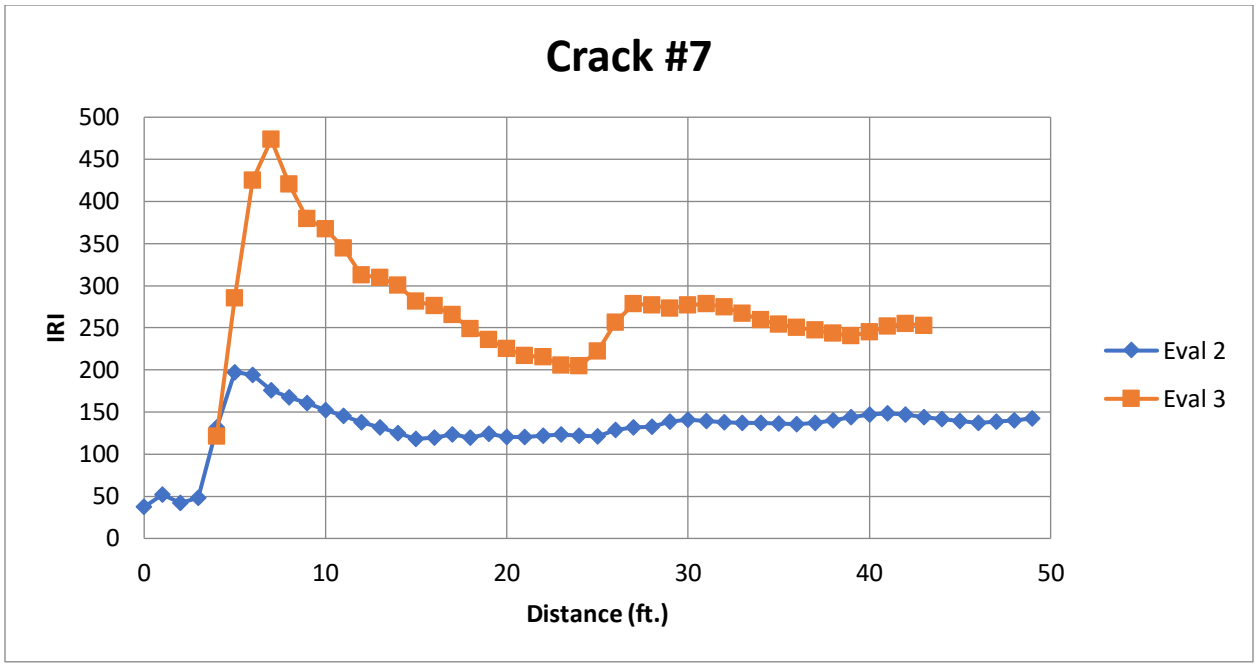

Figure C.11 IRI results of Crack #7

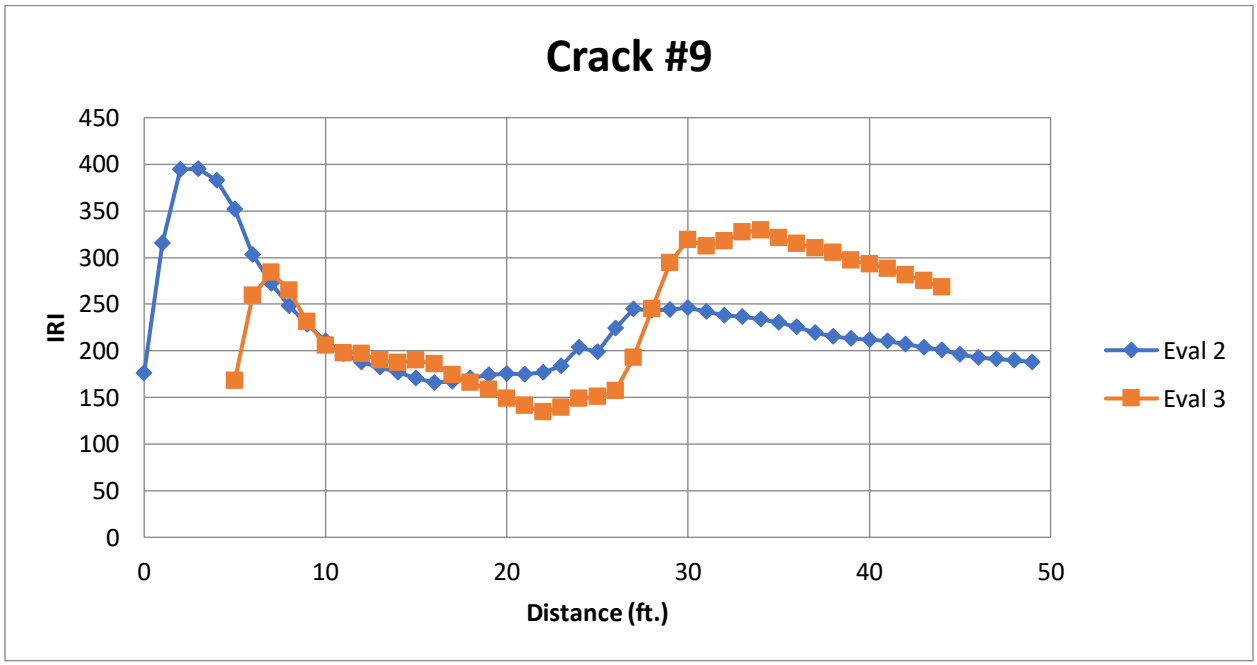

Figure C.12 IRI results of Crack #9

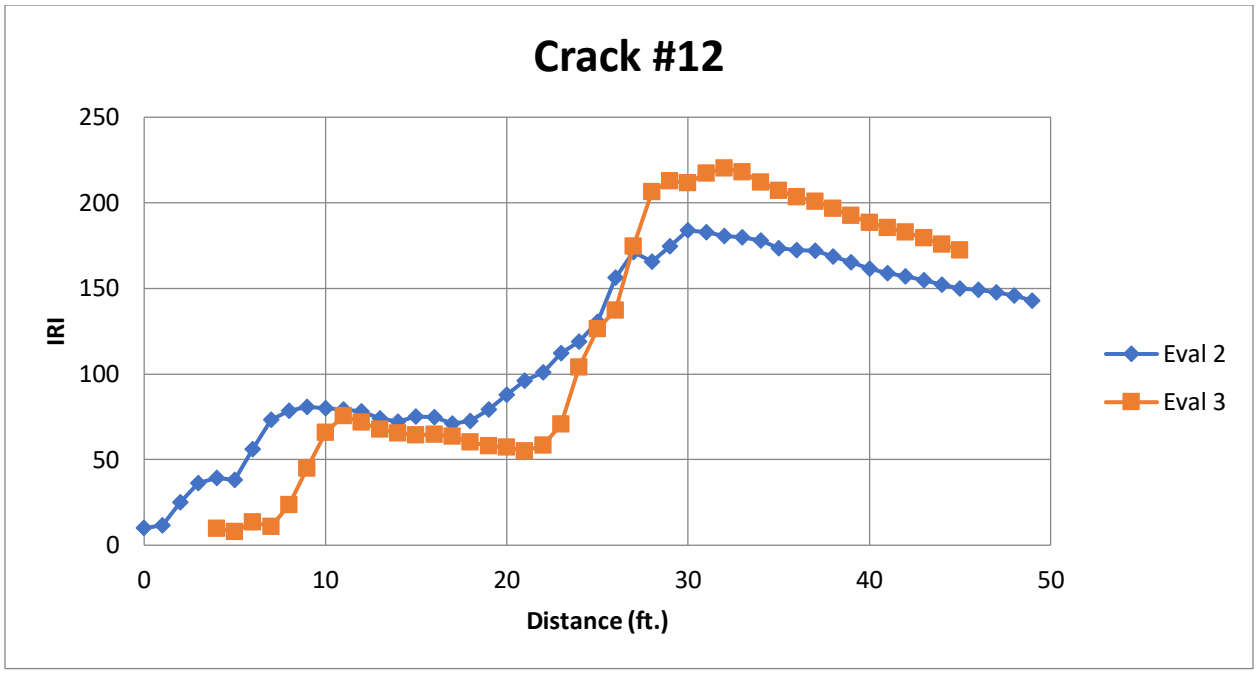

Figure C.13 IRI results of Crack #12

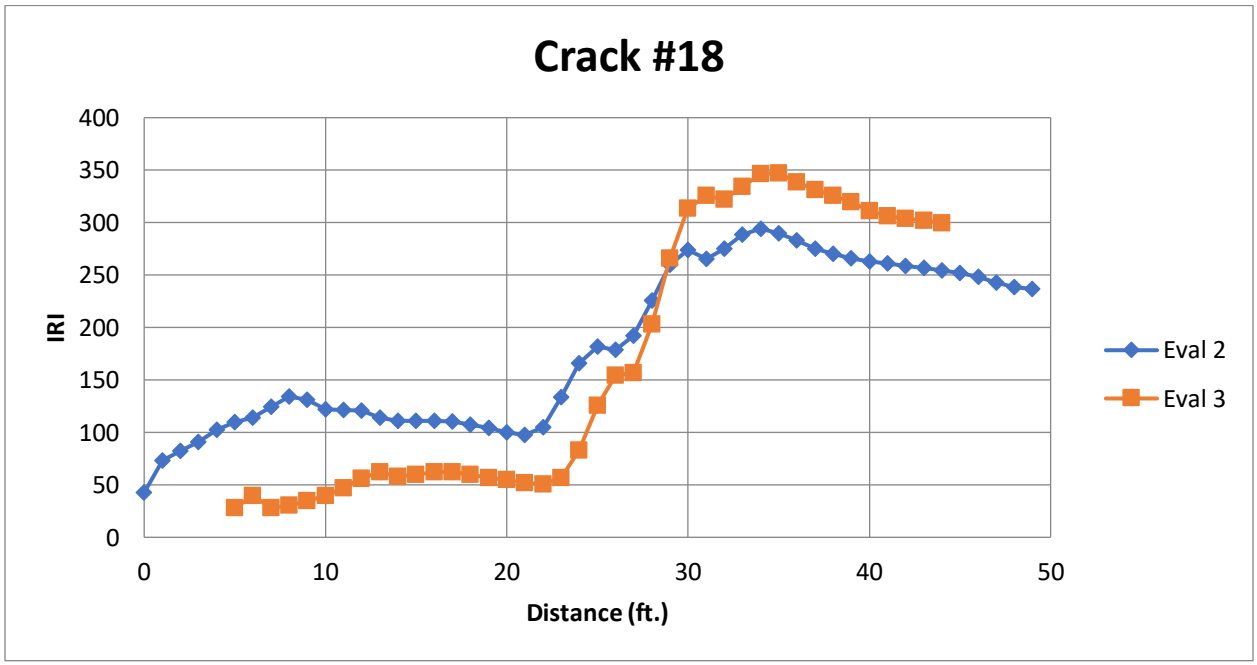

Figure C.14 IRI results of Crack #18

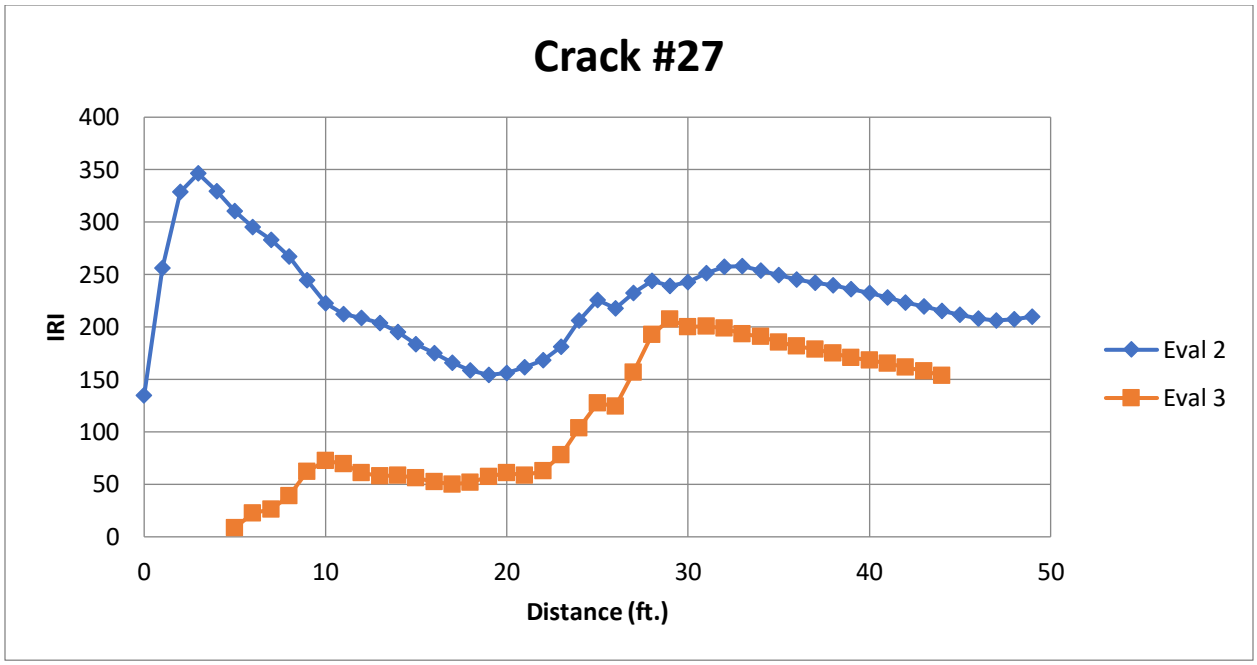

Figure C.15 IRI results of Crack #27

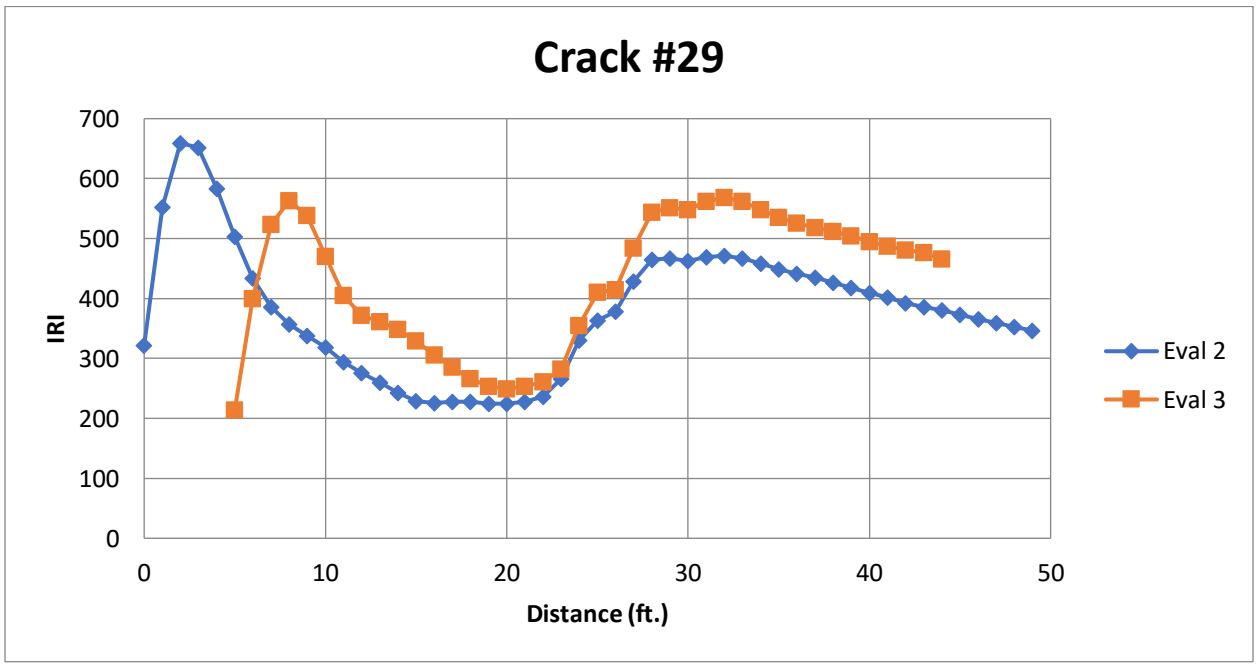

Figure C.15 IRI results of Crack #27

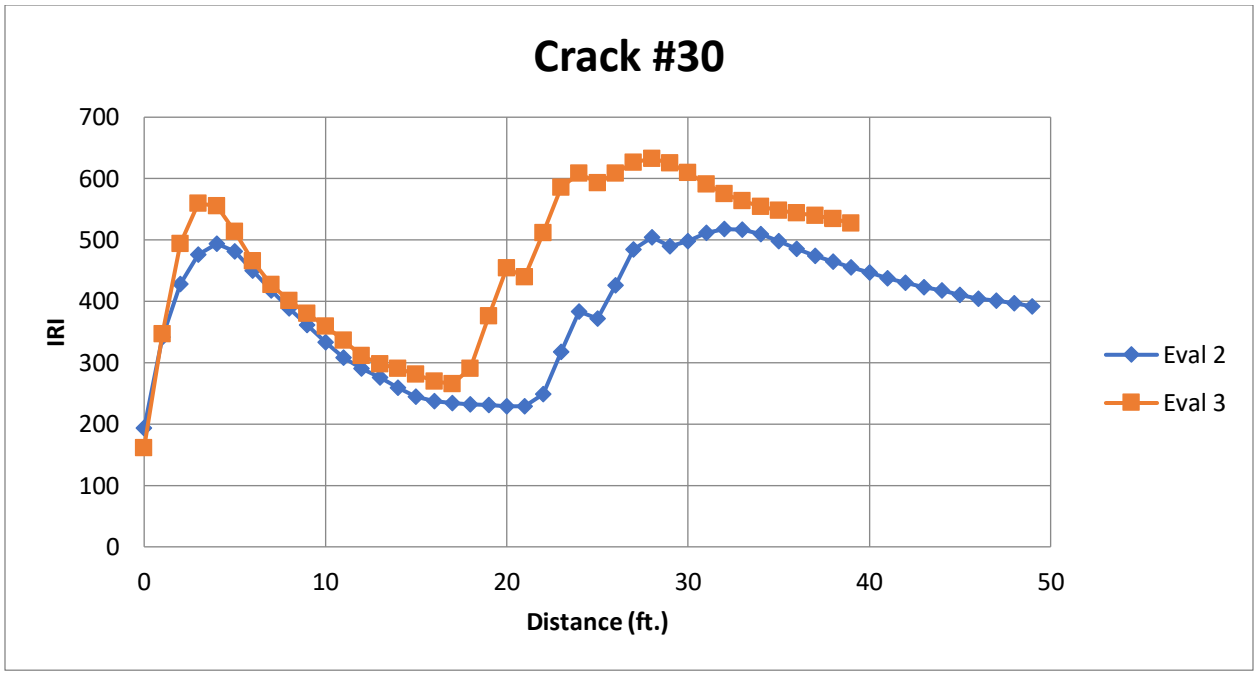

Figure C.16 IRI results of Crack #30

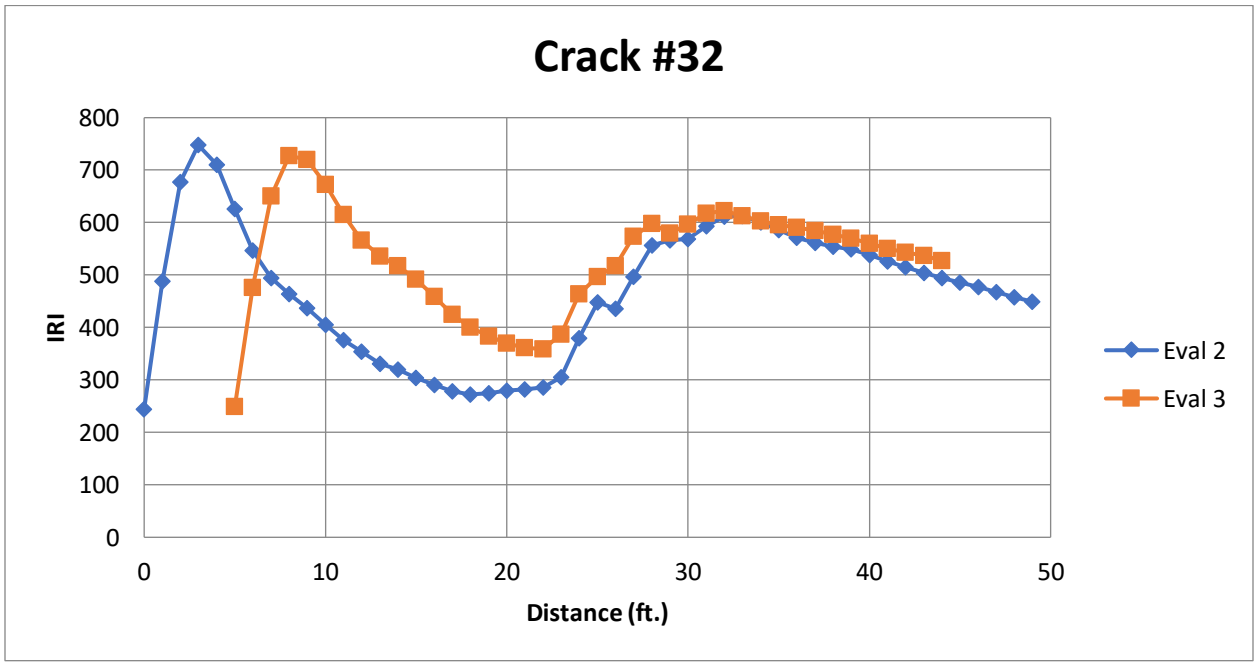

Figure C.17 IRI results of Crack #32

APPENDIX D: STRAIGHTEDGE RESULTS

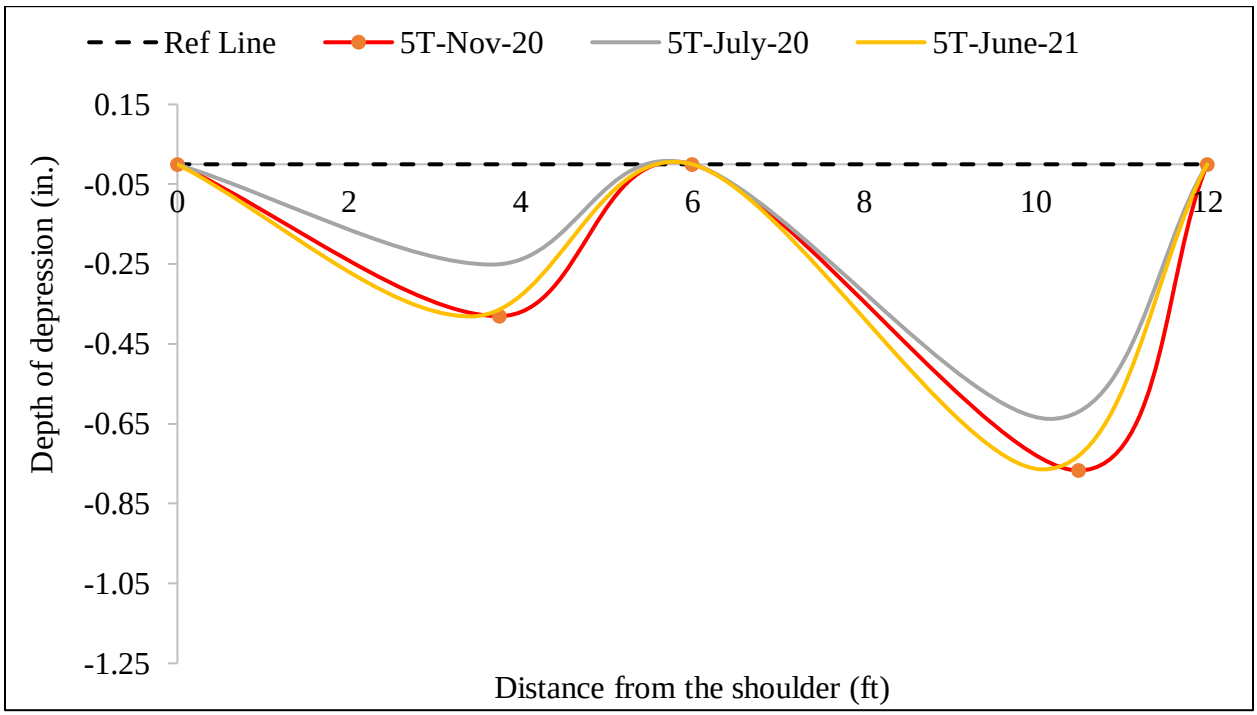

Figure D.1 Transverse Profile of Crack #5

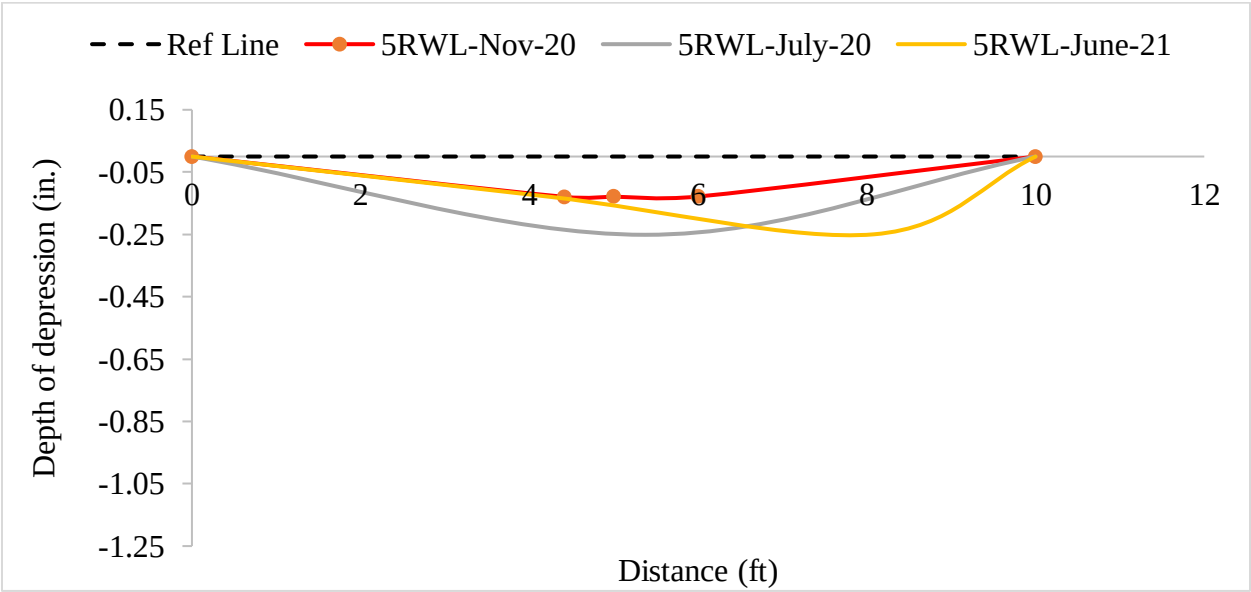

Figure D.2 Longitudinal Profile of Crack #5 (along Right-Wheel-Path)

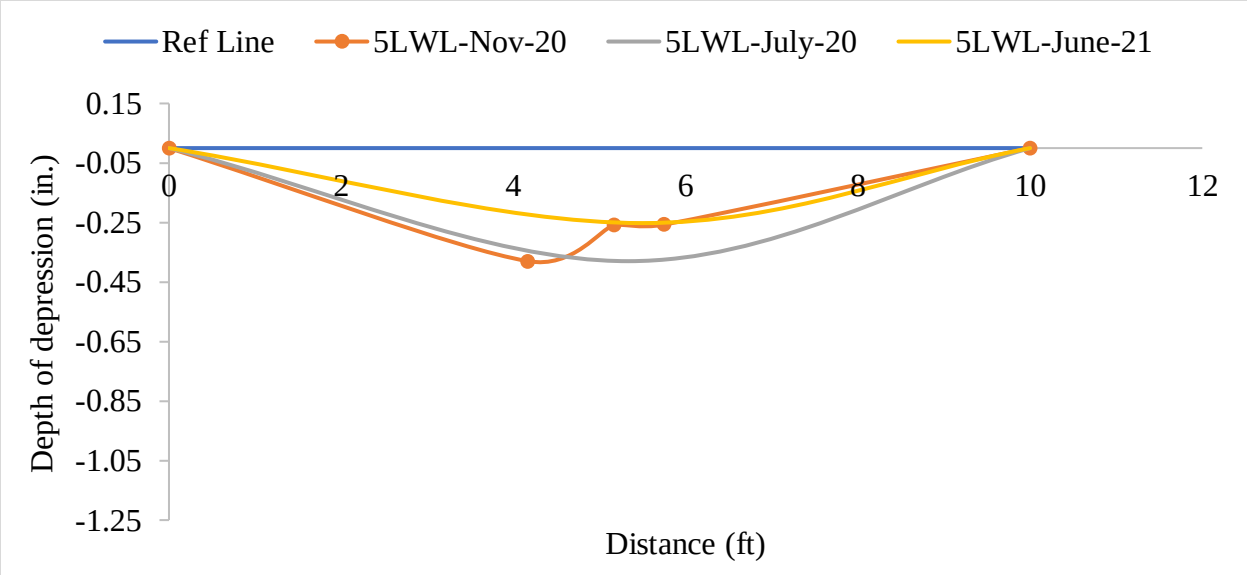

Figure D.3 Longitudinal Profile of Crack #5 (along Left-Wheel-Path)

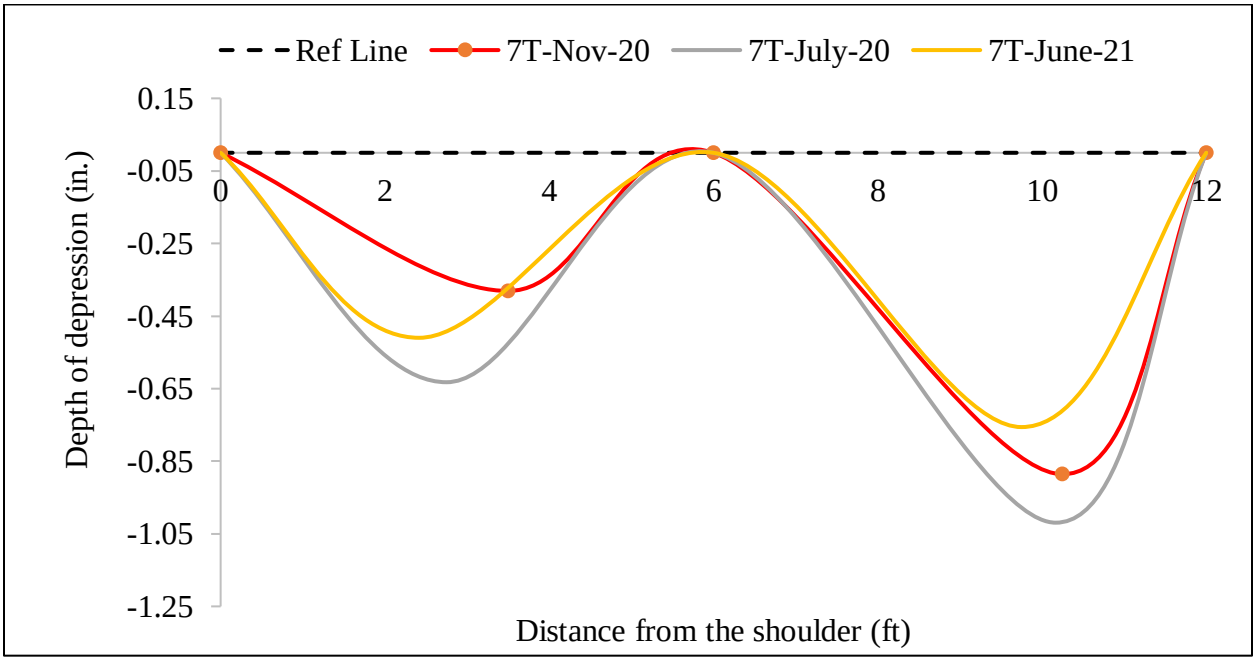

Figure D.4 Transverse Profile of Crack #7

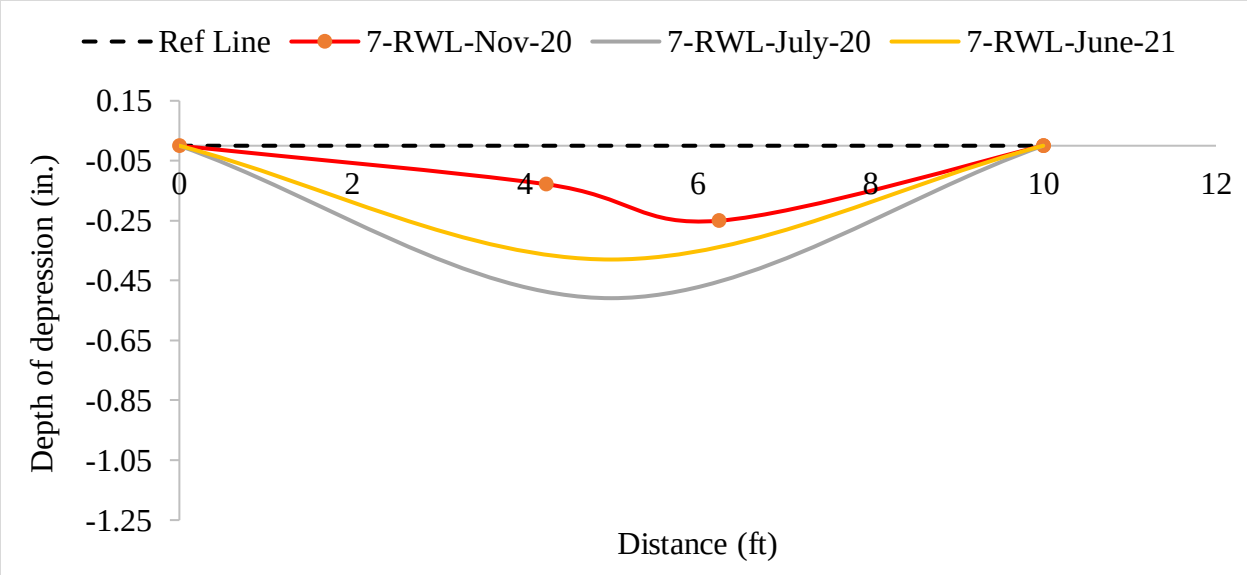

Figure D.5 Longitudinal Profile of Crack #7 (along Right-Wheel-Path)

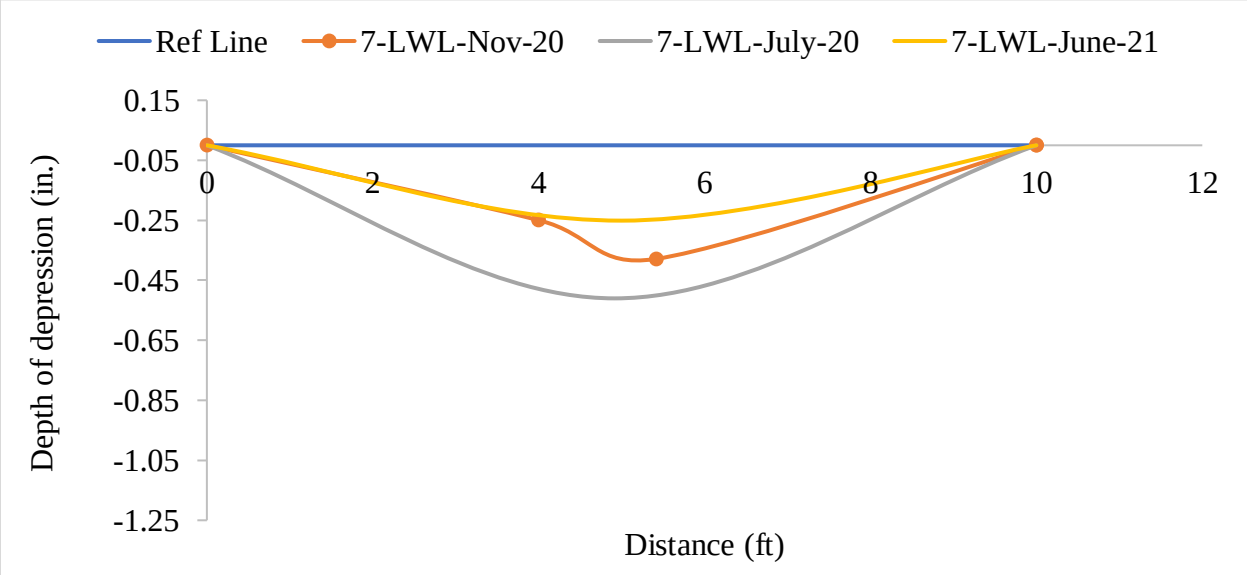

Figure D.6 Longitudinal Profile of Crack #7 (along Left-Wheel-Path)

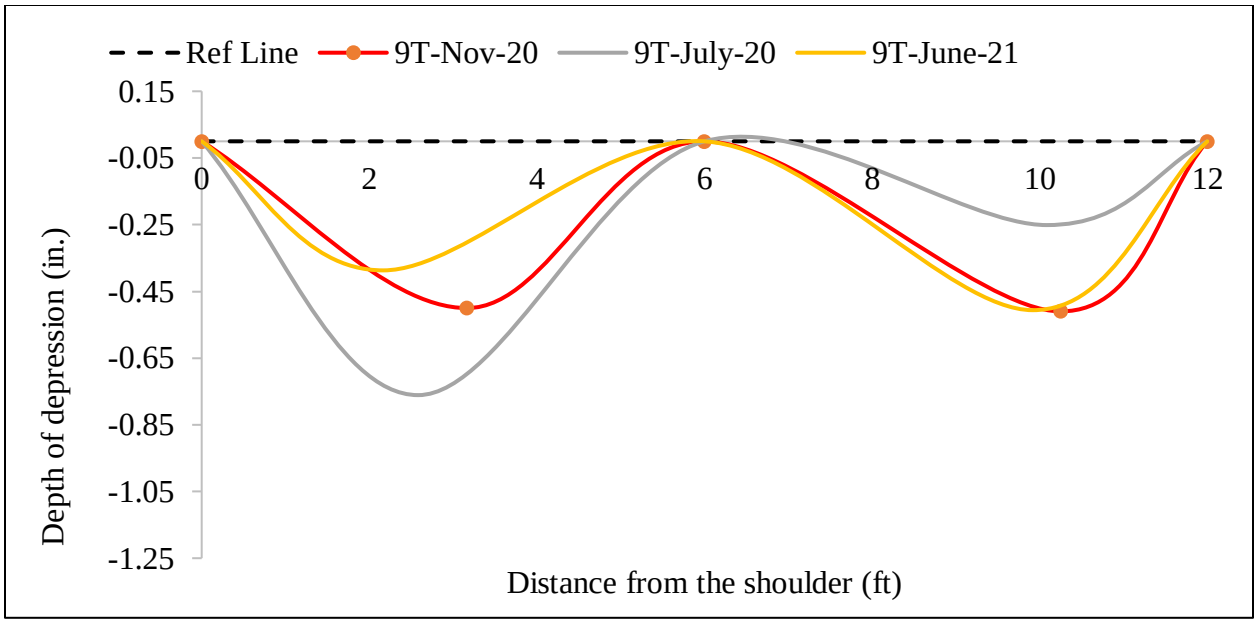

Figure D.7 Transverse Profile of Crack #9

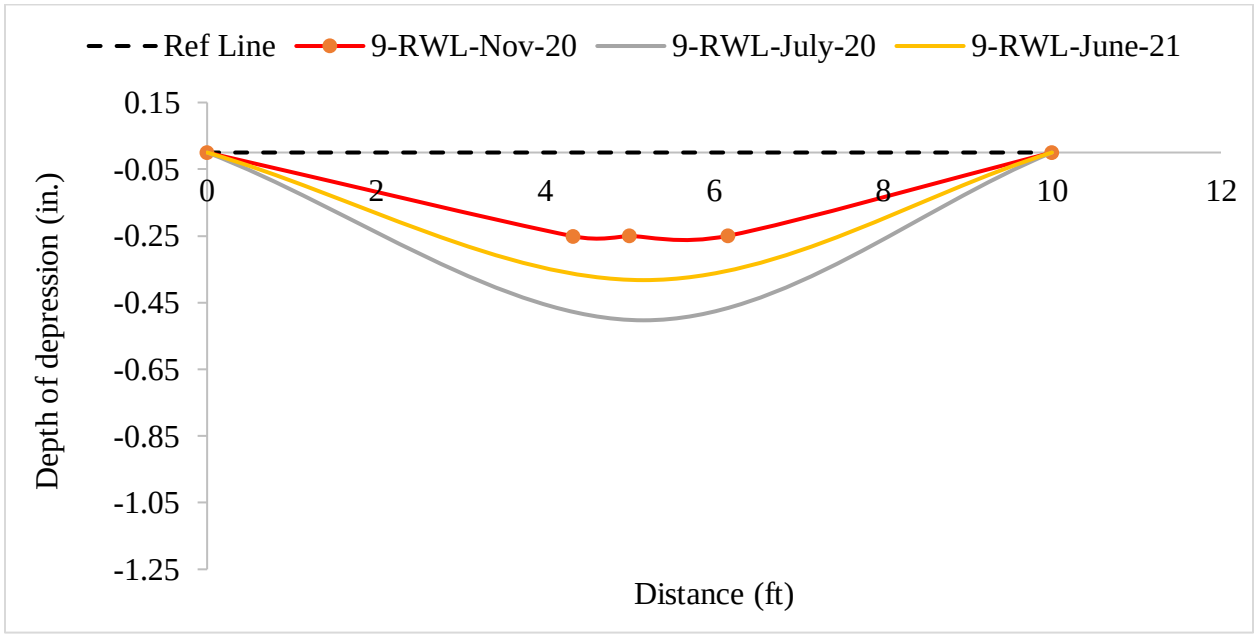

Figure D.8 Longitudinal Profile of Crack #9 (along Right-Wheel-Path)

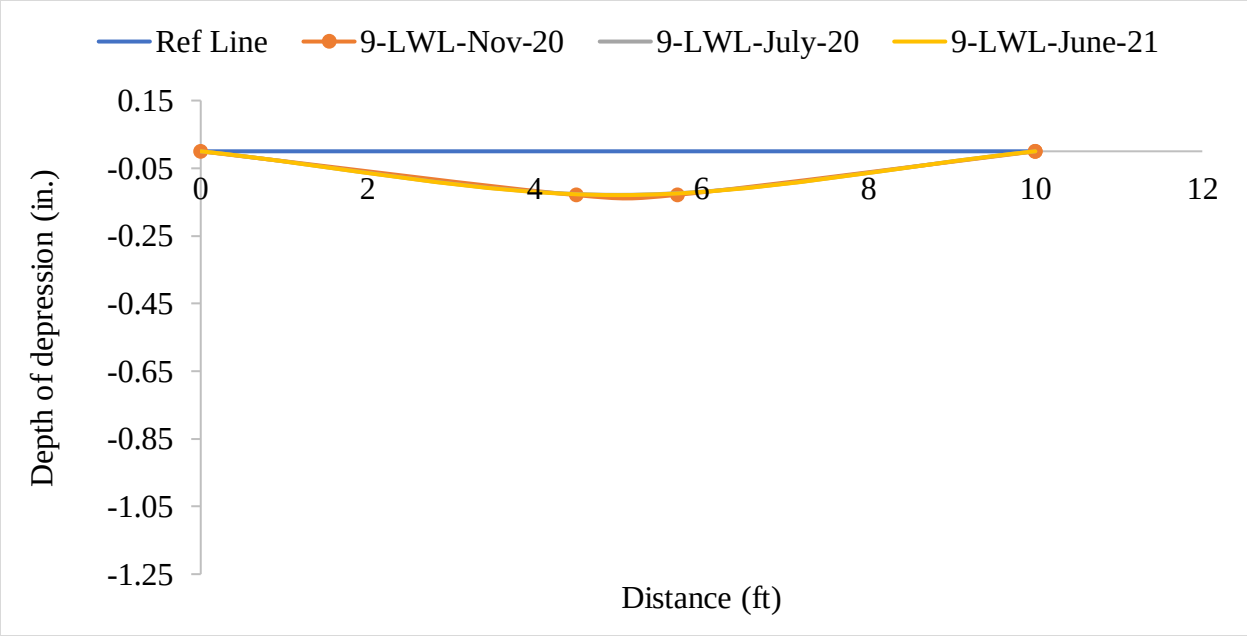

Figure D.9 Longitudinal Profile of Crack #9 (along Left-Wheel-Path)

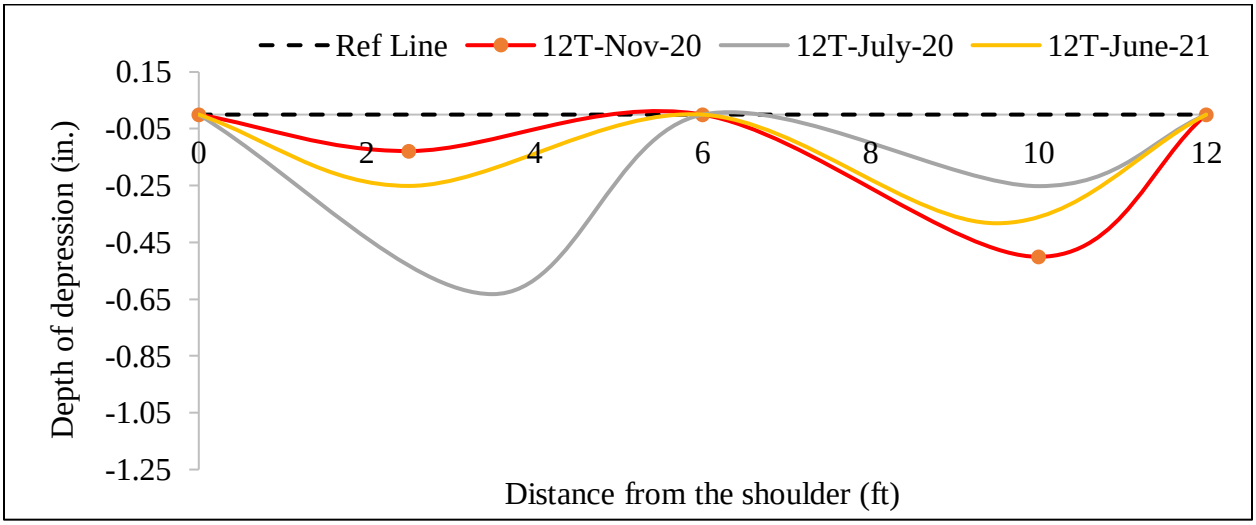

Figure D.10 Transverse Profile of Crack #12

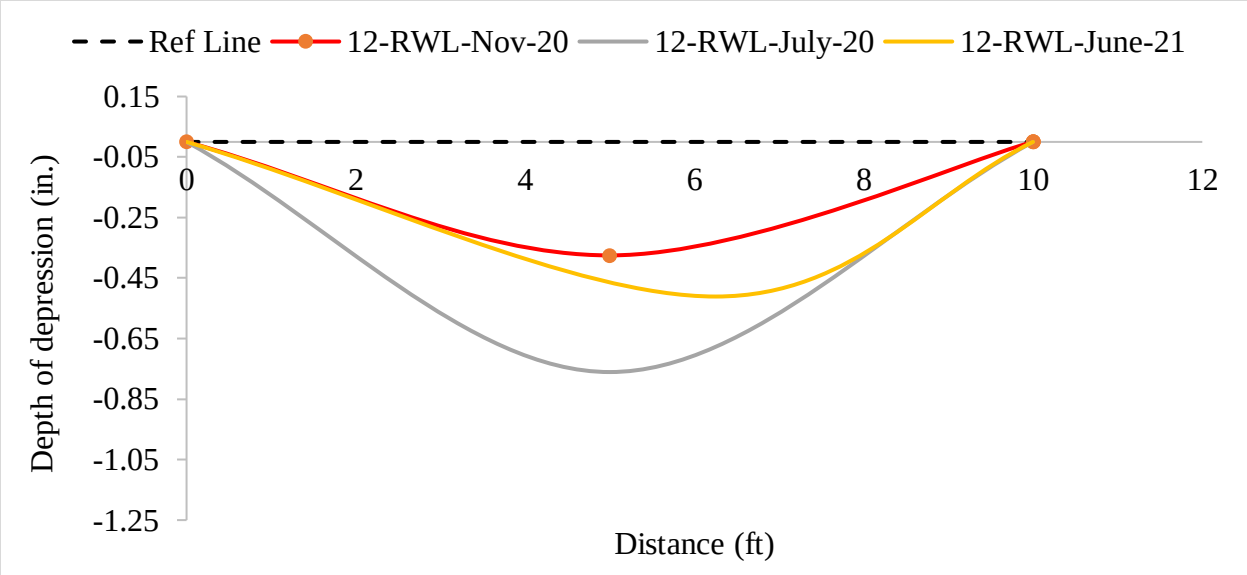

Figure D.11 Longitudinal Profile of Crack #12 (along Right-Wheel-Path)

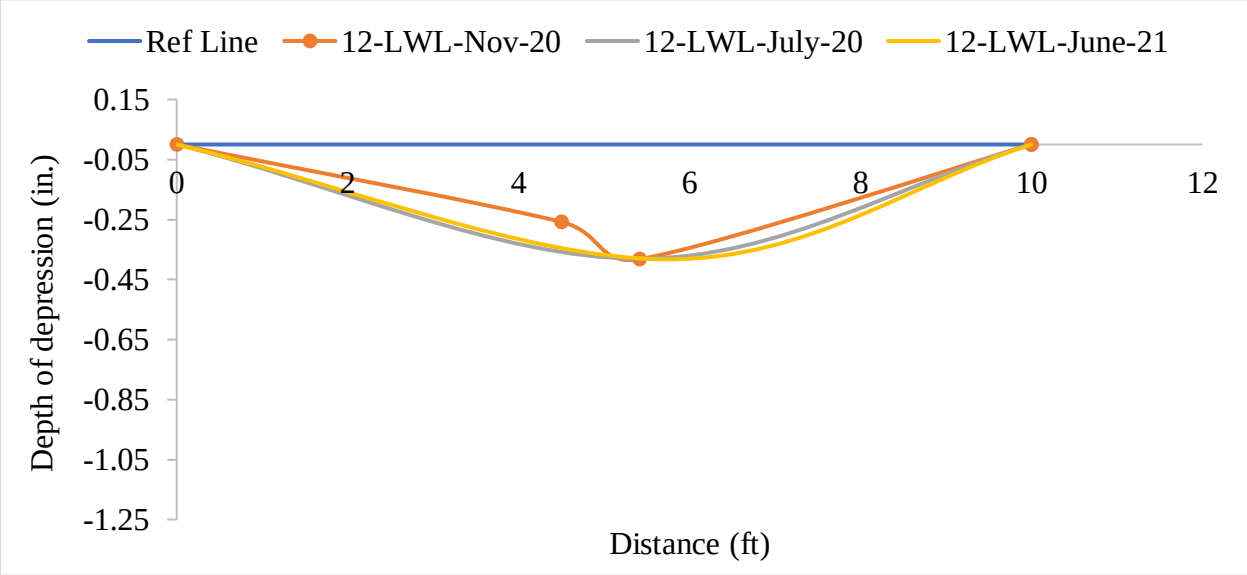

Figure D.12 Longitudinal Profile of Crack #12 (along Left-Wheel-Path)

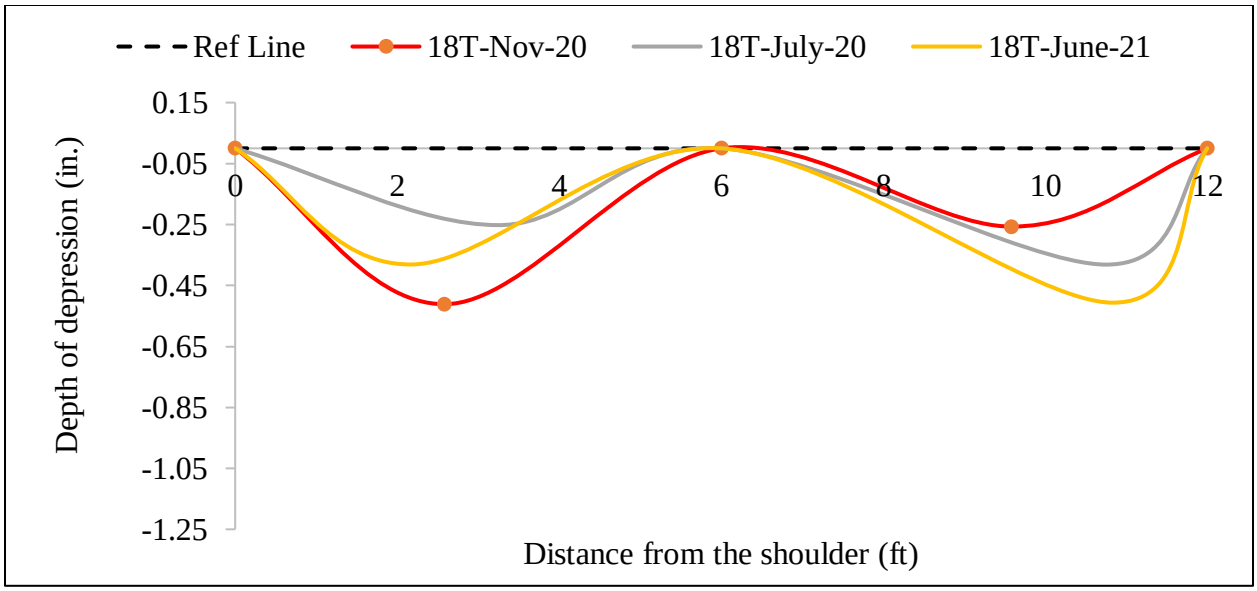

Figure D.13 Transverse Profile of Crack #18

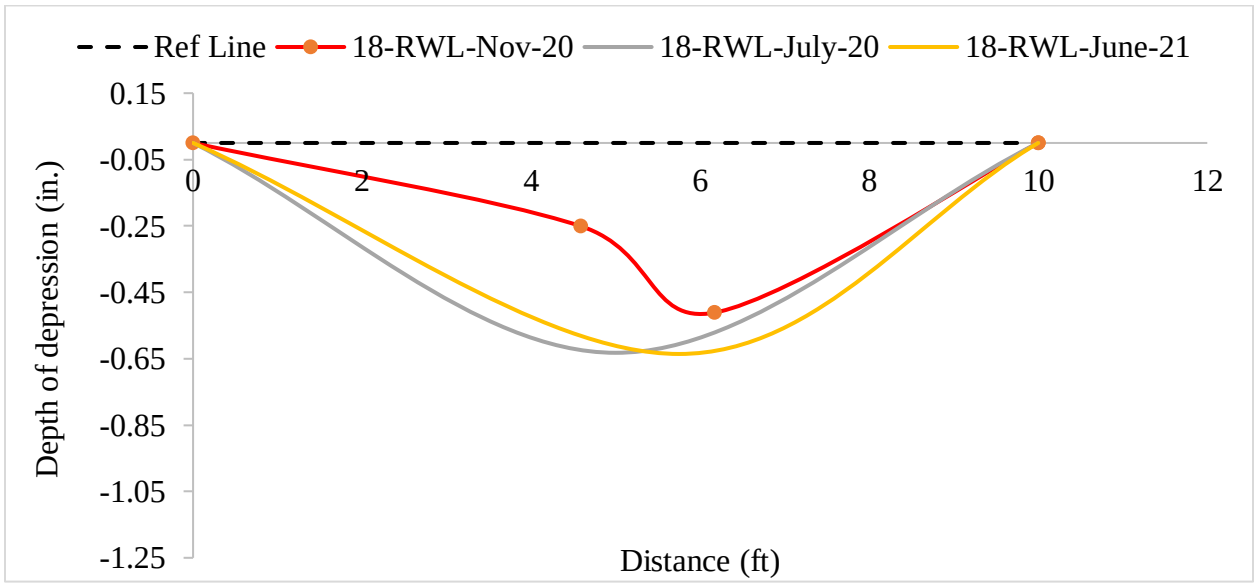

Figure D.14 Longitudinal Profile of Crack #18 (along Right-Wheel-Path)

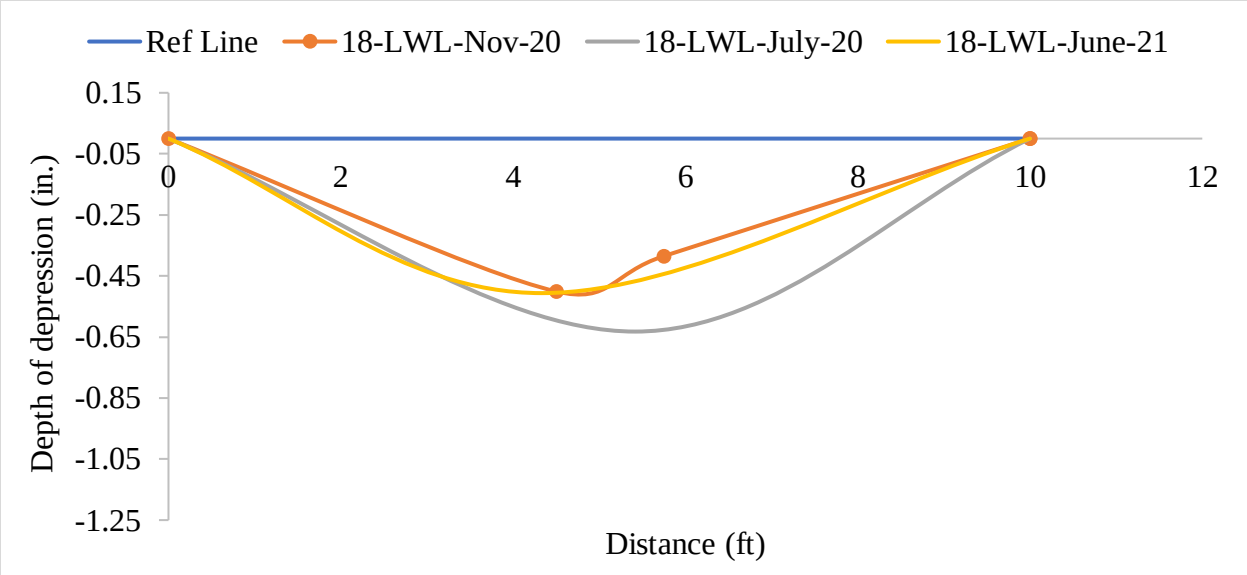

Figure D.15 Longitudinal Profile of Crack #18 (along Left-Wheel-Path)

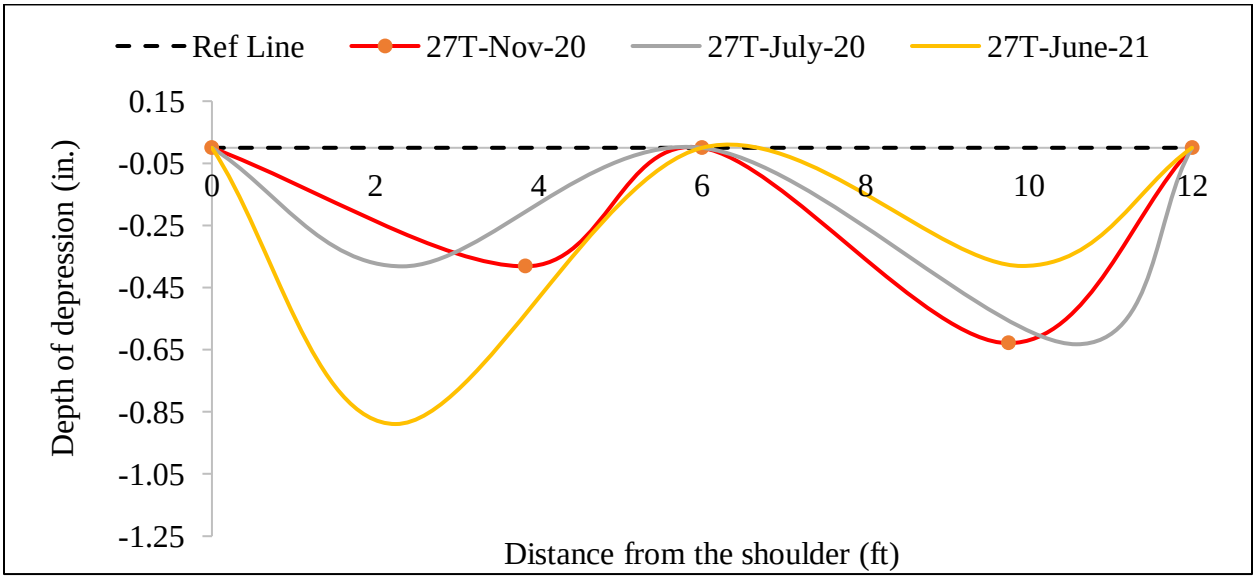

Figure D.16 Transverse Profile of Crack #27

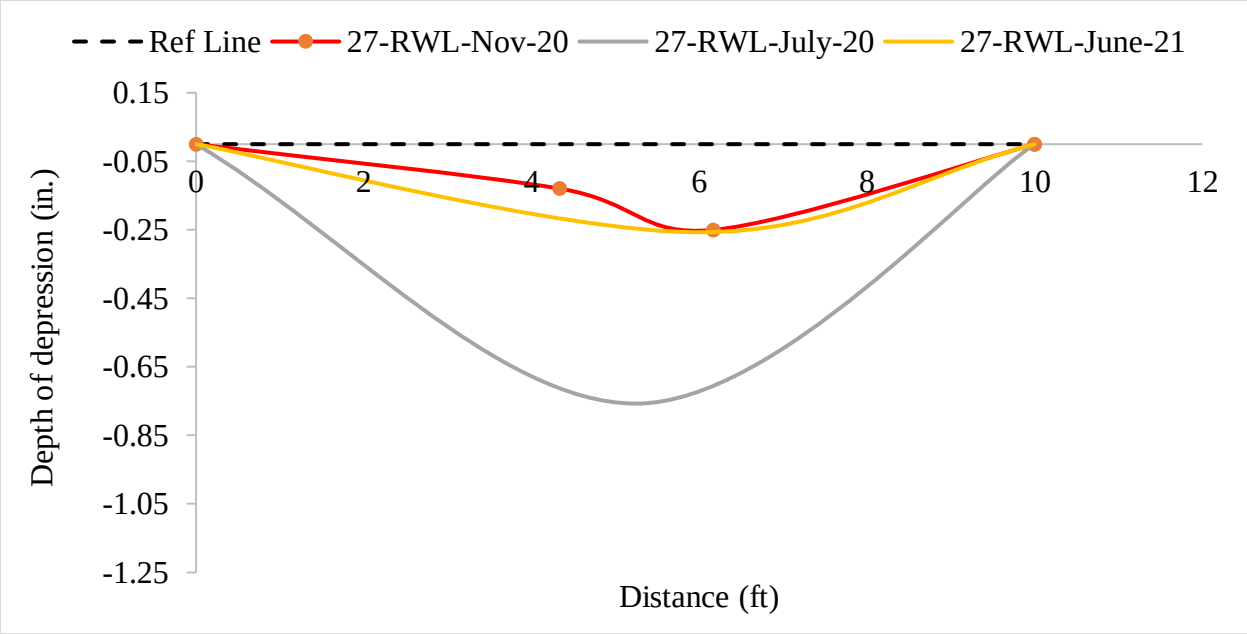

Figure D.17 Longitudinal Profile of Crack #27 (along Right-Wheel-Path)

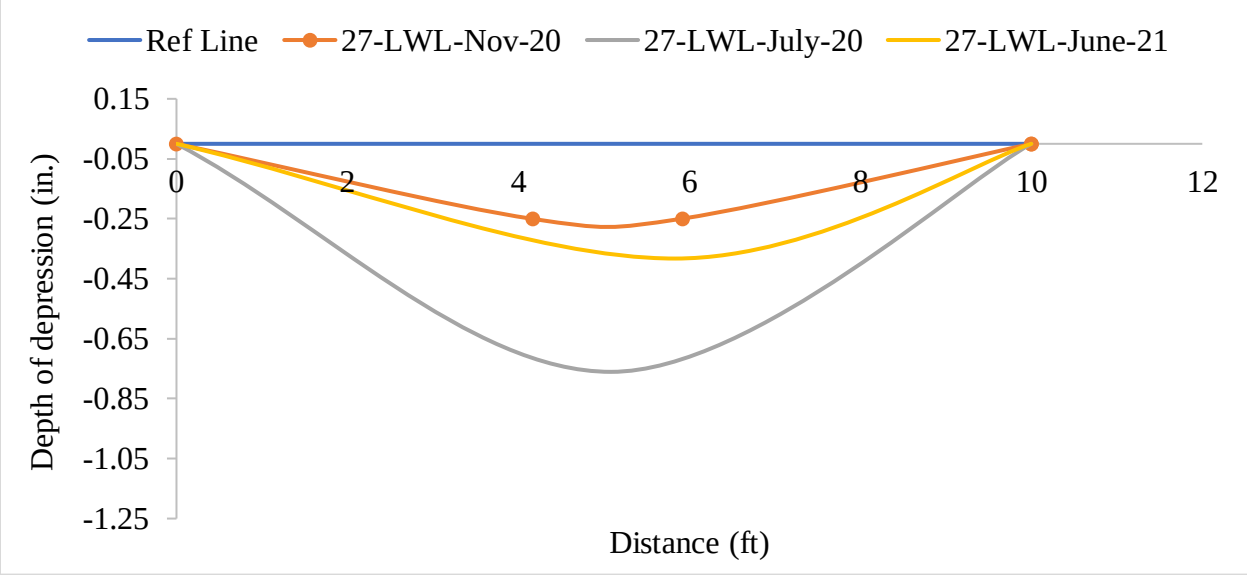

Figure D.18 Longitudinal Profile of Crack #27 (along Left-Wheel-Path)

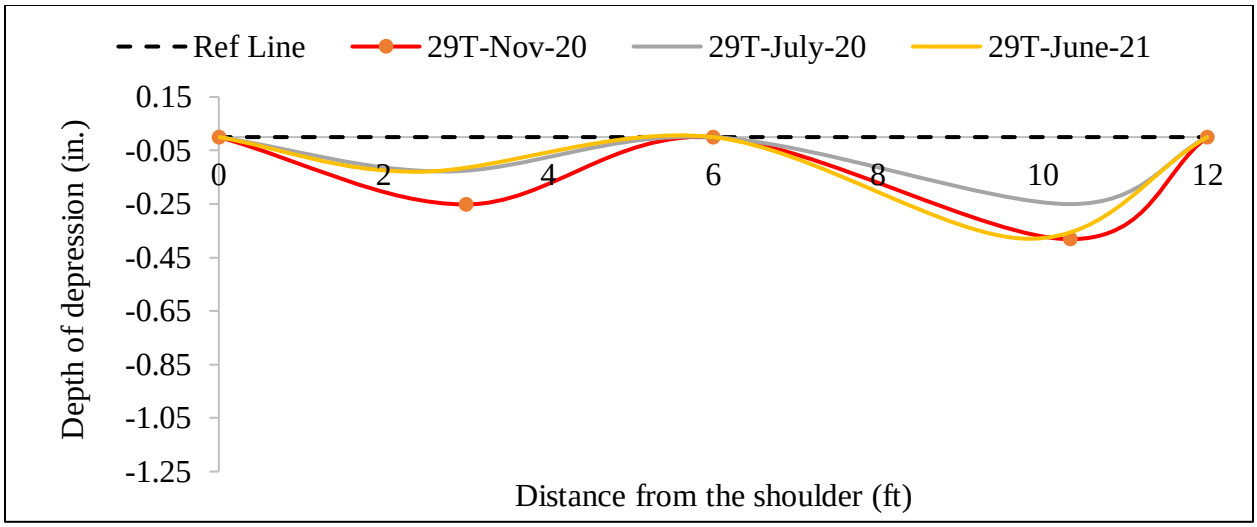

Figure D.19 Transverse Profile of Crack #29

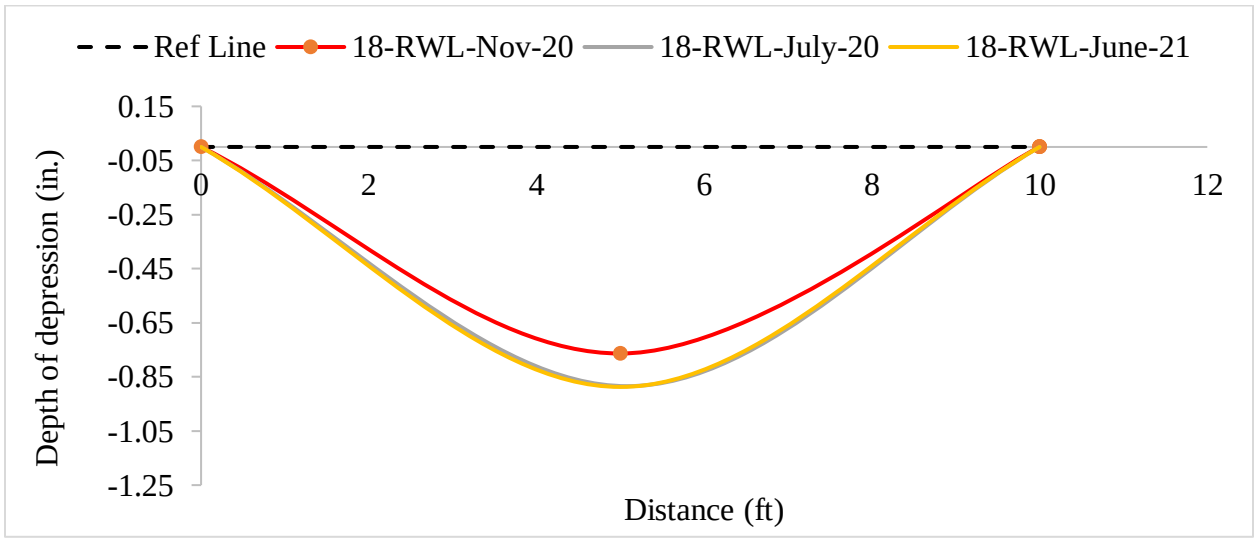

Figure D.20 Longitudinal Profile of Crack #29 (along Right-Wheel-Path)

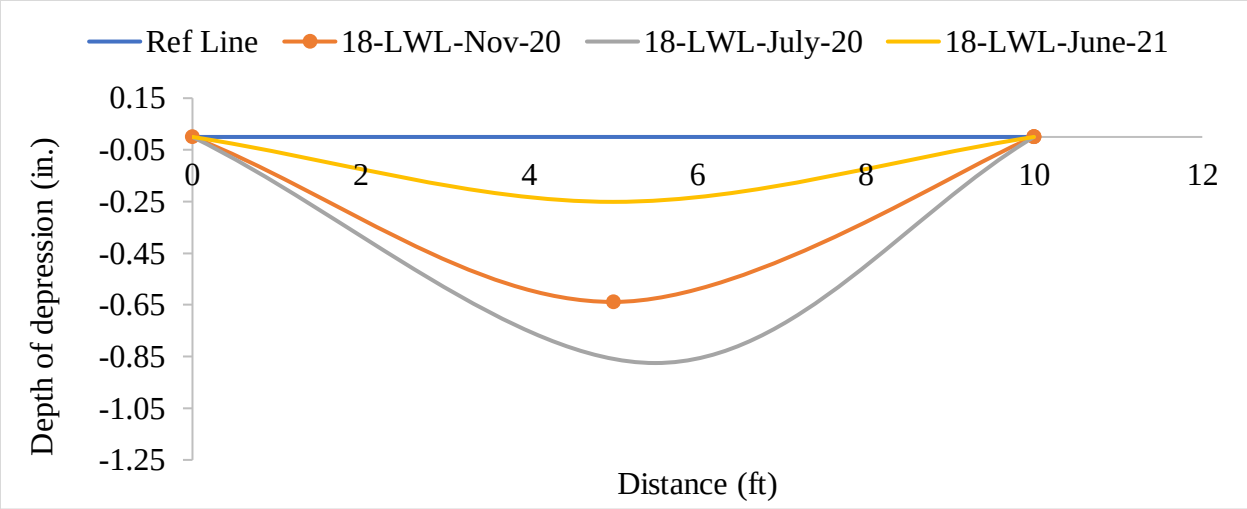

Figure D.21 Longitudinal Profile of Crack #29 (along Left-Wheel-Path)

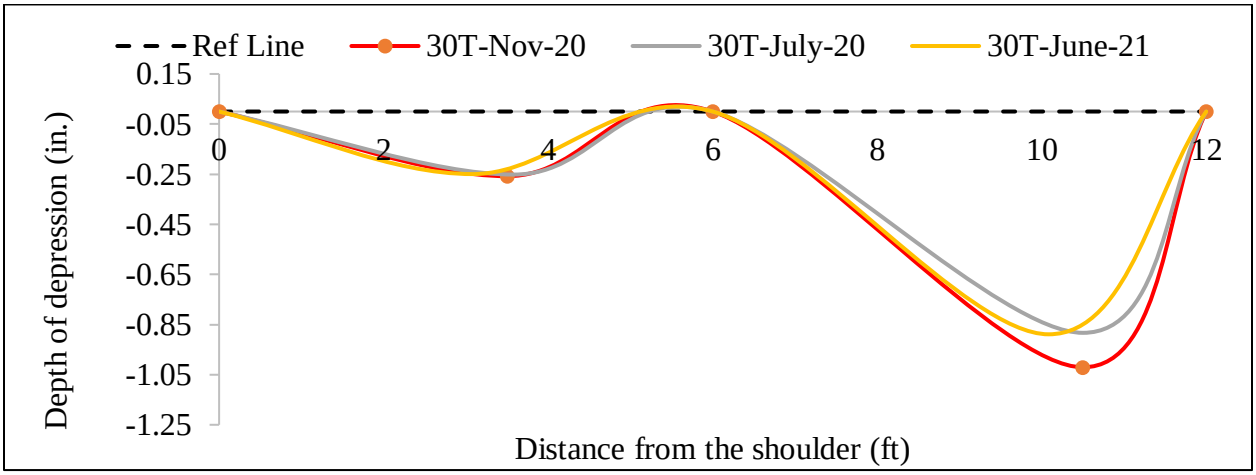

Figure D.22 Transverse Profile of Crack #30

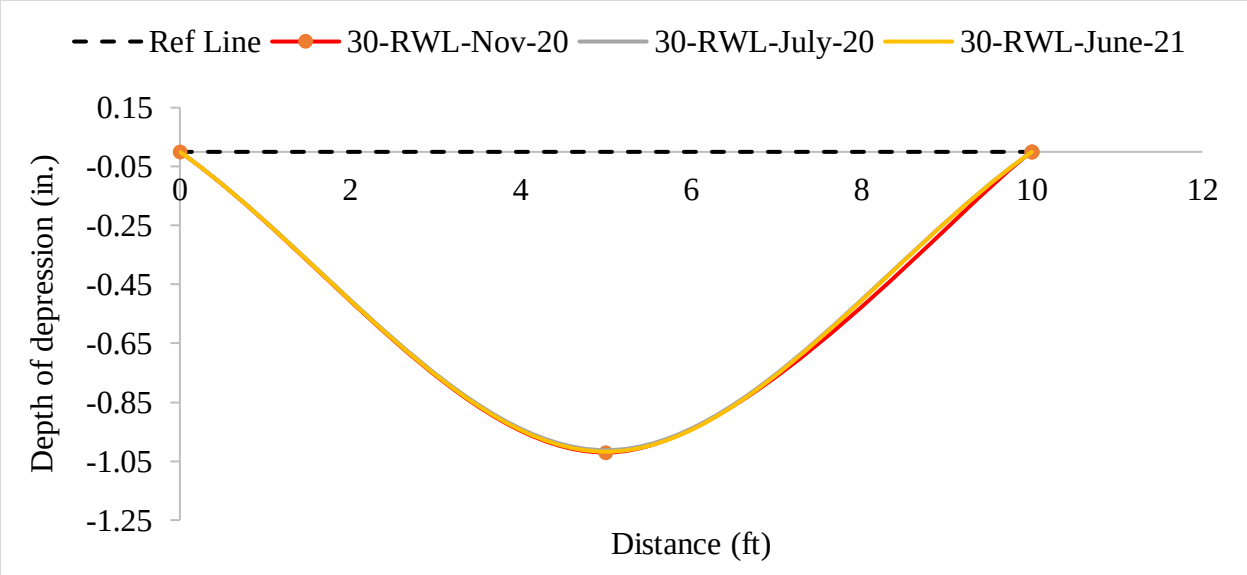

Figure D.23 Longitudinal Profile of Crack #30 (along Right-Wheel-Path)

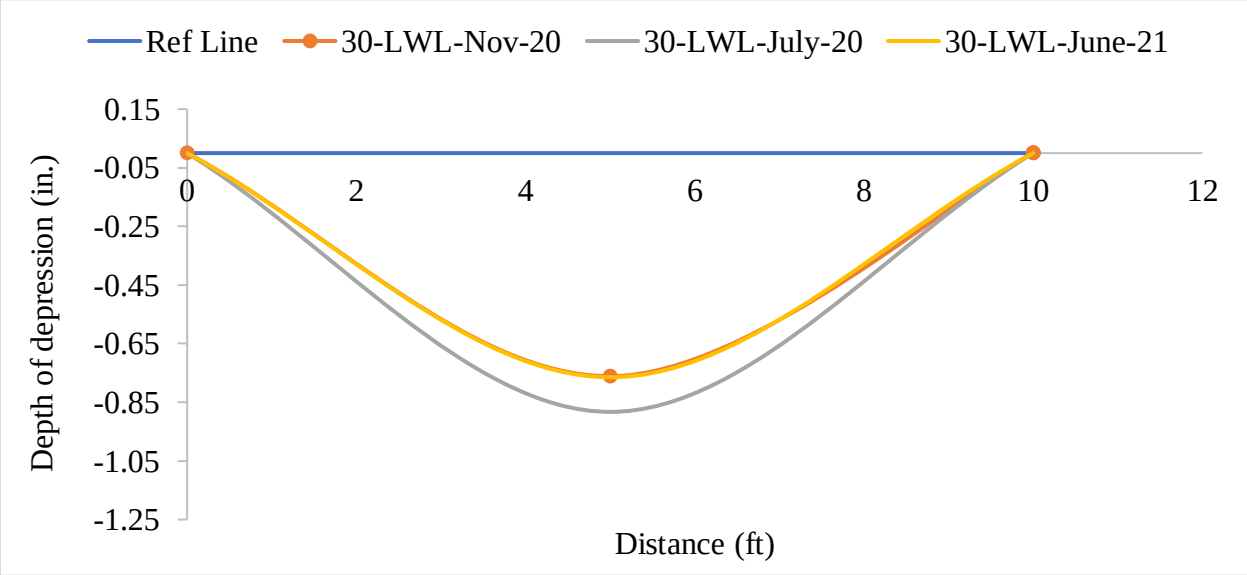

Figure D.24 Longitudinal Profile of Crack #30 (along Left-Wheel-Path)

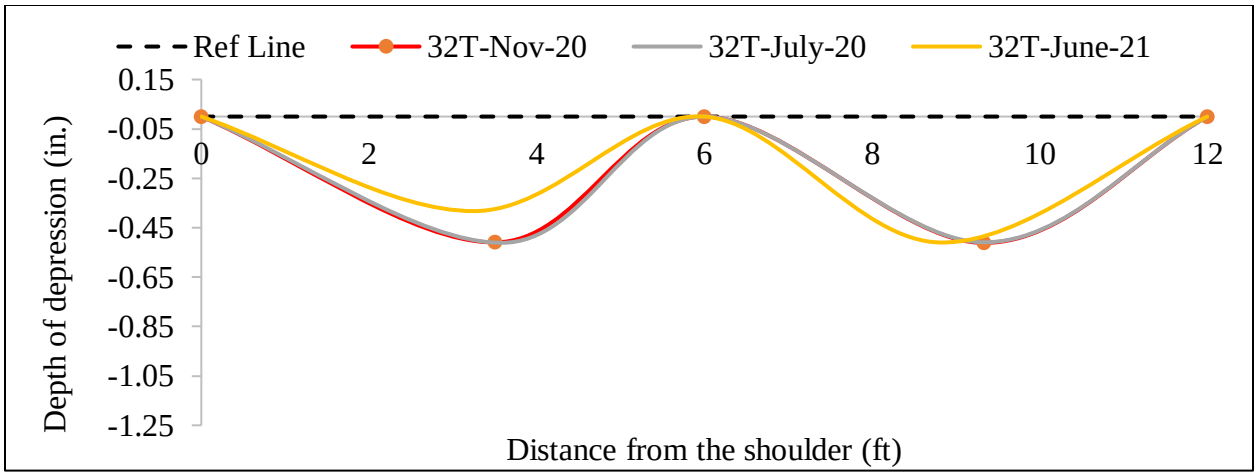

Figure D.25 Transverse Profile of Crack #32

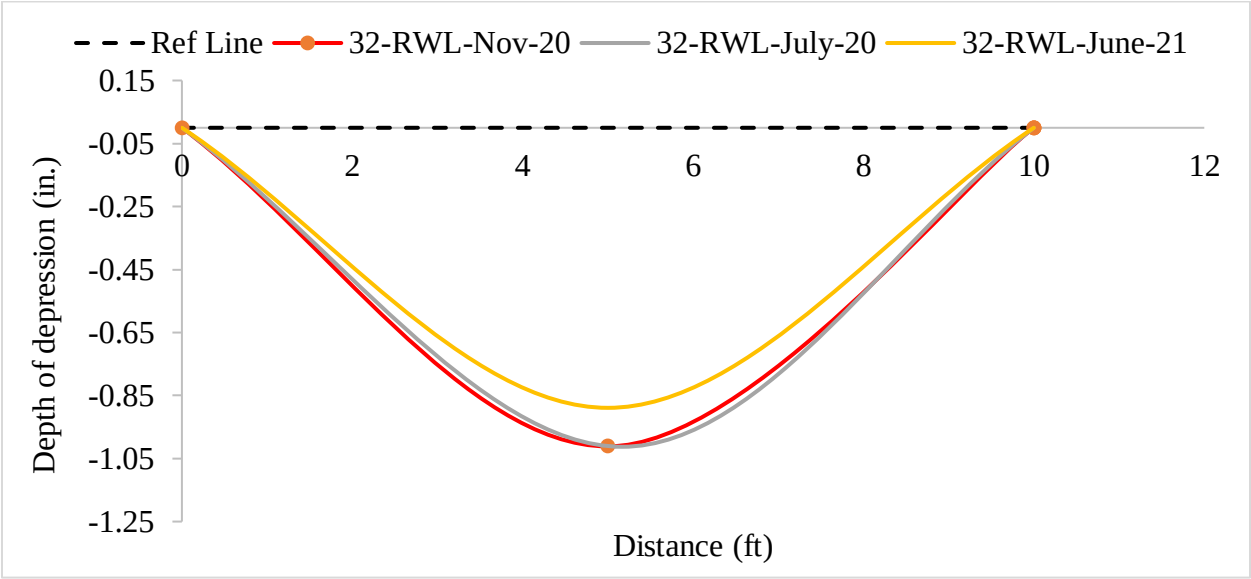

Figure D.26 Longitudinal Profile of Crack #32 (along Right-Wheel-Path)

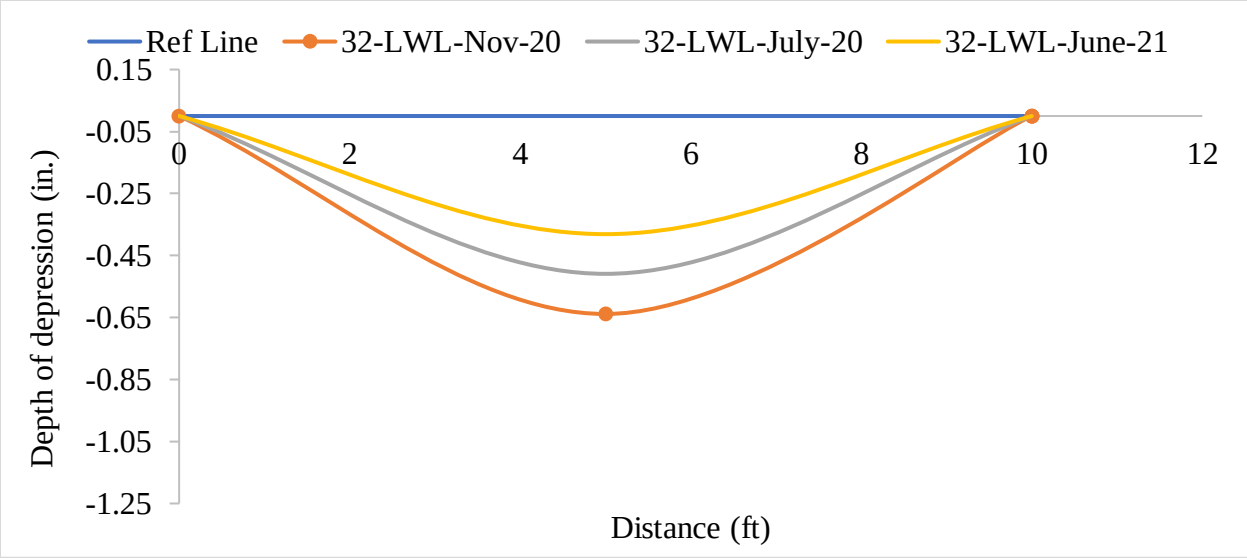

Figure D.27 Longitudinal Profile of Crack #32 (along Left-Wheel-Path)

APPENDIX E: PAVEVISION3D AND PAVE 3D 8K

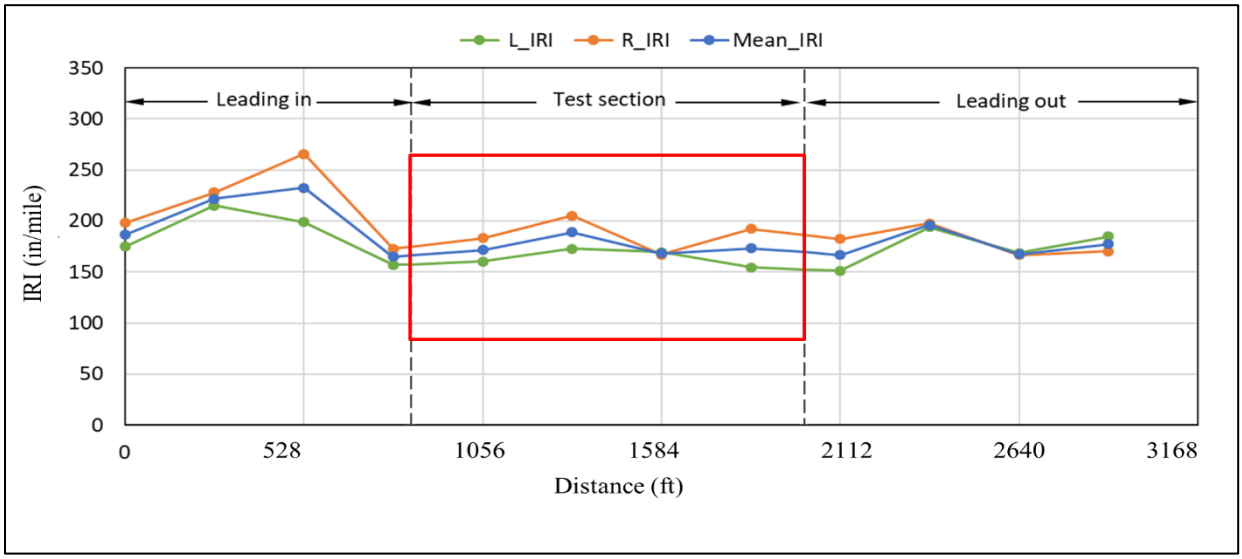

Figure E.1 IRI Plot (Before Repair)

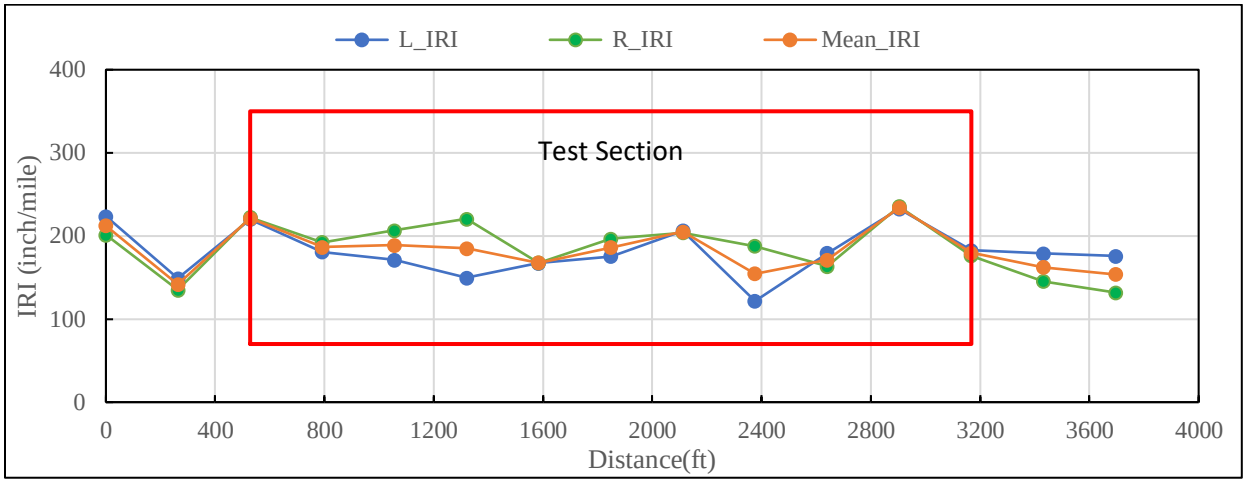

Figure E.2 IRI Plot (Five-months after repair)

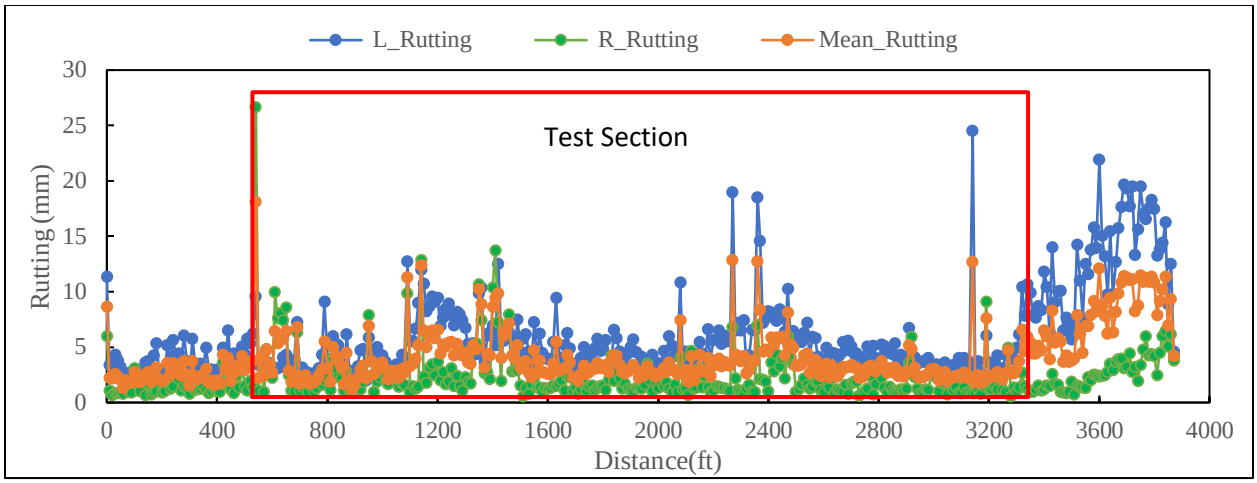

Figure E.3 Summary of Rutting Results (Five-months after repair)

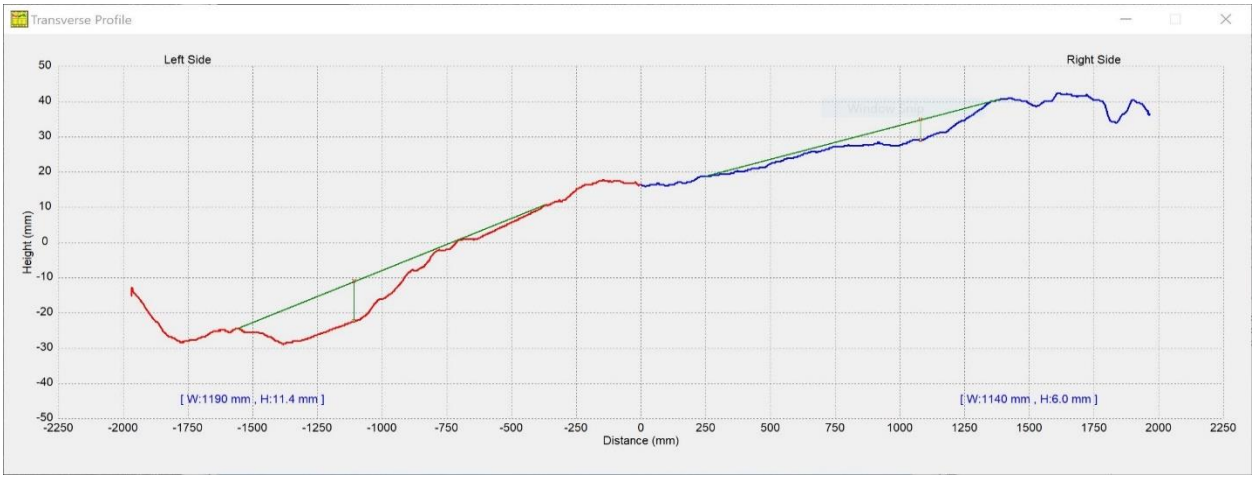

Figure E.4 Transverse Profile at 0 feet

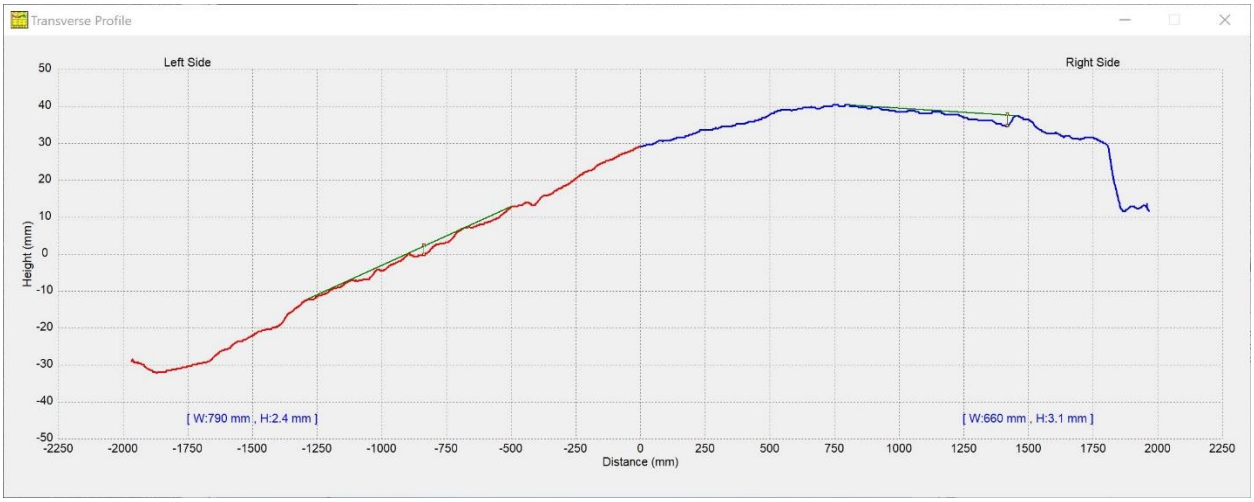

Figure E.5 Transverse Profile at 100 feet

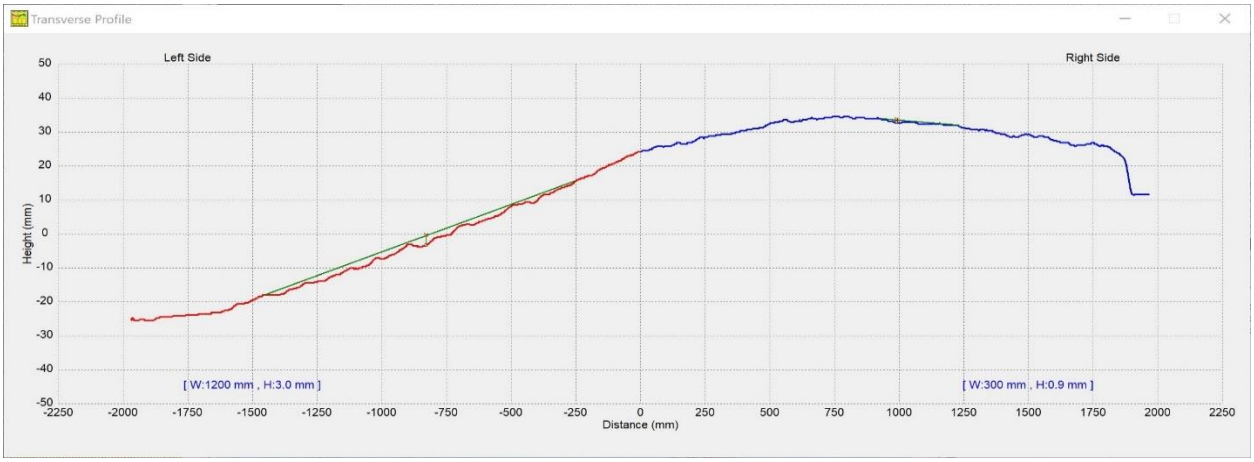

Figure E.6 Transverse Profile at 200 feet

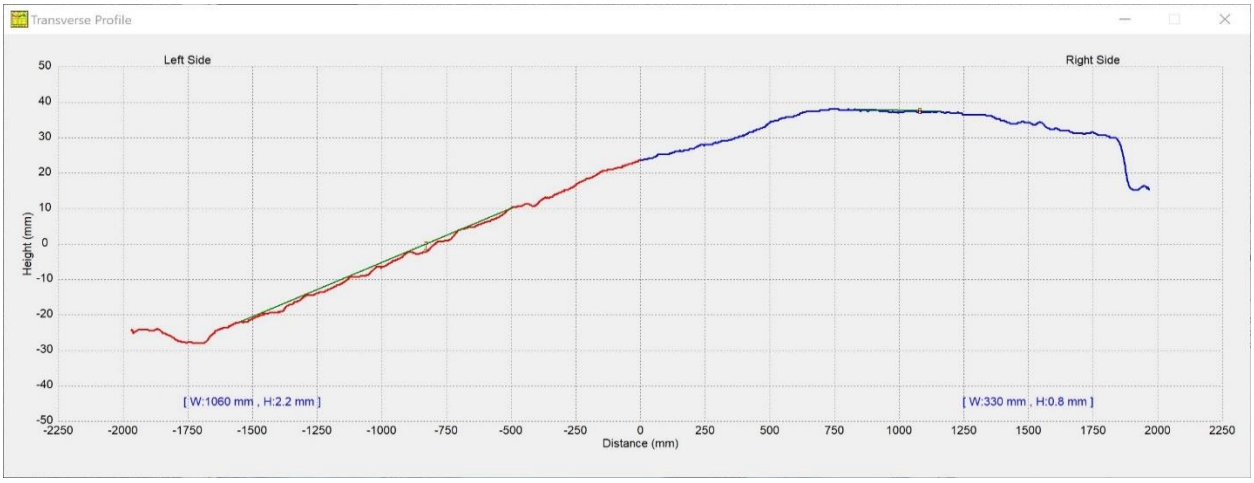

Figure E.7 Transverse Profile at 300 feet

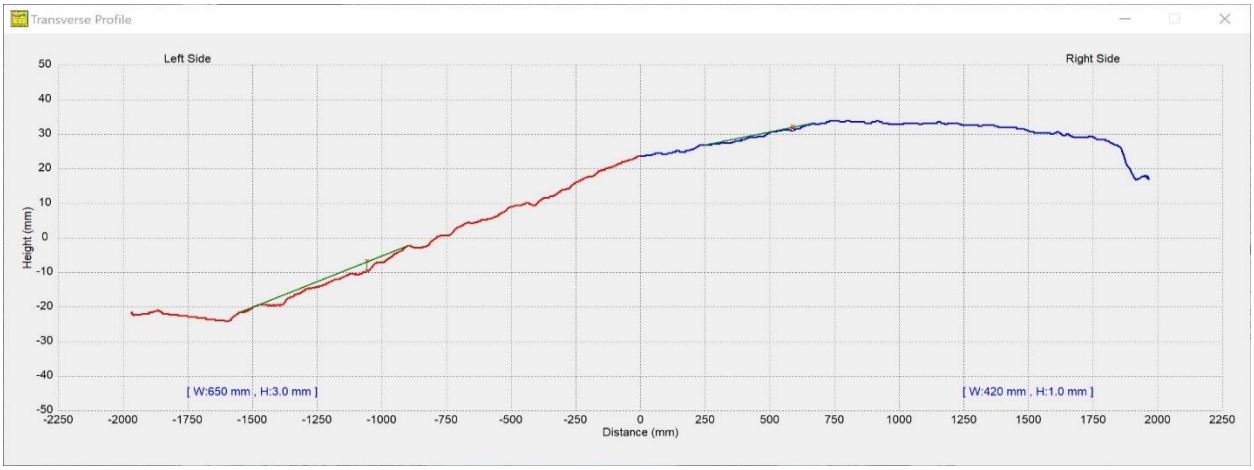

Figure E.8 Transverse Profile at 400 feet

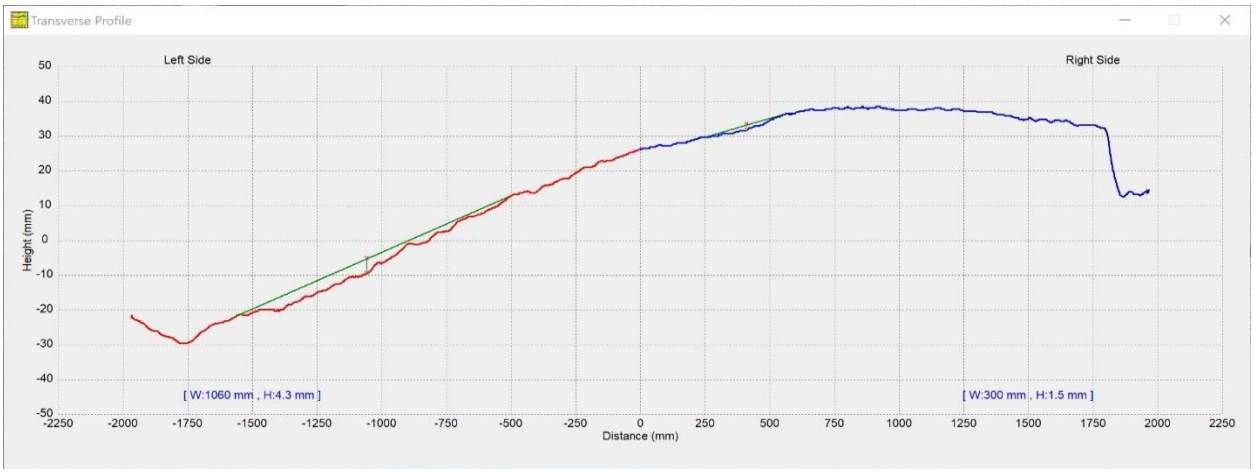

Figure E.9 Transverse Profile at 500 feet

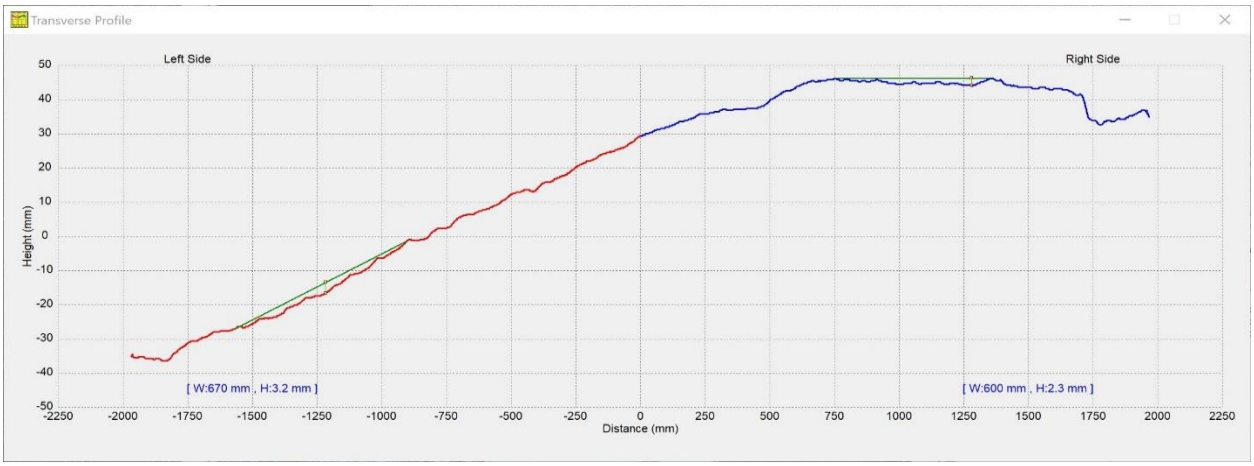

Figure E.10 Transverse Profile at 600 feet

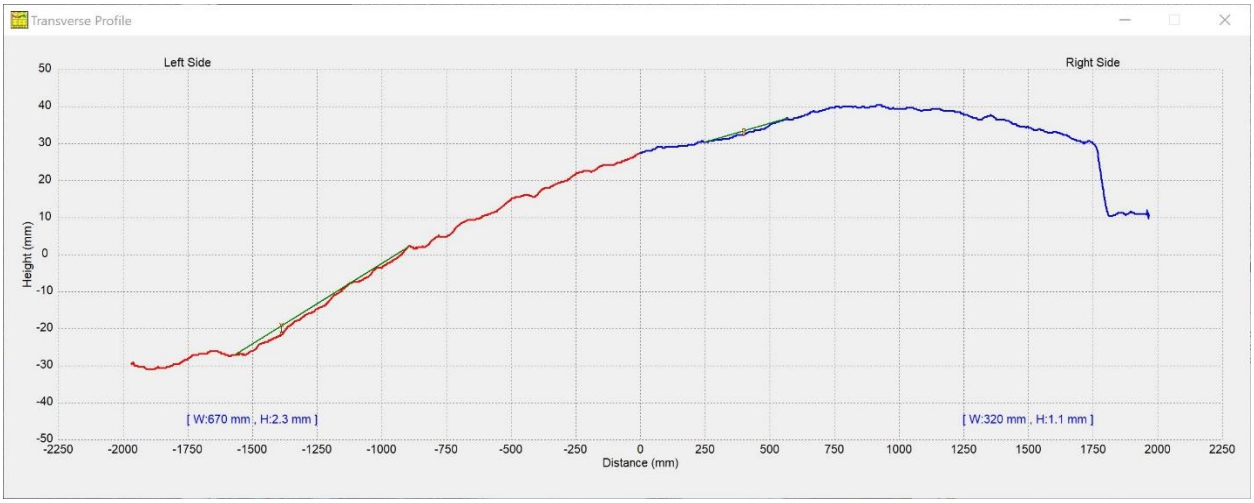

Figure E.11 Transverse Profile at 700 feet

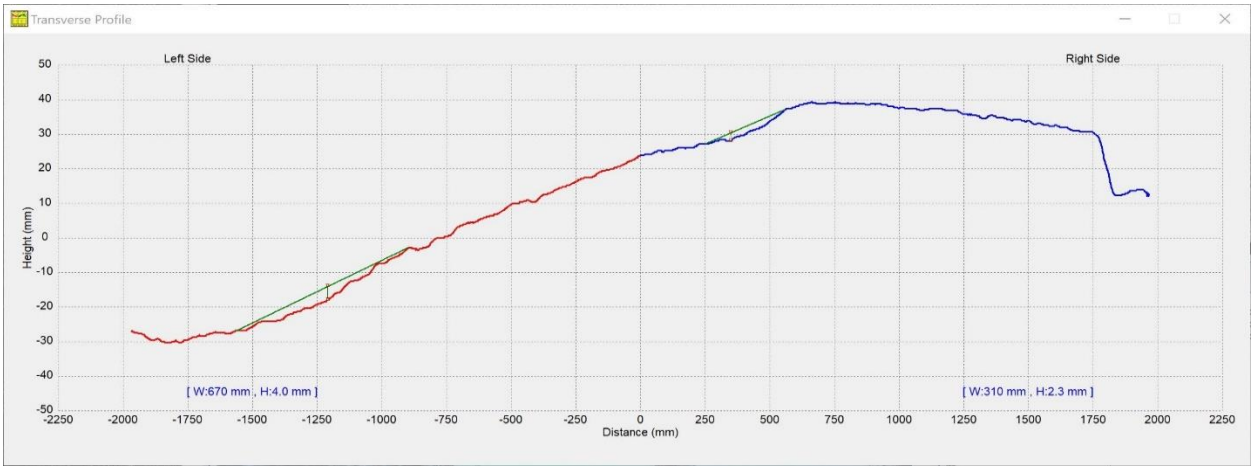

Figure E.12 Transverse Profile at 800 feet

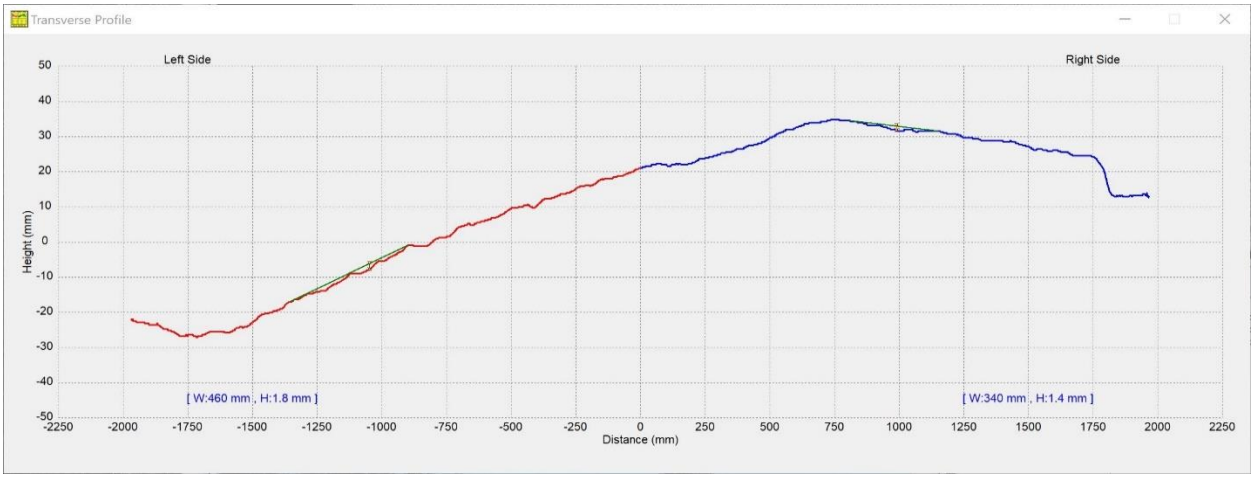

Figure E.13 Transverse Profile at 900 feet

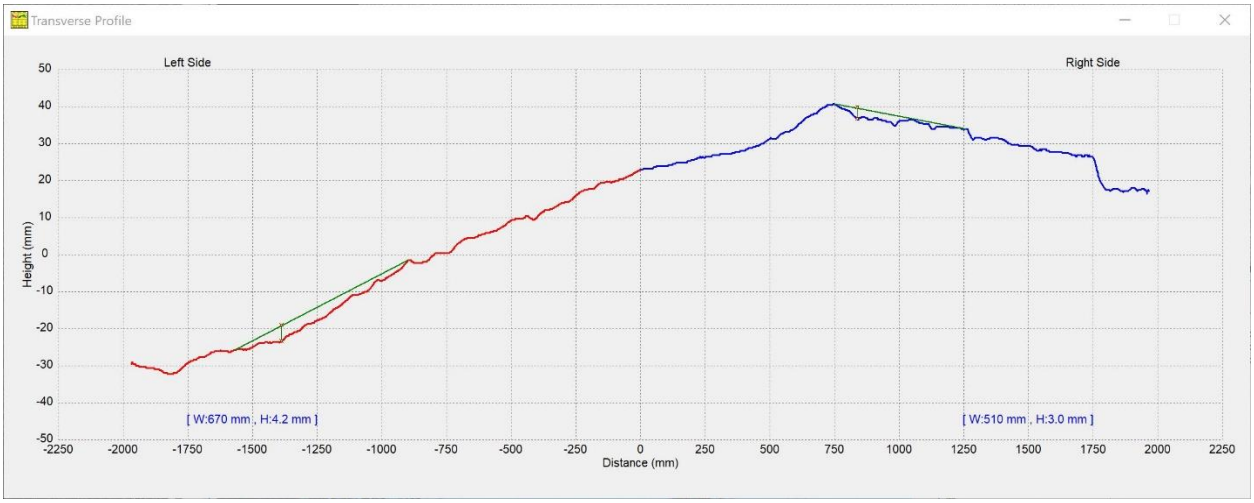

Figure E.14 Transverse Profile at 1000 feet

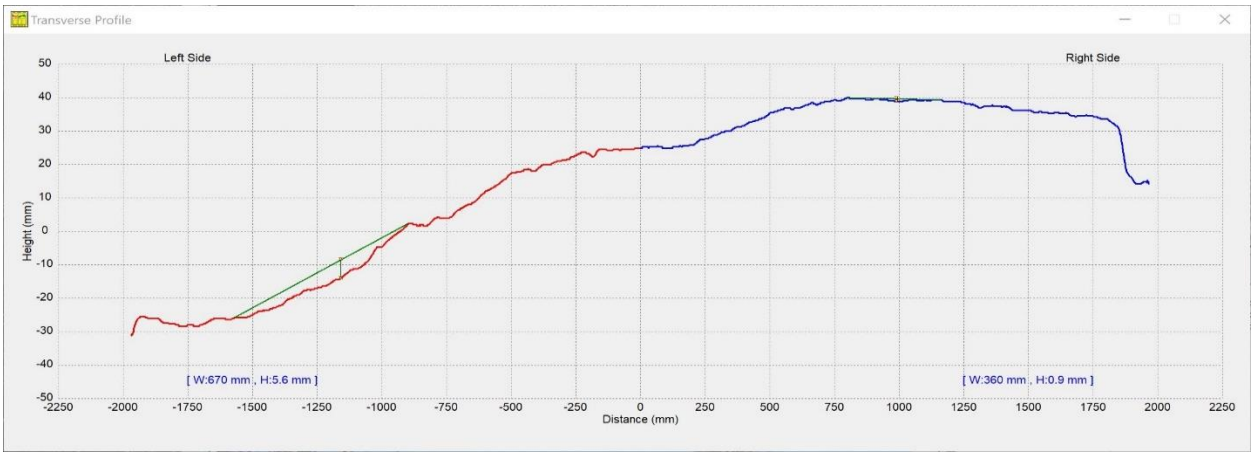

Figure E.15 Transverse Profile at 1100 feet

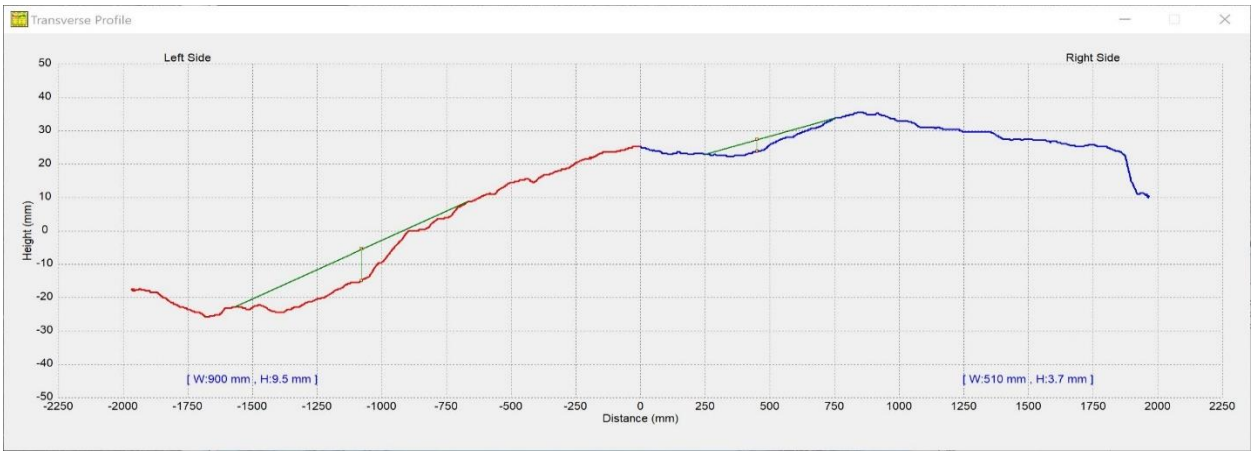

Figure E.16 Transverse Profile at 1200 feet

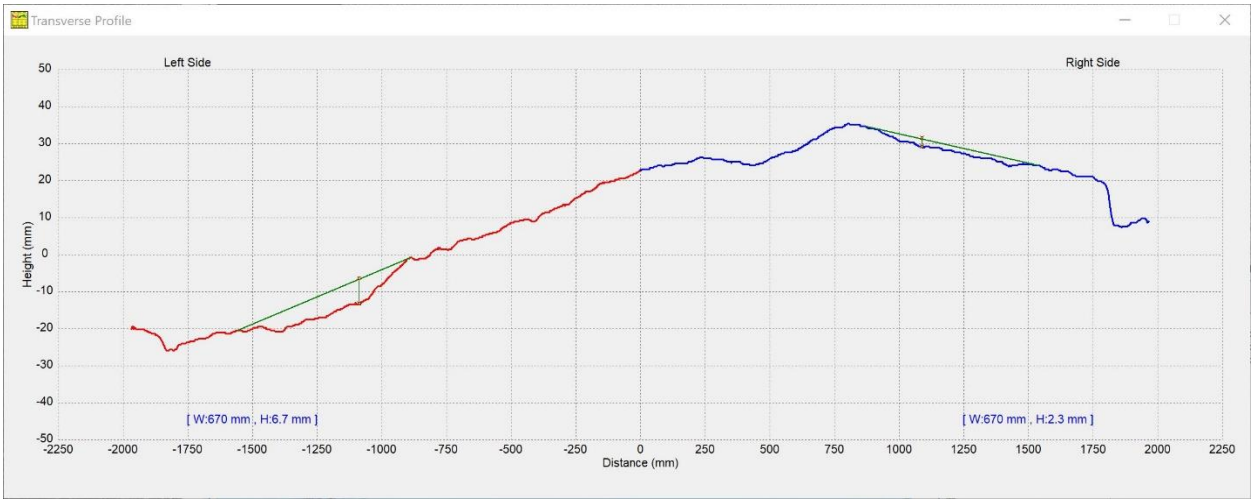

Figure E.17 Transverse Profile at 1300 feet

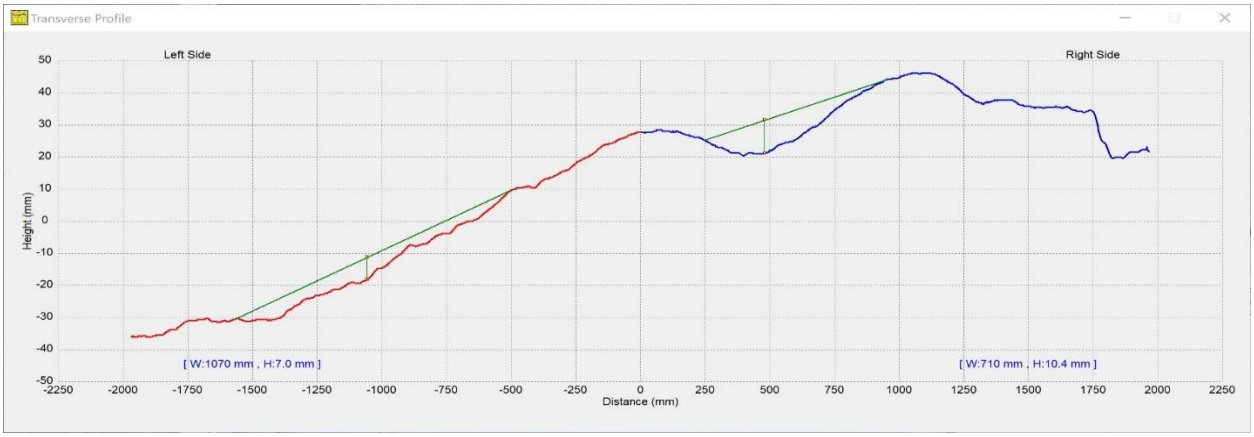

Figure E.18 Transverse Profile at 1400 feet

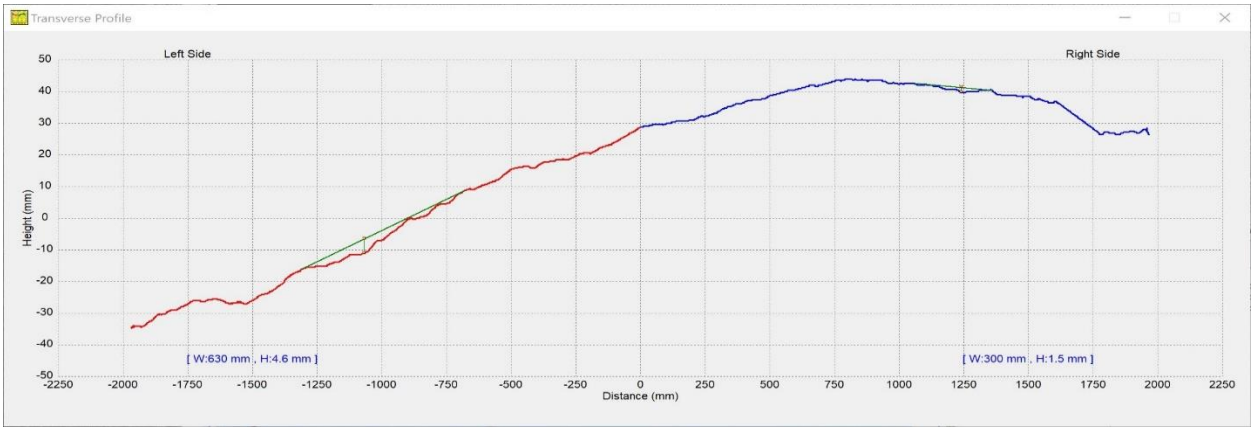

Figure E.19 Transverse Profile at 1500 feet

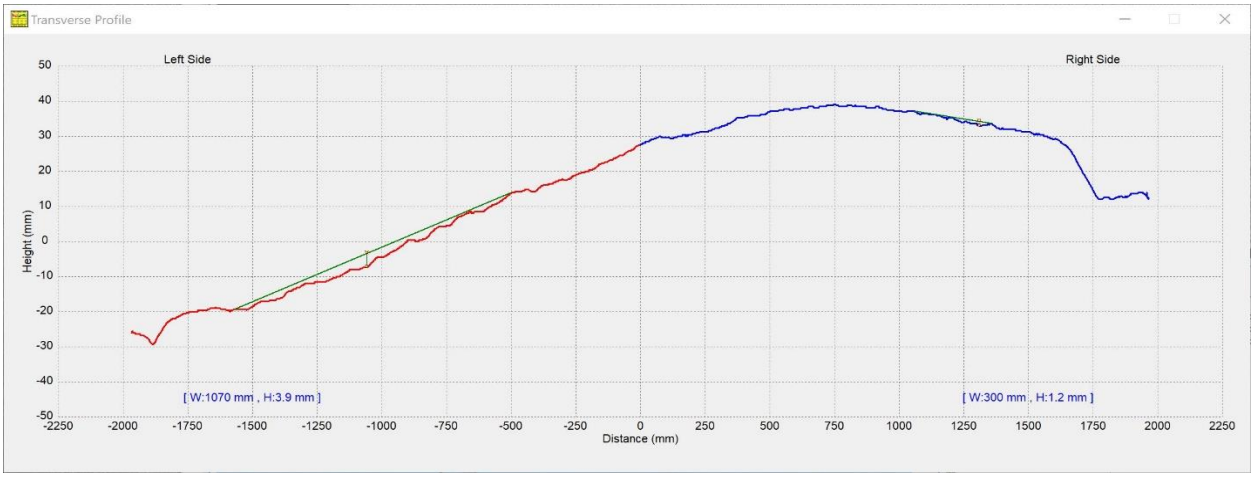

Figure E.20 Transverse Profile at 1600 feet

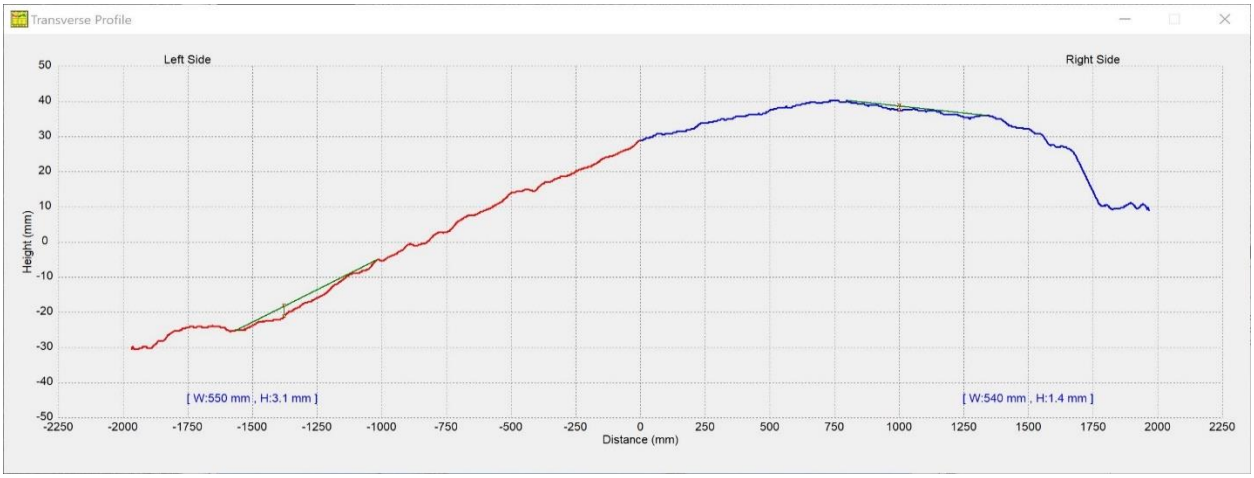

Figure E.21 Transverse Profile at 1700 feet

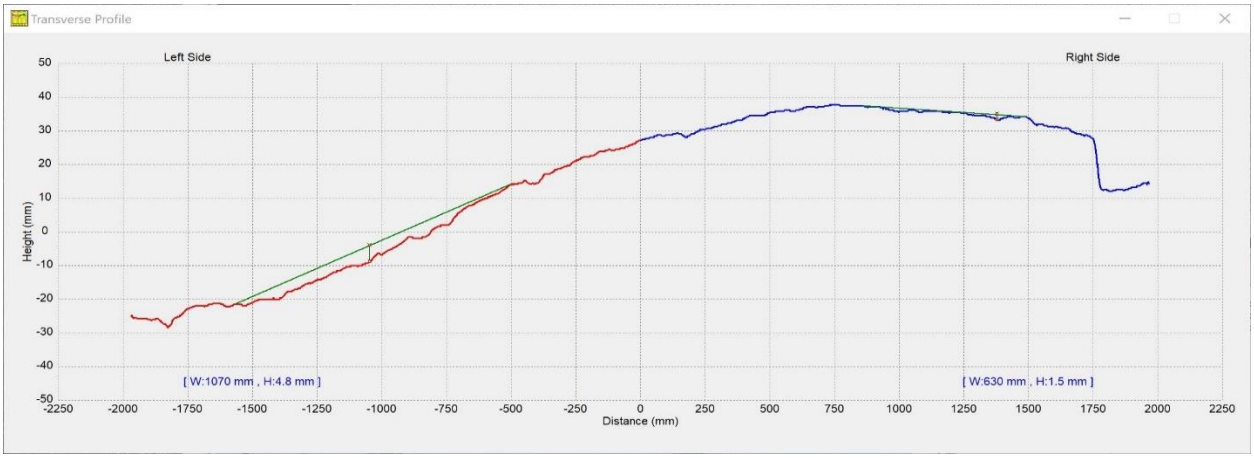

Figure E.22 Transverse Profile at 1800 feet

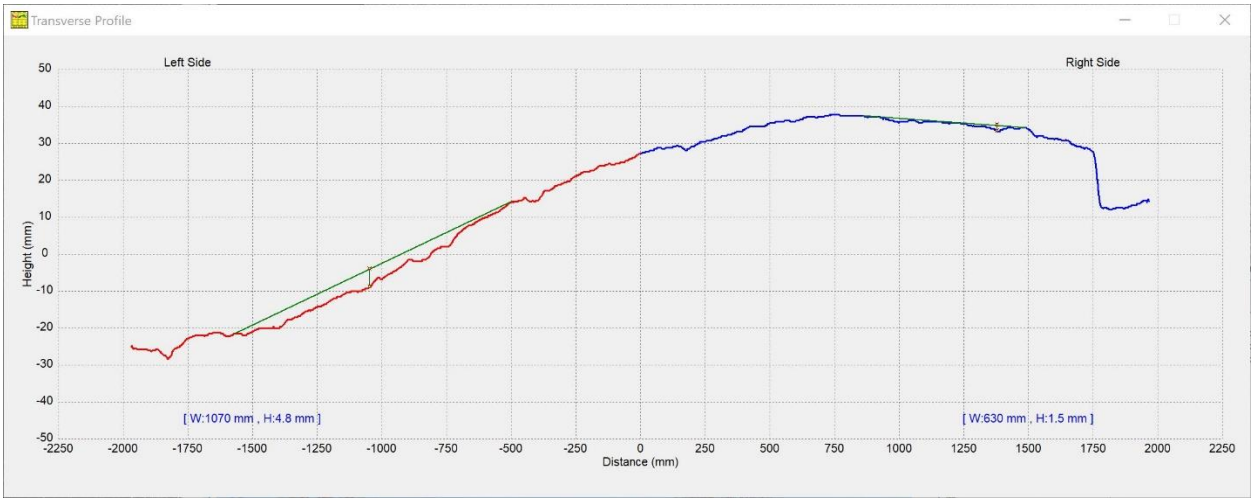

Figure E.23 Transverse Profile at 1900 feet

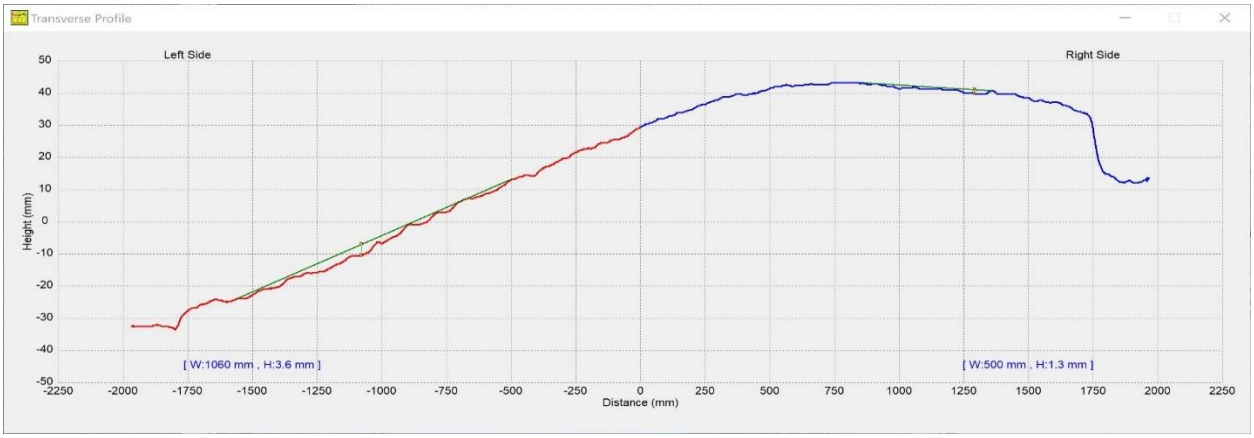

Figure E.24 Transverse Profile at 2000 feet

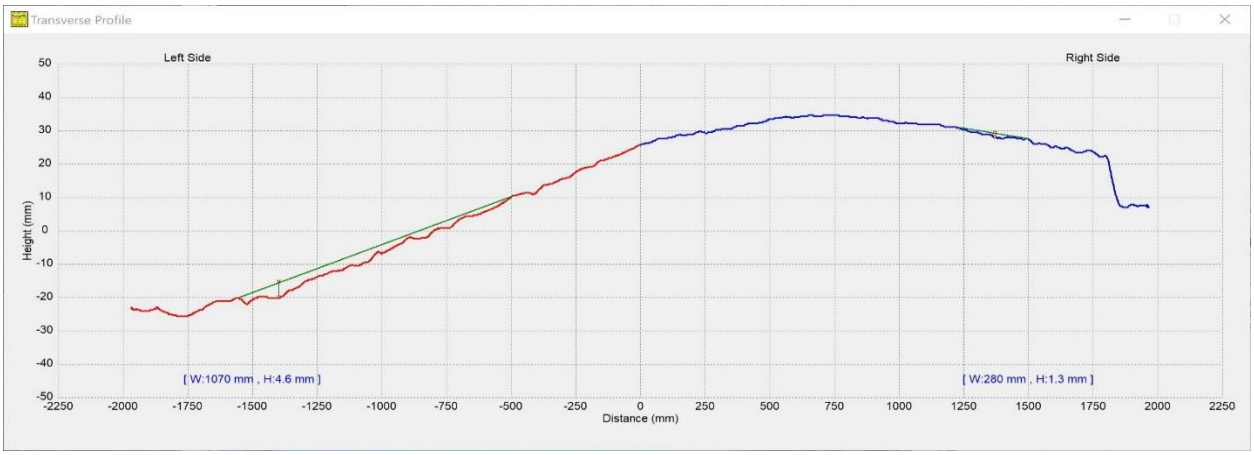

Figure E.25 Transverse Profile at 2100 feet

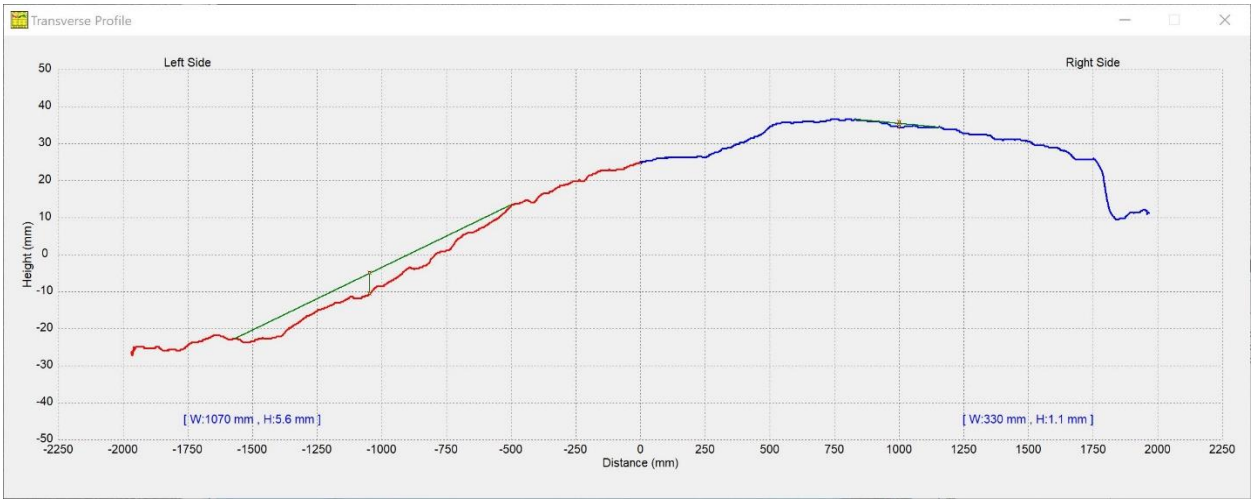

Figure E.26 Transverse Profile at 2200 feet

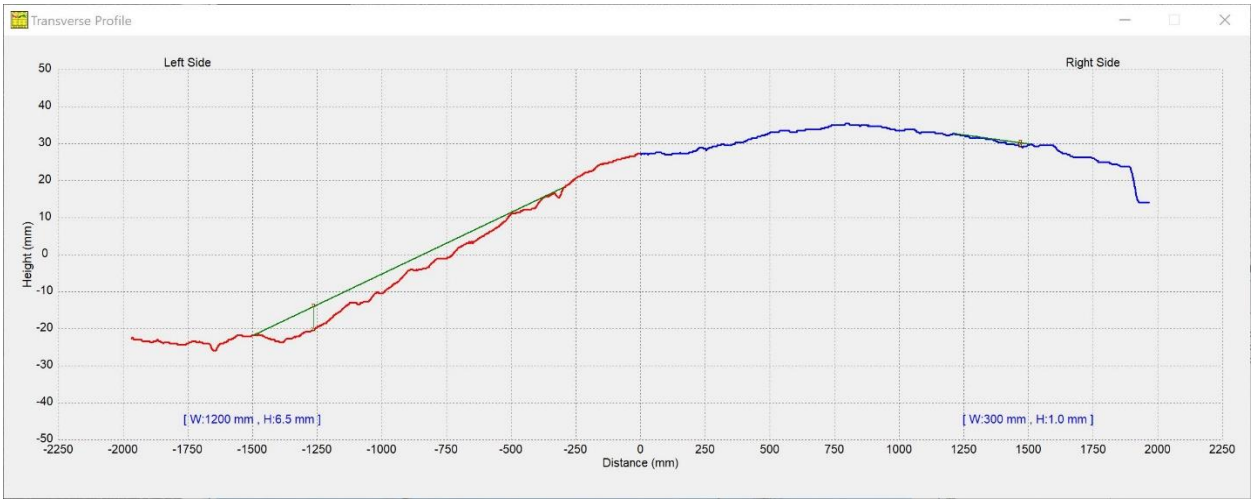

Figure E.27 Transverse Profile at 2300 feet

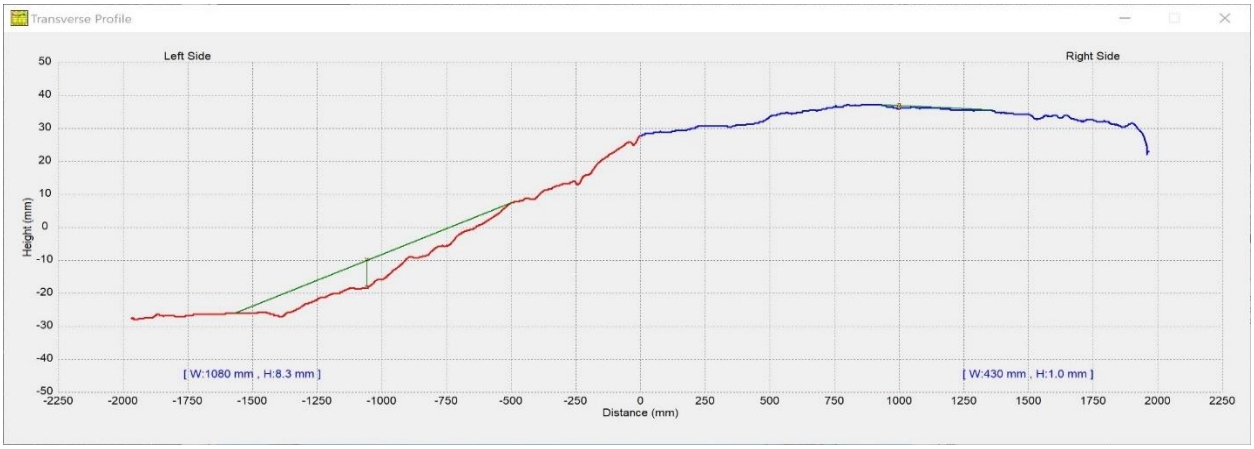

Figure E.28 Transverse Profile at 2400 feet

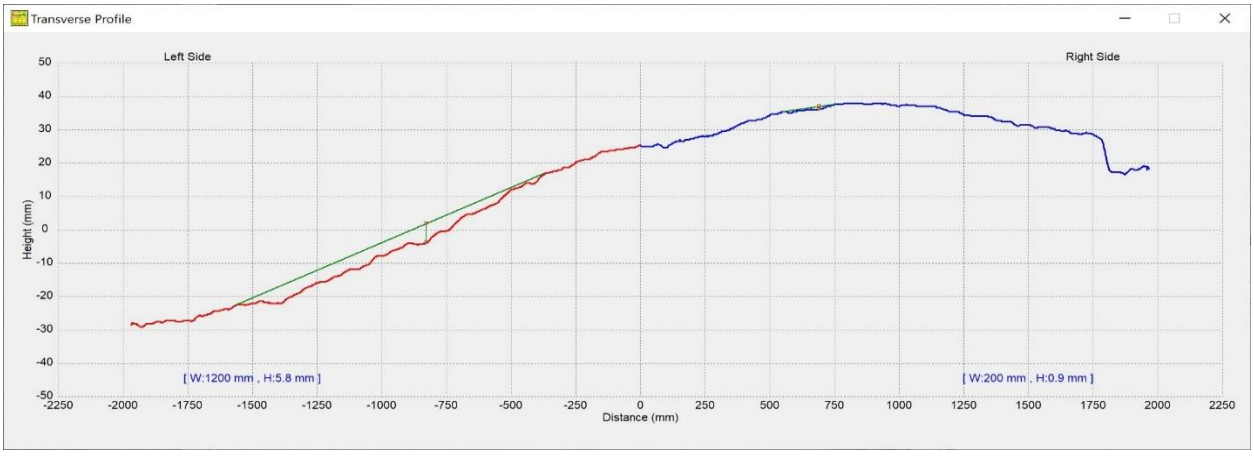

Figure E.29 Transverse Profile at 2500 feet

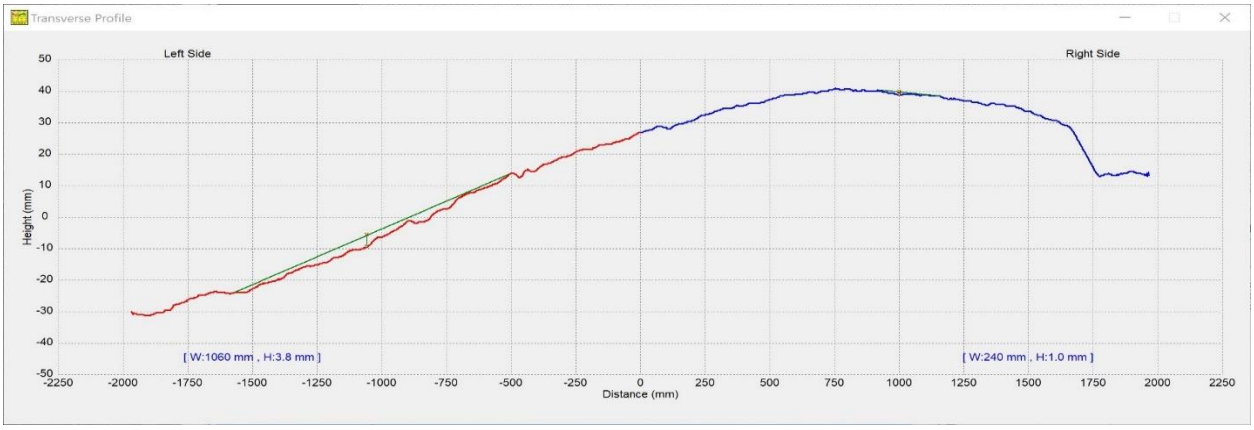

Figure E.30 Transverse Profile at 2600 feet

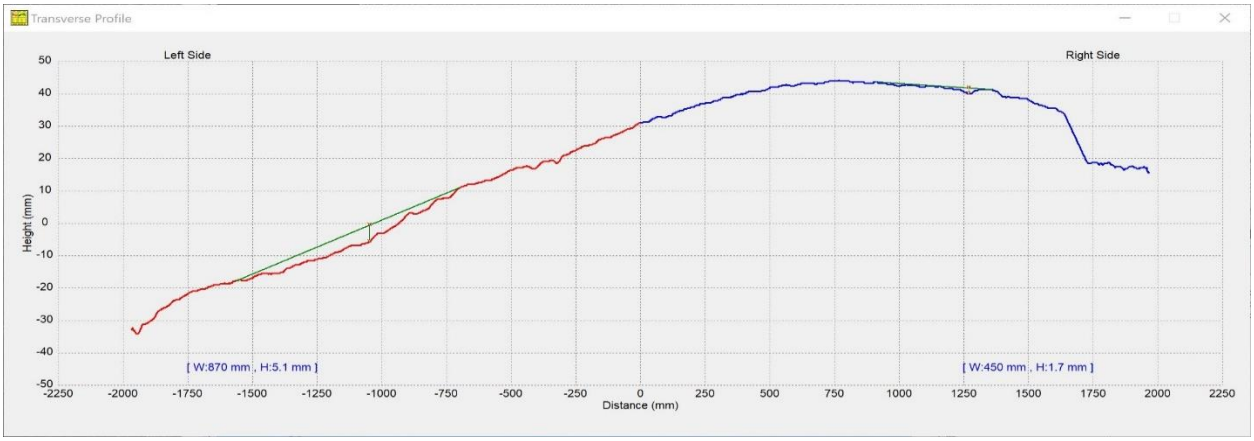

Figure E.31 Transverse Profile at 2700 feet

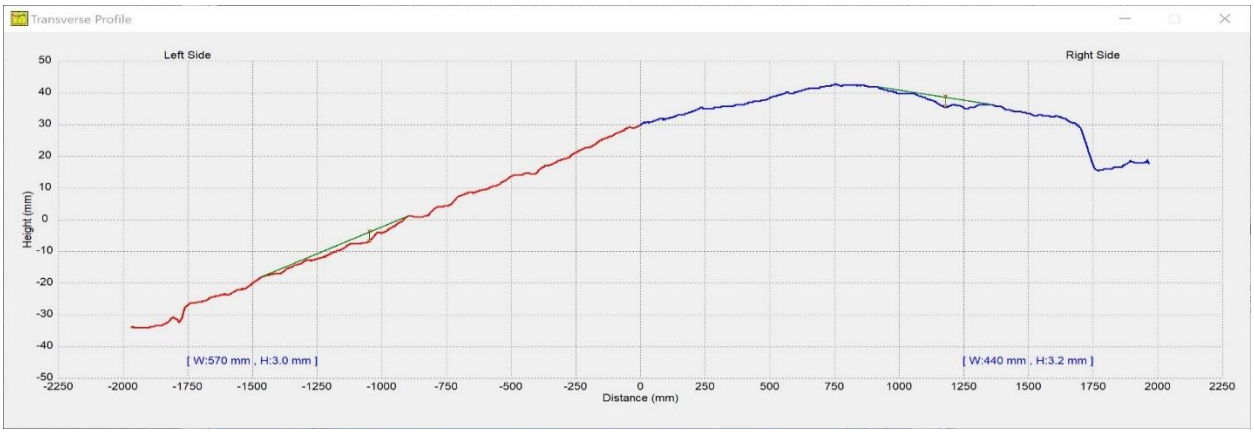

Figure E.32 Transverse Profile at 2800 feet

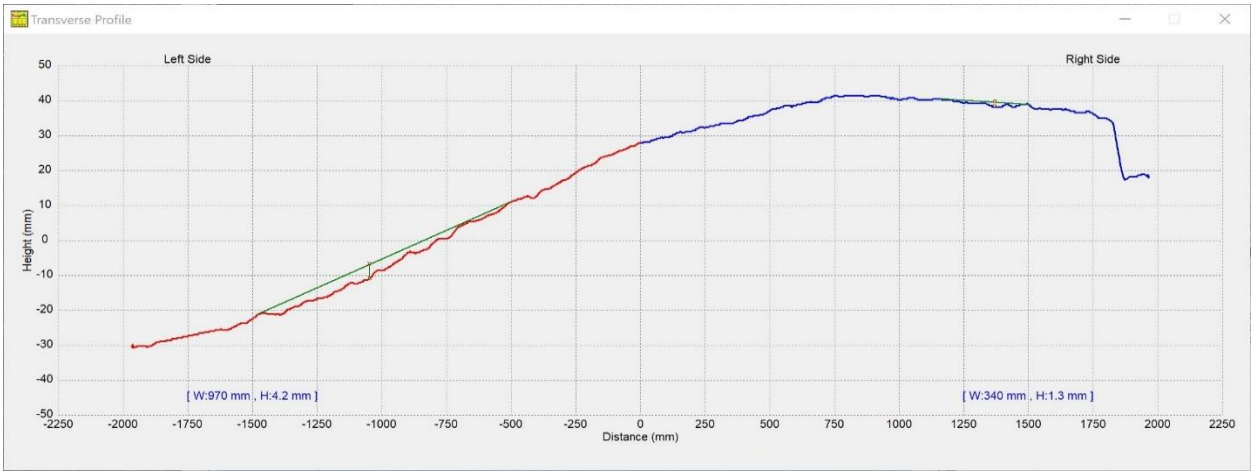

Figure E.33 Transverse Profile at 2900 feet

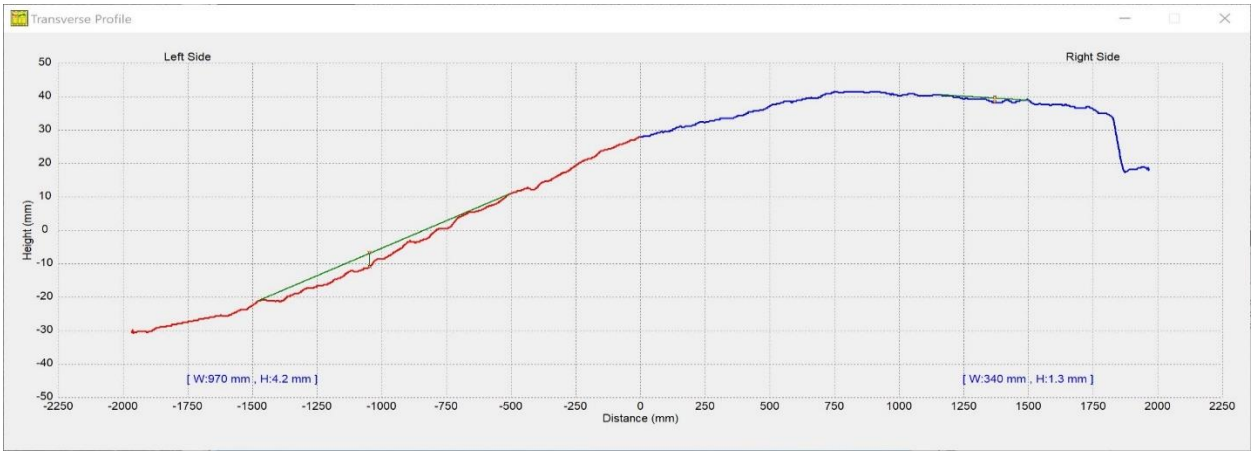

Figure E.34 Transverse Profile at 3000 feet

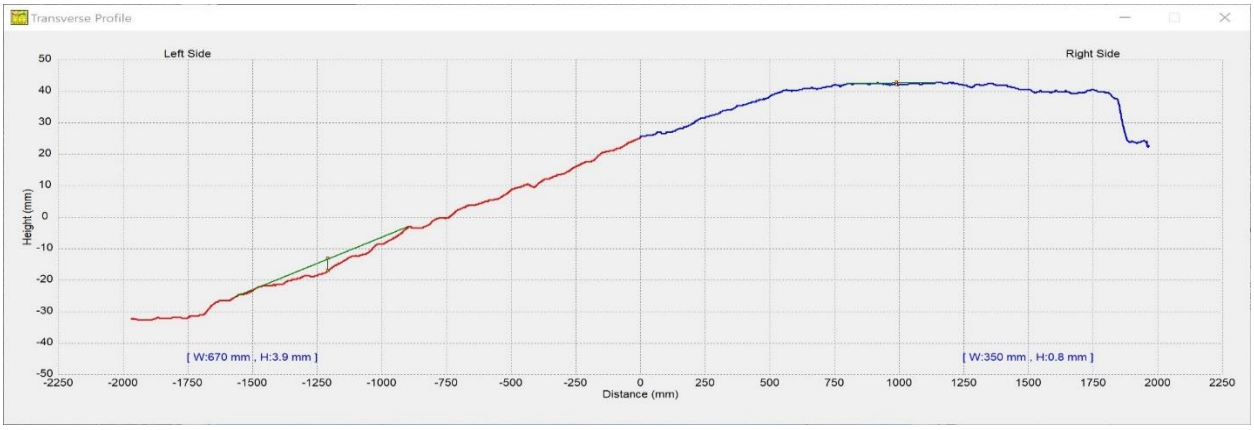

Figure E.35 Transverse Profile at 3100 feet

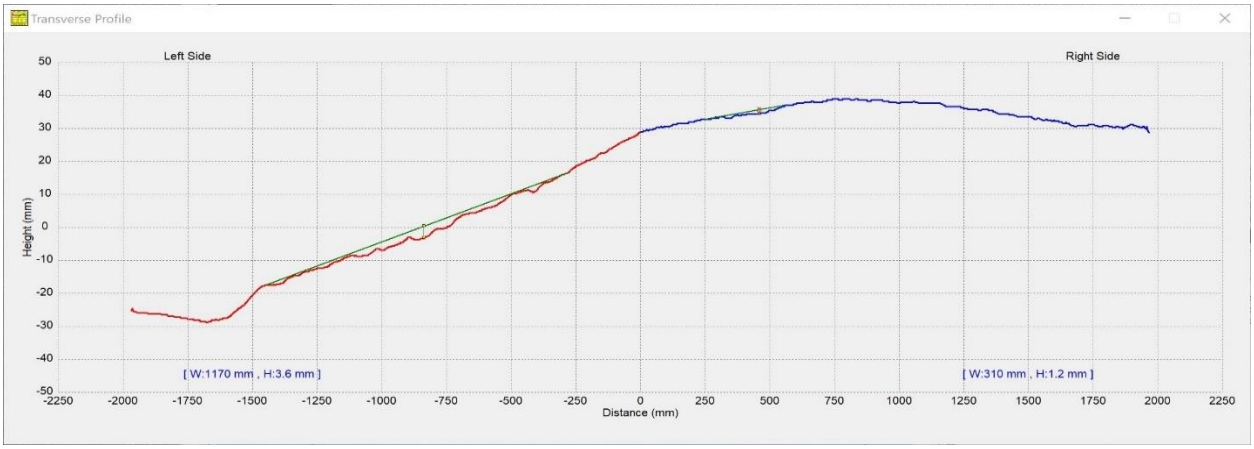

Figure E.36 Transverse Profile at 3200 feet

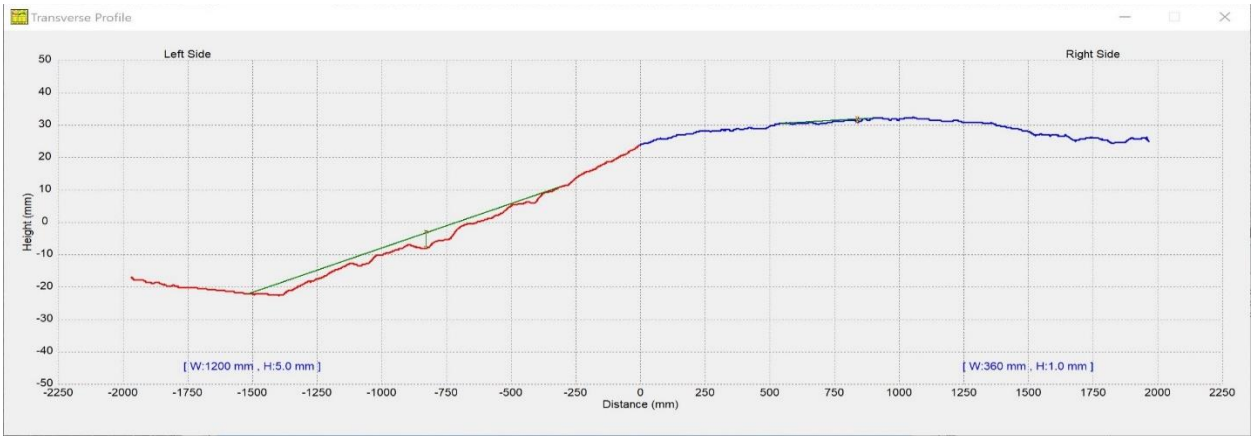

Figure E.37 Transverse Profile at 3300 feet

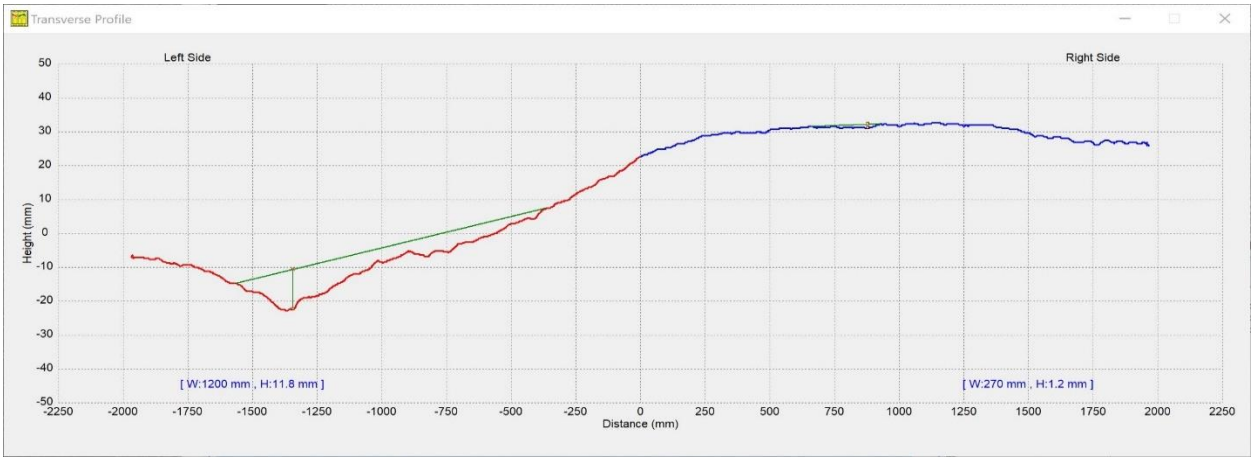

Figure E.38 Transverse Profile at 3400 feet

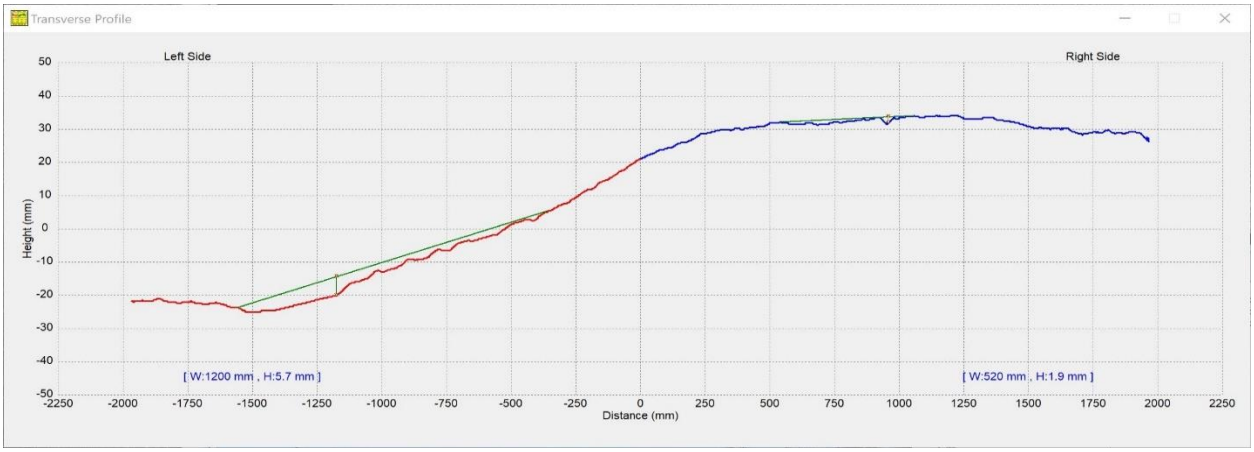

Figure E.39 Transverse Profile at 3500 feet

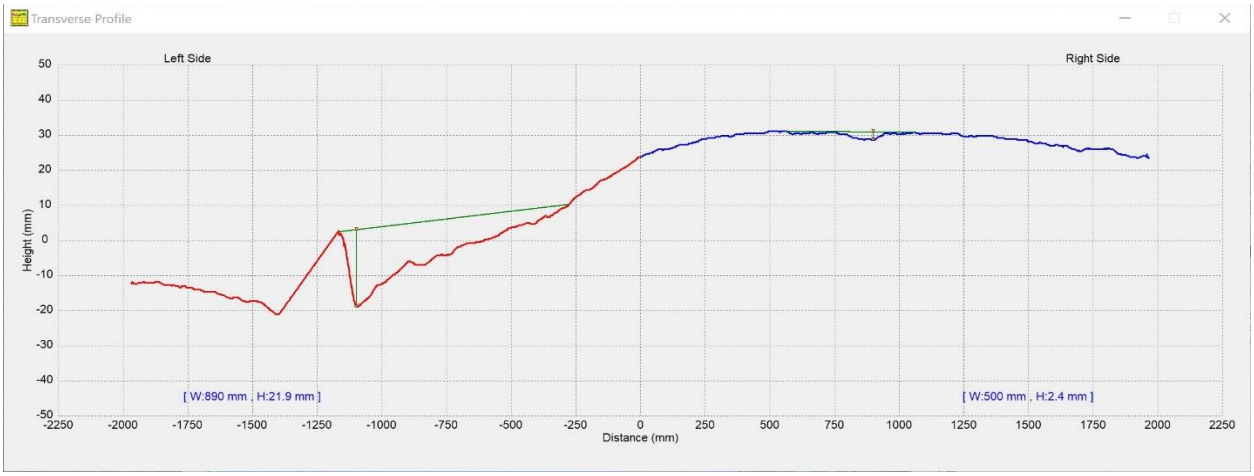

Figure E.40 Transverse Profile at 3600 feet

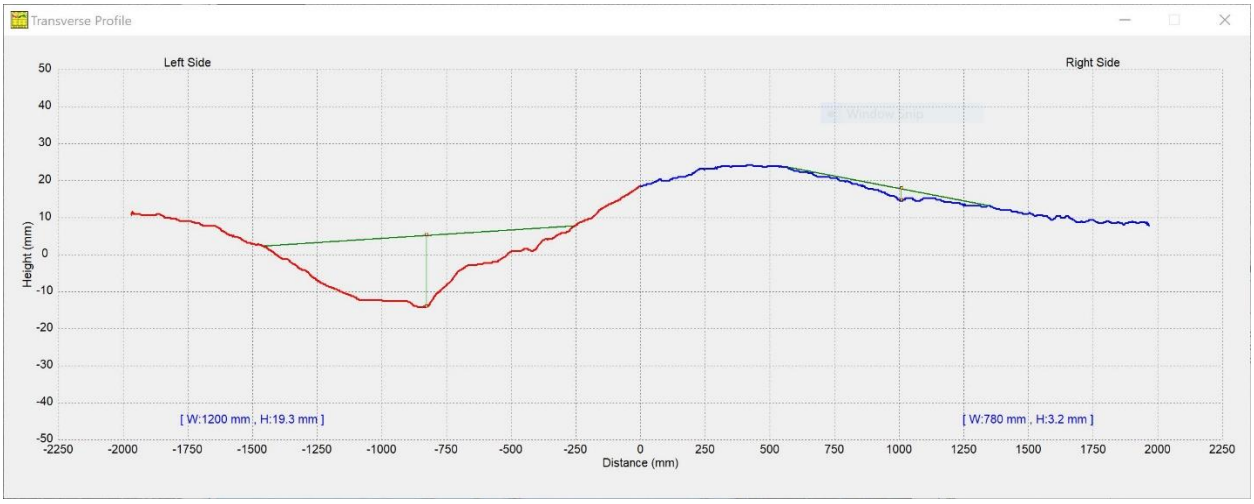

Figure E.41 Transverse Profile at 3700 feet

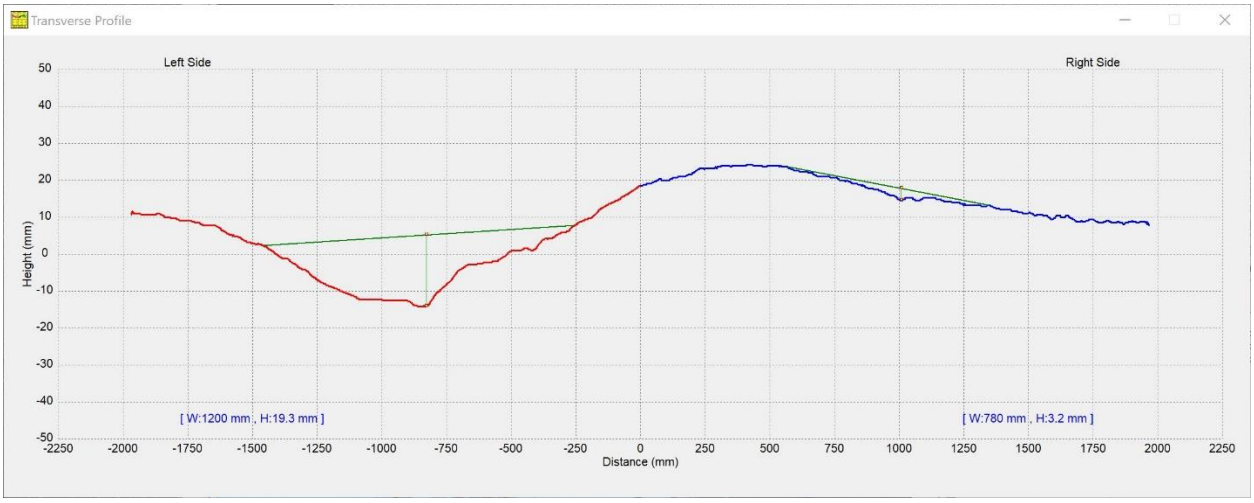

Figure E.42 Transverse Profile at 3800 feet